

STRUCTURE-FUNCTION-ANALYSIS OF DHNA-COA  
THIOESTERASE INVOLVED IN MENAQUINONE  
(VITAMIN K<sub>2</sub>) BIOSYNTHESIS PATHWAY OF  
*STAPHYLOCOCCUS AUREUS*

**Dissertation**

zur Erlangung des Doktorgrades der Naturwissenschaften (Dr. rer. nat.)  
an der Fakultät für Mathematik, Informatik und Naturwissenschaften  
der Universität Hamburg

**Fachbereich Chemie**

vorgelegt von

**Aline Melro Murad**

Hamburg, September 2016

Die vorliegende Arbeit wurde im Zeitraum von Oktober 2013 bis August 2016 in der Arbeitsgruppe von Prof. Ch. Betzel im Laboratorium für Strukturbiologie von Infektion und Entzündung am DESY und am Institut für Biochemie und Molekularbiologie, des Fachbereichs Chemie der Universität Hamburg, durchgeführt.

1. Gutachter: **Prof. C. Betzel**
2. Gutachter: **Prof. R. Bredehorst**

Tag der Disputation: 09.09.2016

For my lovely Family, my lovely Aunt Urma and Grandmother Natália

Love is eternal, unconditional and sovereign

“Não chores por mim. Essa vida não é o fim e sim o começo. Um dia voltaremos a nos encontrar.”

I dedicate this work.

<b>Table of Contents</b>	
List of Abbreviations .....	i
1. Introduction .....	1
1.1. HOSPITAL-ACQUIRED INFECTIONS .....	1
1.2. COMMUNITY-ACQUIRED INFECTIONS (CAI) .....	4
1.3. <i>STAPHYLOCOCCUS AUREUS</i> AND METHICILLIN-RESISTANCE <i>STAPHYLOCOCCUS AUREUS</i> (MRSA) .....	5
1.4. CURRENT AND NEWER THERAPY TREATMENTS FOR MRSA INFECTIONS .....	8
2. Vitamin K: a historical overview.....	12
2.1. DISCOVERY AND CHARACTERIZATION OF AN ANTIHEMORRHAGIC FACTOR - VITAMIN K .....	12
2.2. VITAMIN K <sub>3</sub> – MENADIONE AND VITAMIN K <sub>1</sub> – PHYLLIQUINONE (PHQ) .....	13
2.3. VITAMIN K <sub>2</sub> – MENAQUINONE (MQ) AND ITS ROLE IN THE ELECTRON TRANSPORT CHAIN .....	14
2.4. BIOSYNTHESIS OF MENAQUINONE (MQ) IN BACTERIA .....	16
2.5. VITAMIN K <sub>2</sub> IN HUMANS AND MENAQUINONE AS A NOVEL TARGET FOR ANTIMICROBIAL DRUG DEVELOPMENT .....	18
3. Aim of this work.....	22
4. Material and Methods .....	23
4.1. INSTRUMENTATION AND CHEMICALS.....	23
4.1.1. <i>Instrumentation</i> .....	23
4.1.2. <i>Bacterial strains and plasmids</i> .....	25
4.1.3. <i>Primer</i> .....	26
4.1.4. <i>Buffers, solutions and consumables</i> .....	26
4.2. MOLECULAR BIOLOGY AND BIOCHEMICAL PROCEDURES .....	30
4.2.1. <i>Polymerase chain reaction (PCR)</i> .....	30
4.2.2. <i>Agarose gel electrophoresis</i> .....	31
4.2.3. <i>Restriction digestion, template removal and dephosphorylation</i> .....	31
4.2.4. <i>Site-directed mutagenesis</i> .....	32
4.2.5. <i>Ligation</i> .....	33
4.2.6. <i>DNA purification, concentration determination and sequencing</i> .....	33
4.2.7. <i>Preparation of chemically competent cells</i> .....	34
4.2.8. <i>Transformation of chemically competent bacteria</i> .....	34
4.2.9. <i>E. coli glycerol stock preparation</i> .....	34
4.2.10. <i>Bacterial plasmid and oligonucleotides</i> .....	34
4.2.11. <i>Microbial growth media and selection antibiotics used for E. coli cultivation</i> ....	35
4.2.12. <i>Preparation of cleared lysates</i> .....	35
4.2.13. <i>Affinity chromatography, size exclusion chromatography and anionic/cationic                 exchange</i> .....	35
4.2.14. <i>Precipitation with ammonium sulfate</i> .....	36
4.2.15. <i>Strep-tactin matrix regeneration</i> .....	37

---

4.2.16.	<i>SDS-PAGE</i> .....	37
4.2.17.	<i>Western blot</i> .....	38
4.2.18.	<i>Thermal shift assay</i> .....	38
4.2.19.	<i>Protein quantification</i> .....	39
4.2.20.	<i>Dynamic light scattering (DLS)</i> .....	39
4.2.21.	<i>Circular dichroism (CD)</i> .....	39
4.2.22.	<i>MALDI-ToF Mass Spectrometry</i> .....	41
4.2.23.	<i>Sample preparation for initial crystallization screening</i> .....	41
4.2.24.	<i>Optimization of the crystallization condition</i> .....	42
4.2.25.	<i>Soaking with platinum to obtain heavy atom derivatives</i> .....	43
4.2.26.	<i>Diffraction data collection</i> .....	43
4.2.27.	<i>Data processing and model building</i> .....	44
4.2.28.	<i>Model evaluation</i> .....	45
4.2.29.	<i>Docking studies and peptide rational design</i> .....	45
4.2.30.	<i>Thioesterase activity assays of DHNA</i> .....	45
5.	<b>Results</b> .....	47
5.1.	RECOMBINANT EXPRESSION, PURIFICATION, PHYSICOCHEMICAL CHARACTERIZATION AND SECONDARY STRUCTURE ESTIMATION OF MENF .....	47
5.2.	MENF SEQUENCE ALIGNMENT AND PREDICTION MODEL .....	52
5.3.	RECOMBINANT EXPRESSION, PURIFICATION AND PHYSICOCHEMICAL CHARACTERIZATION OF MENH .....	54
5.4.	MENH SEQUENCE ALIGNMENT AND PREDICTED MODEL .....	57
5.5.	RECOMBINANT EXPRESSION, PURIFICATION, PHYSICOCHEMICAL CHARACTERIZATION AND SECONDARY STRUCTURE ESTIMATION OF DHNA-CoA THIOESTERASE .....	60
5.6.	CRYSTALLIZATION EXPERIMENTS OF <i>S. AUREUS</i> NATIVE DHNA, D16A AND E31N VARIANTS .....	66
5.7.	DIFFRACTION DATA COLLECTION, DATA PROCESSING AND MODEL BUILDING OF <i>S. AUREUS</i> DHNA .....	69
5.8.	<i>S. AUREUS</i> DHNA: STRUCTURE ANALYSIS .....	70
5.9.	4-HYDROXYBENZOYL CoA THIOESTERASE STRUCTURE COMPARISON.....	76
5.10.	PUTATIVE ACTIVE SITE OF <i>S. AUREUS</i> DHNA AND THIOESTERASE ACTIVITY .....	78
5.11.	DESIGNED PEPTIDES AND THIOESTERASE INHIBITION .....	83
6.	<b>Discussion</b> .....	88
6.1.	ISOCHORISMATE SYNTHASE (MENF) .....	88
6.2.	DEMETHYMENTAQUINONE METHYLTRANSFERASE .....	89
6.3.	4-HYDROXYBENZOYL CoA THIOESTERASE (DHNA-CoA THIOESTERASE) .....	90
7.	<b>Summary</b> .....	99
8.	<b>Zusammenfassung</b> .....	100
9.	<b>References</b> .....	102
10.	<b>Appendix</b> .....	126

## Table of Contents

---

11. Acknowledgments .....	127
12. Risks and safety statements .....	129
Curriculum Vitae .....	135
Eidesstattliche Erklärung .....	140

**List of Abbreviations**

AHT - Anhydrotetracycline

AS – Ammonium sulfate

$\alpha$ -HD - HotDog helix

ATP – Adenosine Tri-Phosphate

acyl-AMS - acyl-adenosyl mono phosphate

ACN – Acetonitrile

AmbiCa – Ammonium bicarbonate

APS – Ammonium Persulfate

AML - Acute Myelogenous Leukemia

BCIP - 5-Bromo-4-chloro-3'-indolyphosphate

BFIT - Brown fat adipose tissue thioesterase

BCA – 4-hydroxybenzoyl-CoA

BSI - Bloodstream infection

BSA - Bovine serum albumin

BFIT - Brown fat adipose tissue thioesterase

CDC - Center for Disease Control and Prevention

CACH - Cytoplasmic acetyl-CoA hydrolase

CAI - Community-acquired infections

CA – Community-acquired

ccr - Cassette Chromosome Recombinases

CLABSIs - Central Line-Associated Bloodstream Infections

CD – Circular dichroism

CACH - Cytoplasmic acetyl-CoA hydrolase

CV - Column Volume

DTT – Dithiothreitol

DTNB - 5,5'-Dithiobis(2-nitrobenzoic acid)

DNA – Deoxyribonucleic Acid

dNTP - Deoxyribose nucleoside triphosphate

DLS – Dynamic Light Scattering

DHFL - Dehypoxanthinylfualosine

DMQ – Demethylmenaquinone

DHNA-CoA - 1,4-dihydroxy-2-naphthoyl coenzyme A  
ECDC - European Centre for Disease and Control Prevention  
ESBL - Extended-Spectrum Beta-Lactamase  
*E. coli* – *Escherichia coli*  
EMBL - European Molecular Biology Laboratory  
ELISA - Enzyme-linked immunosorbent assay plate  
FabA - Beta-hydroxydecanoyl thioester dehydrase  
4-HBT - 4-hydroxybenzoyl CoA  
FA – Formic acid  
FPLC - Fast protein liquid chromatography  
FDA - US Food and Drug Administration  
HA – Hospital-acquired  
HAD – Heavy Atom Derivative  
HABA - 4'-hydroxyazobenzene-2-carboxylic acid  
HR - Hydrodynamic radius  
HIV - Human Immunodeficiency Virus  
*HiYbgC* - *Haemophilus influenzae* YbgC  
*HpYbgC* - *Helicobacter pylori* YbgC  
HACO - Health Care-Associated Community-Onset  
HEPES - (4-(2-Hydroxyethyl)-1-piperazineethanesulfonic acid )  
HAIs - Hospital-acquired infections  
ICU - Intensive Care Units  
IDSA - Infectious Diseases Society of America  
IAA – Iodacetamide  
Kb – Kilobase  
K<sub>2</sub>PtCl<sub>4</sub> - Potassium tetrachloroplatinate (II)  
MRSA - Methicillin-Resistance *Staphylococcus aureus*  
MSSA - Methicillin-Susceptible *S. aureus*  
MQ – Menaquinone  
MQH<sub>2</sub> –Menaquinol  
MenF - Isochorismate synthase  
MenD - 2-succinyl-6-hydroxy-2,4-cyclohexadiene-1-carboxylic acid synthase



MenH (*E. coli*) - 2-succinyl-6-hydroxy-2,4-cyclohexadiene-1-carboxylate synthase

MenE - O-succinylbenzoate synthetase

MenC - O-succinylbenzoate synthase

MenB - 1,4-dihydroxy-2-naphthoyl-CoA synthase

MenA - DHNA-octaprenyltransferase

MenG/UbiE/MenH - Demethylmenaquinone methyltransferase

MALDI-ToF - Matrix-Assisted Laser Desorption Ionization - Time of Flight

NHSN - National Healthcare Safety Network

NADH - Nicotinamide adenine dinucleotide reduced

NBT - Nitro-blue tetrazolium

NI - Nosocomial Infections

NNIS - National Nosocomial Infection Surveillance

OSB - O-succinylbenzoate

OBS-CoA - O-succinylbenzoate coenzyme A

OPLS - Optimized Potentials for Liquid Simulations force field

PBP2a - 78-kDa Penicillin-Binding Protein 2a

PhQ – Phylloquinone

PPi – Pyrophosphate

*Pfu* - *Pyrococcus furiosus*

PCR – Polymerase chain reaction

PBS – Phosphate saline buffer

PMSF - Phenylmethane sulfonyl fluoride

*P. profundum* - *Photobacterium profundum*

rRNA – Ribosomal Ribose Nucleic Acid

RS<sup>-</sup> - Radical sulfur anion

R-S-TNB<sup>-</sup> – Radical-sulfur-2-nitro-5-thiobenzoate anion

RT – Room temperature

R&D - Research and Development

RMS – Root mean square

ROS - Reactive Oxygen Species

SAD - Single-wavelength anomalous dispersion/diffraction

SHCHC - 2-succinyl-6-hydroxy-2,4-cyclohexadiene-1-carboxylate

SDM - Site-directed mutagenesis

SDS-PAGE – SDS-Polyacrylamide Gel Electrophoresis

*S. aureus* – *Staphylococcus aureus*

*S. epidermidis* – *Staphylococcus epidermidis*

*S. fleurettii* - *Staphylococcus fleurettii*

*S. sciuri* - *Staphylococcus sciuri*

*S. vitulinus* - *Staphylococcus vitulinus*

SCC<sub>mec</sub> – Staphylococcal chromosome cassette mec

SSI - Surgical site infections

TNB<sup>2-</sup> - 2-nitro-5-thiobenzoate anion

TAE – Tris-acetate-EDTA

TEMED - N,N,N',N'-Tetramethylethane-1,2-diamine

US – United States

UQ – Ubiquinone

VISA - Vancomycin-intermediate *S. aureus*

VRSA - Vancomycin-Resistant *S. aureus*

VRE - Vancomycin-Resistant Enterococcus

v/v – Volume per volume

w/v – Weight per volume

WHO - World Health Organization

## **1. Introduction**

### **1.1. Hospital-acquired infections**

Nosocomial Infections (NI) or Hospital-acquired infections (HAIs) are one of the most serious and concerning problems in the public health care both in developed and developing countries. According to the United States Center for Disease Control and Prevention (US CDC), NI/HAI can be described as an infection which occurs in a period of 48 hours, not having been present at the time of patient hospitalization admission, or within 48 hours after discharge, and the result of medical intervention [1,2]. Nowadays, HAIs are, by far, one of the most common complications among hospitalized patients.

The World Health Organization (WHO) report published by the United Nation - UN in 2011 estimates that out of every 100 hospitalized patients at any given time, 7 in developed and 10 in developing countries might acquire at least one HAI [3]. The CDC report showed a prevalence of 4.5% of HAIs in the USA. Around 2 million patients acquire HAIs per year and approximately 100.000 patients die from HAIs complications [4]. Furthermore, in Europe, the prevalence of HAIs is around 7.1%, representing 4.5 million episodes of HAIs annually and 175.000 die [5–8]. The prevalence of HAI's events for developed countries in a period comprising the years 1995-2010 is shown in Figure 1.

Unfortunately, there is low data available related to developing countries located in Latin America, Asia, and Africa. The HAIs prevalence estimations in these countries are between 5.7 and 19.1%. In Brazil alone, 14% of all hospitalized patients contract infections, and approximately 1 million cases of HAI occur every year resulting in 100.000 deaths (Figure 2) [9].

HAIs contributes to an increase of morbidity (number of incidence of a specified illness within a population during a given time period), mortality (incidence of deaths per 1000 individuals in a population per year from a specified illness) and prolong hospitalization days, time during which patients occupy scarce bed-days. In Europe, patients diagnosed with HAIs lead to a 16 million extra days of hospital stay annually. In developing countries the increase of hospital stay associated with HAIs range between 5 to 30 days [3,10]. Most of the patients who contracted HAI during hospitalization require additional diagnosis and therapeutic interventions, which

increases hospital costs and represent an additional economic burden to the health insurance funds [11,12].

The US CDC estimates an addition of US\$ 5 billion of nosocomial infections costs in the year 2000 [4]. A recent report in 2013 from Zimlichman and co-workers [13] indicates that, in comparison to the data reported in the year 2000, there was an increase of 50%, equivalent to US\$ 9.8 billion. The average costs to treat surgical site HAI were US\$ 18.902 - \$22.667, \$30.919 - \$65.245 to treat central line-associated bloodstream infection, \$36.286 - \$44.220 for ventilator-associated pneumonia treatment and \$603 - \$1.189 for catheter-associated urinary tract infection treatment. A WHO report, in accordance with the European Centre for Disease and Control Prevention (ECDC) report in 2015, indicated that these infections account for a cost of approximately €7 billion per year in Europe [3,14]. Additional costs to treat, for instance, bloodstream infection (BSI) episodes in Europe, oscillated between €4.200 - €3.030. This represents an annual cost of €4 million and €130 million for the healthcare systems in the United Kingdom and France, respectively.

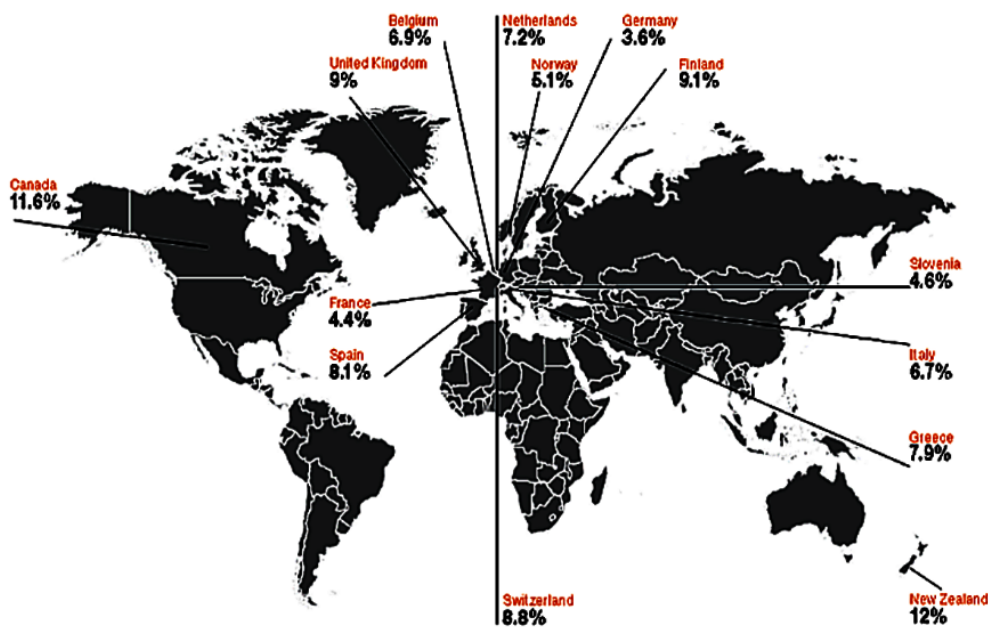


**Figure 1:** Prevalence of health care-associated infection in developed countries, 1995-2010. \*For countries with more than one study, the most recent figures are included. <sup>1</sup>

<sup>1</sup> Reprint authorized by the World Health Organization: Report on the Burden of Endemic Health Care-Associated Infection Worldwide Clean Care is Safer Care, Benedetta Allegranzi, Sepideh Bagheri

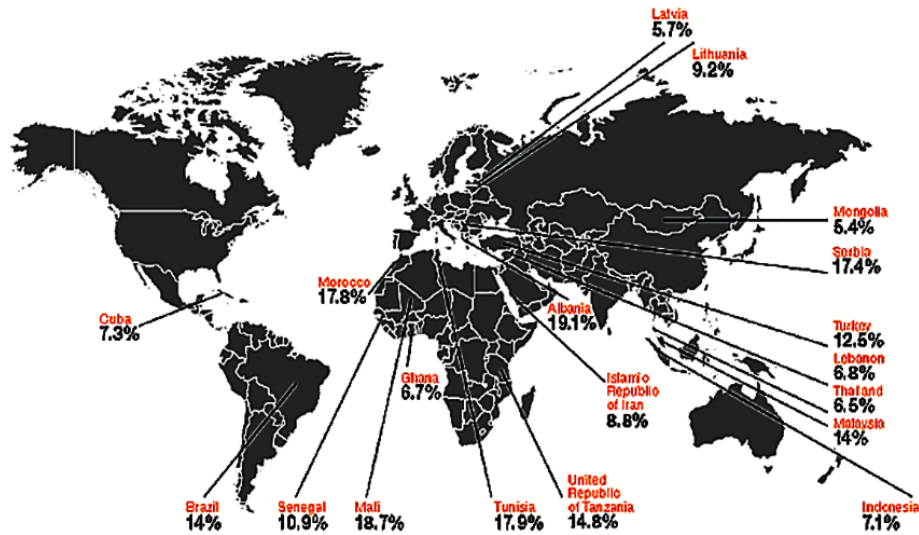


**Figure 2:** Prevalence of health-care-associated infection in developing countries, 1995-2010. \*For countries with more than one study, the most recent figures are included. <sup>1</sup>

Patients submitted to invasive procedures or admitted into intensive care units (ICU) become more susceptible to acquire nosocomial infections in comparison to other hospitalized patients. Implantable medical apparatus, such as urinary catheters, central venous and arterial catheters and endotracheal tubes, which breach normal skin and mucosal barriers, facilitate the colonization by the infectious agents [12]. Data from the US CDC National Nosocomial Infection Surveillance (NNIS) system shows from 500.000 patients analyzed, 97% of HAI were associated with urinary catheters and 87% of primary bloodstream infections with central venous lines [15].

Furthermore, immunocompromised patients are also at risk for contracting HAIs. Patients with leukemia (e.g. acute myelogenous leukemia - AML) or undergoing cancer chemotherapy, for instance, frequently run the risk of developing infections due to low white blood cells counts and the suppression of their immune system [16,17]. In most cases, *Aspergillus* species (90%) and *Candida* species (91%) are the most common infectious agents that colonize immunocompromised patients and cause serious complications, from pulmonary fibrosis to bloodstream infections [18]. Patients

---

undergoing chemotherapy treatment are particularly at risk for contracting infections by encapsulated microorganisms, such as *Streptococcus pneumoniae* or *Cryptococcus neoformans* [19] and to acquire catheter-related complications due to long-term usage [20]. In addition, seropositive patients for the human immunodeficiency virus (HIV), patients under corticosteroids administration, neonates and aged people are also at risk for contracting infections and die due to complications caused by opportunistic HAIs [21–27].

## 1.2. Community-acquired infections (CAI)

Unfortunately, the risk of contracting infections is no longer restricted to the hospital environment. Microorganisms are able to colonize several parts of the human body, such as the respiratory tract and mucosal, the gastrointestinal tract and skin [28]. In normal conditions, many of these microorganisms are harmless and may protect against the invasion of pathogenic organisms. [29]. It is known that nearly 20% of individuals carry at least one type of strain (persistent carriers) without any symptoms of the disease. However, under some circumstances, pathogens are able to enter the host through injuries or breaks in the host defenses (e.g. skin wounds) and cause infections [28]. Most of the time, these infections are restricted to skin, soft tissues, BSI, and pneumonia. The infectious agents are more susceptible to antibiotics therapy and are generally not lethal in comparison to HAI [30–32]. These infections fall into a particular characteristic, designated as Community-acquired infections (CAI).

The US CDC surveillance considers as CAI all the infections that are not nosocomial [1]. In 2002, Friedman *et al.* [33] and Siegman-Igra *et al.* [34] proposed a different definition, in which CAI consists of an infection existing at the time of hospital admission or diagnosed within 48 h of hospitalization, thereby fulfilling one of four criteria. Firstly, patients who received intravenous therapy at home, nursing care by a health care agent, or self-administration of intravenous therapy within 30 days before the infection. Secondly, those who attended hemodialysis or received intravenous chemotherapies in the 30 days before the hospitalization. Thirdly, patients hospitalized in the ICU for 2 days or more within three months. Finally, patients who live in a nursing home or a long-term care facility.

Furthermore, another CAI definition includes all the infections detected within 48 hours after the patient's admission to the hospital or 48 hours after discharge,

without any surgical intervention [35]. The last criteria used to define CAI relates to an important isolate characteristic: antimicrobial susceptibility profiles. The correct classification of CA and HA infection cases are crucial for choosing the suitable antimicrobial intervention. However, classification of HAI and CAI according to antimicrobial susceptibility has become challenging due to the occurrence of resistant bacteria also in the community. Surveys regarding CA bacteria resistance are reported, especially for fluoroquinolones and the emergence of extended-spectrum beta-lactamase (ESBL)-producing *E. coli* strains [36] and Methicillin-Resistant *Staphylococcus aureus* [37,38]. The epidemiological complexity of CA strains in health care sites and exchange of HA strains among the community has demonstrated that a delimitation between CA and HA became difficult [39].

### **1.3. *Staphylococcus aureus* and Methicillin-Resistance *Staphylococcus aureus* (MRSA)**

In the end of the 19th century, the Scottish surgeon Alexander Ogston (1844-1929) discovered the major cause for pus in abscesses. Observing a stained smear on the microscope, Ogston detected the presence of micrococci (“kokos” means berry, in Greek), rounded organisms found in a great number organized into clusters. In 1882, he named these micrococci clusters “staphylococci” (from the Greek, “staphyle” means grape-like) [40]. Two years later, the German surgeon Anton J. Rosenbach (1842-1923) isolated two *Staphylococcus* strains and named them according to their pigment: *Staphylococcus albus* (renamed to *Staphylococcus epidermidis*) presenting white pigmentation and *Staphylococcus aureus* showing a gold coloration [41].

*S. aureus*, a Gram-positive cocci cluster belonging to the Staphylococcaceae family, is a facultative anaerobic bacterium, non-motile cocci with 1 µm in diameter. It is possible to be distinguished from other staphylococcal species mainly by demonstrating positive results to catalase, in which the bacteria is able to convert hydrogen peroxide into water and oxygen [42]. *S. aureus* is also a common human commensal bacterium. Around 30% of the human population are *S. aureus* asymptomatic carriers [43]. However, amongst 200 *Staphylococcus* species reported, *S. aureus* is the most virulent species. *S. aureus* produces several virulence factors which

---

contribute to the cell wall attachment, cell–cell interactions, immune evasion as well as tissue damage during host colonization [44,45].

In the year 1928, Sir Alexander Fleming changed the history of medicine and propelled the world into a new era of therapeutic drugs, the “antibiotic era”. Fleming noticed that *Staphylococcus* colony plates contaminated with a mold (*Penicillium notatum*) inhibited the bacterial growth [46]. Later on, the active compound, named penicillin, had its  $\beta$ -lactam structure determined using X-ray crystallography by Dorothy C. Hodgkin and co-workers [47]. Despite the discovery of penicillin in the early years of the 20<sup>th</sup> century, clinical trials of penicillin were carried out only in the 1940s. Penicillin, the first antimicrobial, was widely used for *S. aureus* treatment. However, in early 1942, strains of *S. aureus* resistant to the  $\beta$ -lactam ring of penicillin were detected in hospitals [48,49]. By the beginning of the 1960s, 80% of *S. aureus* isolated both in the community- and hospital-acquired infections worldwide were resistant to penicillin. The acquisition of a plasmid encoding for a penicillin-hydrolyzing enzyme (penicillinase) was the resistance molecular determinant. Penicillinase has the ability to cleave the beta-lactam ring and inactivate the antimicrobial molecule, defining the first wave of resistance within the antibiotic era [50].

In order to overcome pandemic infections caused by the penicillin-resistant *S. aureus*, methicillin, a semi-synthetic derivative of penicillin with the beta-lactam ring resistant to  $\beta$ -lactamase cleavage was introduced in the early 1960s. *S. aureus* penicillin-resistant infections soon decreased following the methicillin introduction [51]. However, within one year the first case of *S. aureus* resistant to the designed methicillin was identified in a patient in Colindale, United Kingdom [52]. Investigations revealed that the resistance against methicillin was due to the production of an additional 78-kDa penicillin-binding protein, known as PBP2a (or PBP2’), which has a remarkably low affinity for all semi-synthetic penicillin derivatives (e.g., methicillin, nafcillin and oxacillin) present in the *mecA* gene [53]. The *mecA* gene is positioned within the *mec* operon along with two regulatory genes *mecI* (encoding the repressor protein MecI) and *mecR1* (encoding the signal transducer protein MecR1). The genetic element encoding the methicillin resistance carrying the site-specific recombinases (cassette chromosome recombinases – *ccr*) was identified and assigned as staphylococcal SCC*mec* [54]. It was speculated the methicillin resistance molecular



mechanism was highly transmissible among staphylococcal species, since the *mecA* gene was found to be widely distributed in *S. aureus*, as well as in coagulase-negative staphylococci, especially in the *S. epidermidis* group [55,56]. In fact, the SCC*mec* element belongs to a particular type of mobile genetic element. The *ccr* gene complex comprises one or two site-specific recombinases genes (invertase-resolvase family), which catalyze the excision of SCC*mec*, as well as its integration (site- and orientation-specific) into the chromosome cassette [54]. In addition to the *ccr* and *mec* gene complex, the SCC*mec* element also includes three joining regions (J1-J3) located between the *ccr* and *mec* complexes as well as adjacent to *orfX* [53]. Previously called “Junkyard”, the J regions have significant importance, since they may be targets for plasmids or transposons carrying supplementary antimicrobial as well as heavy metal resistances [50].

Although the nucleotide sequence of the *ccr* genes demonstrated to be highly diverse among several *Staphylococcus* species, the *mecA* genes seem to be extremely similar. *Staphylococcus sciuri*, *S. fleurettii* and *S. vitulinus*, for instance, share 85, 86 and 94% nucleotide identities regarding the *mecA* gene homologs, respectively [57]. Found among all species, the *mecA* gene homolog of *S. sciuri* was considered being the evolutionary precursor of the *mecA* gene. Further surveys regarding the *mecA* gene, in fact, pointed out that another *Staphylococcus* species, *S. fleurettii*, was likely to have developed the *mecA* gene due to an environment selective pressure caused by the beta-lactam antimicrobial. The origin/reservoir of SCC*mec* is still unknown and there are speculations point to another methicillin-susceptible commensal animal *Staphylococcus* species that lived at the same time with *S. fleurettii* and was likely involved in the SCC*mec* formation. *S. fleurettii*, as well as *S. aureus*, are commensal bacteria found in humans and animals [58–61]. Evidence suggests that methicillin-susceptible *S. aureus* (MSSA) may be acquired by horizontal transference of the SCC*mec* elements [62], therefore emerging in a new strain resistant to all beta-lactam antibiotics and leading to outbreak infections.

Until the late 1980s, MRSA was considered to be life-threatening only in the health-care associated infections. However, in 1993, the first case of community-acquired MRSA was identified and reported for an isolated part of Australia without any closely health-care facility [63]. Similar cases of MRSA among communities were reported in the USA for patients who had never been hospitalized and had no history or

---

risk factors for MRSA infections [64], constituting the latest wave of antimicrobial resistance.

MRSA is a versatile and highly adaptive species, thus it is able to infect any body system and cause a wide spectrum of infections. In a survey performed by Filice and co-workers [65], *S. aureus* was isolated more than 2.000 times during the study period. Overall, 73% of the patients suffered from pneumonia, bacteremia or urinary tract infections incited by MRSA and 23.6% patients died within six months due to MRSA infections. In the period comprising 2009-2010, the US CDC National Healthcare Safety Network (NHSN) reported that the most frequently HAI-related to MRSA was a central line-associated bloodstream infection – CLABSIs (54.6%), catheter-associated urinary tract infections (58.7%), ventilator-associated pneumonia (48.4%) and surgical site infections - SSI (43.7%) [66]. Furthermore, MRSA is also associated with skin infections such as abscesses, follicular carbuncle [67–69], cellulitis with black necrotizing tissue [70] and orbital cellulitis [71]. MRSA can cause ear, nose and throat infections leading to otitis media, otitis externa, sinusitis, and mastoiditis [72–76]. Severe life-threatening infections, such as bacteremia, endocarditis, and septicemia [77–79] frequently require a combined antimicrobial treatment intervention.

#### **1.4. Current and newer therapy treatments for MRSA infections**

The MRSA infections treatment comprises a multistep process. Firstly, removal of the contaminated tissue, as well as infected medical devices is necessary. Secondly, a laboratory test to determine its antibiogram (antibiotic susceptibility) is essential, since the result gives the directives of the type of therapy needed to proceed. Posteriorly, antibiotic therapy should be implemented [80].

The first antimicrobial choice for staphylococcal infections remains the  $\beta$ -lactams due their established efficiency. Vancomycin, although being inferior to  $\beta$ -lactam drugs, is the major therapeutic choice to treat MRSA. Vancomycin, belonging to the glycopeptide class, is administrated intravenously intermittently or continuous. The antimicrobial activity depends on the ability of vancomycin to bind and inactivate cell wall synthesis precursors, localized at the division septum in *S. aureus* [81]. Vancomycin is also recommended to treat less severe bacteremia and endocarditis when combined with semisynthetic penicillin. Therapy with this antimicrobial, however,

should be monitored, once nephrotoxicity has been demonstrated [80,82]. Due its slow bactericidal activity, selective pressure had stimulated the emerging of *S. aureus*, as well as MRSA resistant to vancomycin. Vancomycin-intermediate *S. aureus* (VISA) and vancomycin-resistant *S. aureus* (VRSA) due to the acquisition of *vanA* gene have become reality [83]. VRSA is particularly concerning due to the high probability of interspecies exchange of genetic resistant genes. VRSA contains both *vanA* and *mecA* resistance determinants of vancomycin-resistant Enterococcus (VRE) and MRSA [83,84], resulting in a multiple drug resistance and narrowing the choices of antimicrobial therapies for MRSA infection treatments. In addition, point mutations in the regulatory genes, leading to the thickening of the cell wall, avoid the diffusion of vancomycin into the division septum providing a protective barrier for the bacteria [85].

Linezolid, the first available oxazolidinone antimicrobial, binds to the V domain of the 23S ribosomal RNA (rRNA) of the 50S subunit and inhibits the protein synthesis [86]. Linezolid, a bacteriostatic synthetic drug used for salvage therapy, showed good results against MRSA. With excellent bioavailability, no hepatic or renal damage and good drug penetration into the lungs, linezolid demonstrated to be a good alternative for vancomycin therapy, especially for ventilator-associated HAIs and HA-pneumonia [87–89]. However, severe side effects have been reported for linezolid therapy, such as thrombocytopenia and myelosuppression, as well as cases of bacterial resistance [90–92]. The resistance mechanism involves the mutations on the domain V regions of 23S rRNA genes, as well as to the 50S ribosomal proteins L3 and L4 encoding genes [93–95], indicating that the resistance is generated spontaneously due to antibiotic selective pressure rather than genetic exchange [96–98]. Other agents for salvage therapy include Quinuspristin-dalfopristin (limited use due to myalgia and arthralgia adverse events) [99], trimethoprim-sulfamethoxazole for bacteremia and endocarditis infection as an alternative for vancomycin [100] and tigercycline, first licensed as a drug from glycylicycline class recommended as 2<sup>nd</sup> and 3<sup>rd</sup> –line for MRSA infections [101].

Another example of antimicrobials in clinical use is daptomycin, a cyclic lipopeptide derivative from *Streptomyces roseosporus* fermentation. Therapy with daptomycin is usually well tolerated and demonstrated good results for BSI, endocarditis, as well as skin and soft skin tissue infection. In addition, daptomycin is also recommended for bacteremia and endocarditis in the case of resistance levels to vancomycin or renal failure [80]. Although a good penetration into the lungs was

observed, administration of daptomycin for pneumonia treatment is not recommended due to its inactivation by the pulmonary surfactants [102]. However, bacteria resistance is reported for bacteria grown under sublethal concentrations for daptomycin [103–105]. The antimicrobial pressure resulted in the accumulation of single point mutations leading to a reduction of *S. aureus* susceptibility to daptomycin therapy.

The lipoglycopeptide dalbavancin is also used in MRSA infection treatments and clinical trials experienced 87% of successes during treatments, especially for catheter-related BSI [78,106]. This lipoglycopeptide forms a stable dimer and binds to the D-Ala-D-Ala peptide of the bacterial membrane portion, thus avoiding the cross-linking formation of peptidoglycan [106–108].

Approved by the United States Food and Drug Administration – FDA in June 2013, telavancin is an effective therapy for limited use when no other option is available involving skin and skin structure infections [106,109,110]. Ceftaroline fosamil is the first FDA approved broad-spectrum cephalosporin and is, in general, a well-tolerated therapy with high affinity to PBP2a of MRSA. However, therapy with ceftaroline may induce hypersensitivity, including anaphylaxis. Further studies regarding the safety of this drug are currently in progress [111].

Recently, the RX-P873, a novel protein synthesis inhibitor provided by Melinta Therapeutics (New Haven, CT), from the ESKAPE Pathogen Program, showed excellent activity results against *S. aureus*, as well as for *Pseudomonas aeruginosa* infections. The authors demonstrated that this new drug was more potent and has a rapid bactericidal activity in comparison to other established therapeutic treatments, such as vancomycin and daptomycin. This result indicates that RX-P873 may constitute a suitable substitute for intracellular bacterial infections, especially for Gram-negative bacteria strains [112]. Many other antimicrobials are under development and Table 1 summarizes the latest antibiotics under development, as well as the main target on the bacteria.

Despite the pharmaceutical companies' efforts in attempting to solve the microbial resistance, the antibiotic production pipeline has begun to decrease. According to the US CDC, the number of novel antibiotics accepted by the FDA has decreased over the past three decades.

**Table 1:** Summary of new drugs under development to treat MRSA infections. Based on Kumar & Chopra, 2013 [113].

Main bacterial structure target	Antimicrobial	Clinical Studies	Reference
Cell membrane/ Cell Wall inhibitors	MX-2401	Pre-clinical tests	[114]
	Tripkopeptin C (TPPC)		[115]
	Oritavancin	Phase III	[116]
	Teicoplanin	Approved in EU, except in the US	[117–119]
	TD1792	Phase II	[120–122]
	Brilacidin (PMX-30063)	Phase II	[123,124]
	XF-73		[125]
	Sanguinarine		[126]
Protein synthesis inhibitor	Oxazolidinones		[127,128]
	Torezolid (TR701)		[129–131]
	Omacycline (PTK-0796)	Phase II	[132]
	Eravacycline (TP-434)	Phase II complete	[133]
	Plazomicin (ACHN-490)	Phase II	[134]
	GSK1322322	Pre-clinical tests complete	[135,136]
DNA synthesis inhibitors	Moxifloxacin	FDA approved	[137]
	Delafloxacin (RX3341)	Phase II	[138]
	Finaxifloxacin (BAY35-3377)	Pre-clinical tests	[139]
	Nadifloxacin (WCK771)		[140,141]
	JNJ-Q2	Phase II	[142,143]
	ACH-702		[144,145]
	Iclaprim	Phase III	[146,147]
Fatty acid synthesis inhibitors	Tricosan and Isoniazid		[148,149]
	AFN-1252		[150,151]
	Fab-001 (MUT056399)	Phase II	[152]
	CG400549		[153,154]

In 2014, for instance, only four antimicrobial drugs were approved by this regulatory agency [155,156]. In addition, the Infectious Diseases Society of America

(IDSA) reported that in 2013 only a few antimicrobial drugs were in phase 2 or 3 of development [157–159]. As also discussed by Silver [160], the antimicrobial pipeline has not stagnated. Most of the newly discovered drugs were submitted to improvements and continue to use similar strategies of drugs that are already in clinical use [161]. The significant reduction of new drugs developed has led to a drug discovery void, which can be attributed to several key reasons. As difficulties in the discovery of drugs with novel mechanisms of action combined with low financial returns to the pharmaceutical industries [162,163]. The discovery of novel drugs, as well as novel strategies to slow down the resistance, is undoubtedly an important and challenging mission for the Research and Development (R&D) sector in a post-antibiotic era.

## **2. Vitamin K: a historical overview**

### **2.1. Discovery and characterization of an antihemorrhagic factor - vitamin K**

Studies performed by Carl Peter Henrik Dam (1895–1976) at the Biochemistry Institute at the University of Copenhagen led to the discovery of a coagulation vitamin. While the cholesterol biosynthesis pathway in chicks was investigated in 1929, the research observed an unexpected disease. Chicks treated with cholesterol- or any other fat-free diet for longer than 2-3 weeks demonstrated subcutaneous, gut, muscular and some organ hemorrhages [164]. Later, MacFarlane and co-workers in Canada and Holst and Halbrook at the University of California reported the same hemorrhagic disease in chicks [165,166]. Blood tests performed by Schönheyder showed those chicks had normal levels of calcium and fibrinogen and that neither an increase in thrombokinase nor a decrease of antithrombin were detected in the plasma. In addition, there were no morphological or pH changes in the blood cells or in the plasma. The only change observed in the plasma of sick animals was lower levels of prothrombin and the clotting time (several hours for a sick animal in comparison to 1-5 min for a normal chick).

They speculated that hemorrhagic disease, frequently referred to as scurvy-like, was due to the lack of hydrosoluble lipids, such as vitamin A, D and E and especially ascorbic acid - vitamin C. In 1935, experiments conducted by Dam and co-workers with supplemented or depleted diets of fat-soluble vitamins resulted in no differences in the decrease of hemorrhage. Neither the administration of vitamin A and D in the form of

concentrates or oils in sick chicks nor large doses of vitamin C were effective to prevent the disease [167,168]. However, by feeding sick animals with green leaves (e.g. alfalfa) and certain animal meat (e.g. hog liver), this situation could be reversed. By excluding the possibility of vitamins A, C, D and E as being responsible for the elimination of the disease, Dam, therefore, postulated that the presence of a new fat-soluble vitamin in green leaves and in hog liver would be responsible for the coagulation, naming it vitamin “K” (“K” for “Koagulation”, in German and Scandinavian languages).

After the discovery that a fat-soluble vitamin was responsible for preventing coagulation disorders, the efforts moved towards the isolation and characterization of vitamin K. It was known that green leafy vegetables such as alfalfa and kale, tomatoes, hog liver fat, putrefied fishmeal and many bowls of cereal were a source of this vitamin. Herman James Almquist, from the University of California College of agriculture described, in 1936, the process in which the vitamin K could be purified from alfalfa leaves. In addition, Almquist could also purify vitamin K from dry alfalfa meal by distillation, which also results in a yellowish oil containing great amounts of vitamin K [169]. Later, in 1939, Binkly and co-workers [170,171] were successful in isolating vitamin K<sub>1</sub> from alfalfa in a high purity and elucidating its structure, as well as vitamin K<sub>2</sub> from putrefaction fish meal [172].

## **2.2. Vitamin K<sub>3</sub> – Menadione and Vitamin K<sub>1</sub> – Phylloquinone (PhQ)**

The parent structure of all vitamin Ks possess a common structure of a 2-methyl-1,4-naphthoquinone aromatic ring, however, the structures diverge from each other in the composition of the side chain at the 3-site. The molecular structure of vitamin K<sub>3</sub> or menadione (Figure 3 A) only has a 2-methyl-1,4-naphthoquinone ring, has no side chain and does not occur in nature, but it can be synthesized artificially and alkylated to menaquinone (vitamin K<sub>2</sub>) in the human gut [173].

In vitamin K<sub>1</sub> (or phylloquinone) (Figure 3 C) the side chain is composed of four isoprenoid residues with three saturated phytyl subunits and this form is synthesized in cyanobacteria and green leafy vegetables, such as kale and broccoli [174]. The phylloquinone is located in the chloroplasts and participates in the electron transfer cofactor of photosystem I - PSI [167].

---

The first studies concerning the biosynthesis of phylloquinone were performed for the cyanobacteria *Synechocystis* sp. Homolog enzymes which encode for the menaquinone pathway (Men) were identified in *Synechocystis* comparing the genome of *E. coli*. In addition, knockouts in five of these genes blocked the PhQ synthesis, confirming the presence of the Men pathway as the route of PhQ biosynthesis in cyanobacteria [175].

### **2.3. Vitamin K<sub>2</sub> – Menaquinone (MQ) and its role in the electron transport chain**

Menaquinone (MQ) is considered the most ancient isoprenoid lipoquinone. MQ is one of the most widespread microbial respiratory quinones found in many groups such as Archaea, green sulfur bacteria, green filamentous bacteria, flavobacteria, as well as in  $\gamma$ - $\delta$ - $\epsilon$ -proteobacteria [176,177]. MQ has a low midpoint redox potential [Eo' (MQ/MQH<sub>2</sub>)  $\sim$ -80 mV] and its appearance can be connected to the early stages of evolution, before the existence of oxygenic photosynthetic organisms [178]. Another type of lipoquinone, the ubiquinone (UQ), is only found in  $\alpha$ - and  $\beta$ -prokaryotes [179], as well as in human mitochondria and in other bilayer membrane organelles (e.g. endoplasmic reticulum and Golgi vesicles). The most common UQ in humans is Q<sub>10</sub> (the 10 refers to the number of isoprene units). In other species, the number of isoprene units may vary, for instance, Q<sub>9</sub> in mouse, Q<sub>1-8</sub> in *E. coli* and Q<sub>6</sub> in *Saccharomyces cerevisiae* [180].

The size of the isoprenoid side chain is variable among species (Table 2), however, the most common MQ is composed of 5-13 prenyl units. [180,181]. The side chain of the MQ is frequently completely unsaturated, but some organisms present the side chain moderately or fully saturated [179]. In addition, the length and saturation bonds of the isoprene chain frequently depend on the growth temperature and affects the redox potential of the lipoquinone [182], allowing bacteria to modify the isoprene length and saturation according to environmental changes and their respiratory requirements. In some cases, diverse groups of lipoquinones occur in different taxonomic groups of species, therefore the amount of isoprene in the side chain is an important characteristic for species taxonomy [179].



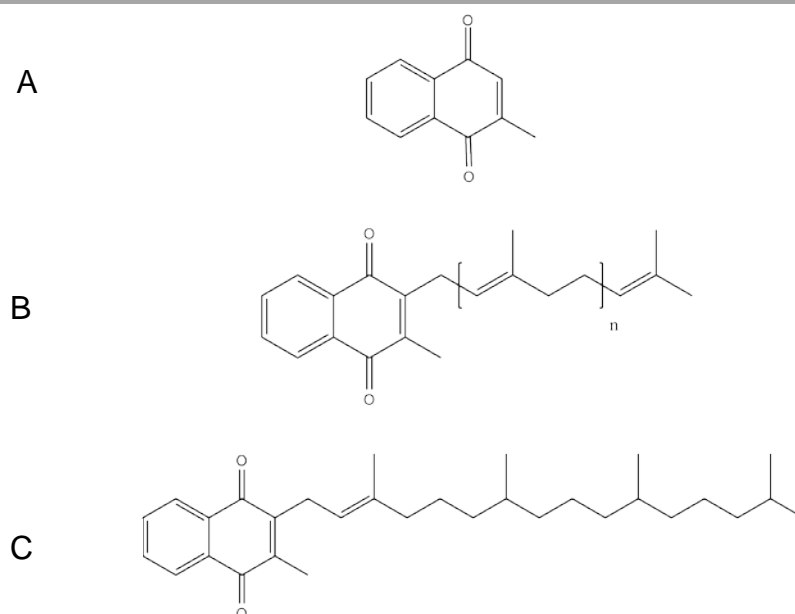


**Figure 3:** Chemical structures of A: menadione (K<sub>3</sub>), B: menaquinone (K<sub>2</sub>) and C: phyloquinone (K<sub>1</sub>), respectively. The figure was created using the ChemDraw program (PerkinElmer Inc.).

Found almost entirely in the bacterial membrane (about 85-90%), MQ is an important constituent in the respiratory and photosynthetic electron transport chain, as an electron carrier in the cytoplasmic membrane of prokaryotes. In addition, MQ plays an important role during oxidative phosphorylation, active transport and endospore formation in some species of Gram-positive bacteria [183,184].

The respiration of prokaryotic cells occurs in the cell membrane. Throughout aerobic growth, electrons go into the electron transport chain by the NADH dehydrogenase I [185], transfer two electrons to MQ and, consequently, to cytochrome c, producing a reduced form of cytochrome C. Cytochrome C oxidase transfers the electrons to an oxygen atom, the terminal electron acceptor. At the end of this process, a water molecule, as well as a pH and an electrochemical gradient are formed across the membrane. The protons return to the bacterial cytoplasm through the F<sub>0</sub> subunit of the F<sub>0</sub>F<sub>1</sub> ATP synthase and the F<sub>1</sub> subunit associates two pyrophosphates (PPi) with adenosine monophosphate (AMP) generating ATP [186]. Consequently, lipoquinones, acting as electron carriers, have an important function in electron transport, assisting the ATP generation [187]. Many bacteria during the respiratory process have flexibility regarding the terminal electron acceptor. Some bacteria take advantage of other compounds such as nitrite, nitrate (reduced to nitrite by nitrate reductase), sulfate, sulphite, thiosulfate, sulfur, Fe(III) metal oxyanions, fumarate (reduced to succinate by

fumarate reductase during anaerobic growth) and others [181,188,189]. In addition to the electron transport chain, MQ is also related to other functions such as cell wall membrane protection against lipid oxidation promoted by reactive oxygen species (ROS), as well as the transport of molecules across the cell membrane [178,190].

**Table 2:** Lipoquinone found in some species. The underlined represent the most dominant quinone isolated in different species.

Species	Lipoquinone	Reference
<i>S. aureus</i>	<u>MQ</u> <sub>7</sub> , <u>MQ</u> <sub>8</sub> , MQ <sub>6</sub> , MQ <sub>5</sub> , MQ <sub>4</sub>	[191]
<i>Bacillus subtilis</i>	<u>MQ</u> <sub>-7</sub>	[192]
<i>Mycobacterium tuberculosis</i>	MQ <sub>9</sub> (H <sub>2</sub> ), MQ <sub>9</sub> ,	[193]
<i>E. coli</i>	<u>Q</u> <sub>8</sub> , Q <sub>7</sub> , Q <sub>6</sub> , Q <sub>5</sub> , Q <sub>4</sub> , Q <sub>3</sub> , Q <sub>2</sub> , Q <sub>1</sub> , <u>MQ</u> <sub>8</sub> , MQ <sub>9</sub> , MQ <sub>7</sub> , MQ <sub>6</sub>	[194]
<i>Streptomyces</i> spp	<u>MQ</u> <sub>9</sub> (H <sub>6</sub> ), MQ <sub>9</sub> (H <sub>8</sub> ), MQ <sub>9</sub> (H <sub>4</sub> ), MQ <sub>9</sub> (H <sub>2</sub> ), MQ <sub>9</sub>	[195]

The majority of Gram-positive bacteria, including *S. aureus*, use only menaquinone in the electron transport chain during respiration [196]. Consequently, menaquinone biosynthesis is critical for maintenance of the energy production, and thus crucial for the Gram-positive bacteria survival [179,197,198].

## 2.4. Biosynthesis of menaquinone (MQ) in bacteria

Early experiments demonstrate the origin of all atoms of the MQ ring junction. Through radioactive isotopes molecules, it became clear that MQ is a compound was originated from the shikimate pathway with all shikimate carbons combined through chorismate into the naphthoquinone ring of MQ. The last carbons are provided by  $\alpha$ -ketoglutarate, the C-3 prenyl side chain originates from the mevalonate pathway and the methyl group in the position C-2 is provided by the cofactor S-Adenosylmethionine [199,200]. The MQ biosynthesis has been widely studied in *E. coli* and *B. subtilis* and

through an extensive mutagenesis investigations of genes associated to the biosynthetic pathway, eight genes, named *menA-H*, were identified to be crucial for MQ biosynthesis [201,202].

MQ biosynthesis (Figure 4) starts with chorismate, an intermediate compound of aromatic amino acids, indole derivatives, salicylic acid and alkaloids, resultant from the shikimate pathway. Chorismate is isomerized by MenF (isochorismate synthase), the first enzymatic step from the MQ biosynthetic pathway [203]. MenD (2-succinyl-6-hydroxy-2,4-cyclohexadiene-1-carboxylic acid synthase), a thiamine diphosphate-dependent enzyme, catalyzes the conjugation addition (Stetter-like) of isochorismate with  $\alpha$ -ketoglutarate to form the intermediate 2-succinyl-5-enolpyruvyl-6-hydroxy-3-cyclohexadiene-1-carboxylate [204]. The removal of pyruvate and the formation of carbon dioxide is performed by MenH (*E. coli*) (2-succinyl-6-hydroxy-2,4-cyclohexadiene-1-carboxylate synthase) yielding the 2-succinyl-6-hydroxy-2,4-cyclohexadiene-1-carboxylate (SHCHC) formation [205]. SHCHC is dehydrated by MenC (O-succinylbenzoate synthase) to form a stable intermediate O-succinylbenzoate (OSB) [206]. MenE (O-succinylbenzoate synthetase) converts OSB to a thioester OBS-CoA [207]. The cyclization of the naphthalene aromatic ring (Dieckmann-type) of OBS-CoA is performed by MenB (1,4-dihydroxy-2-naphthoyl-CoA synthase) producing 1,4-dihydroxy-2-naphthoyl-CoA (DHNA-CoA) [208] and the hydrolysis of the thioester bond with formation of water is executed by DHNA-CoA thioesterase [209]. DHNA is prenylated by MenA (DHNA-octaprenyltransferase) producing demethylmenaquinone (DMQ) [196] and DMQ is methylated by MenG/UbiE/MenH (*S. aureus*) (demethylmenaquinone methyltransferase) using S-adenosylmethionine as a methyl donor to form menaquinone (vitamin K<sub>2</sub>) [210].

During genome databank screening analysis regarding MQ necessities for growth, Hiratsuka and co-workers [211] discovered that some organisms of the  $\epsilon$ -proteobacteria lacked the *men* gene orthologues, despite knowing that most of them synthesize MQ. Through further surveys including mutagenesis, radioisotope tagging and genetic engineering, the futasine pathway was identified (Figure 5).

Likewise as for the menaquinone pathway, the futasine pathway uses chorismate to initiate. The early steps of the futasine pathway begin with the condensation of chorismate, inosine and phosphoenolpyruvate by MqnA forming futasine. MqnB or futasine nucleosidase hydrolyze the hypoxanthine ring to form

---

dehypoxanthinylfutalosine (DHFL). Afterward, the MqnC is involved in the cyclization of DHFL and MqnD converts DHFL into 1,4-dihydroxy-6-naphthoate (DHNA). The subsequent enzymatic reactions are hypothesized to be similar to the classical menaquinone pathway [212,213].

## **2.5. Vitamin K<sub>2</sub> in humans and Menaquinone as a novel target for antimicrobial drug development**

Vitamin K<sub>2</sub> plays an important role as a cofactor for the blood coagulation cascade in humans, which depends exclusively on food intake to obtain vitamin K. Hydroquinone, a reduced form of vitamin K<sub>2</sub>, functions as a cofactor in the carboxylation by  $\gamma$ -glutamyl carboxylase producing  $\gamma$ -carboxyglutamic acid in plasma [167]. Calcium ions are also important since all vitamin K-dependent proteins bind to Ca<sup>2+</sup> and are essential for an increase in bone mass. Without vitamin K<sub>2</sub>, carboxylation does not occur and synthesized proteins do not undergo post-translational modifications leading to inactive clotting factors (e.g. II, VII, IX, and X) [214] and, consequently, bleeding disorders.

Vitamin K<sub>2</sub> in humans and in bacteria possess different functions within cells. In contrast to bacteria, the electron transport chain of humans requires only ubiquinone and the menaquinone biosynthesis pathway is absent. Due to its essential role in bacteria growth, virulence, and survival, menaquinone biosynthesis has received attention as a promising drug target. *In vitro* studies with MenA of *Mycobacterium tuberculosis* showed that the inhibition of this enzyme could not be recovered even when introducing high concentrations of exogenous vitamin K<sub>2</sub>. Menaquinone deficient bacteria, consequently may not accomplish required levels of electron transport chain products and do not survive in this environment [215].

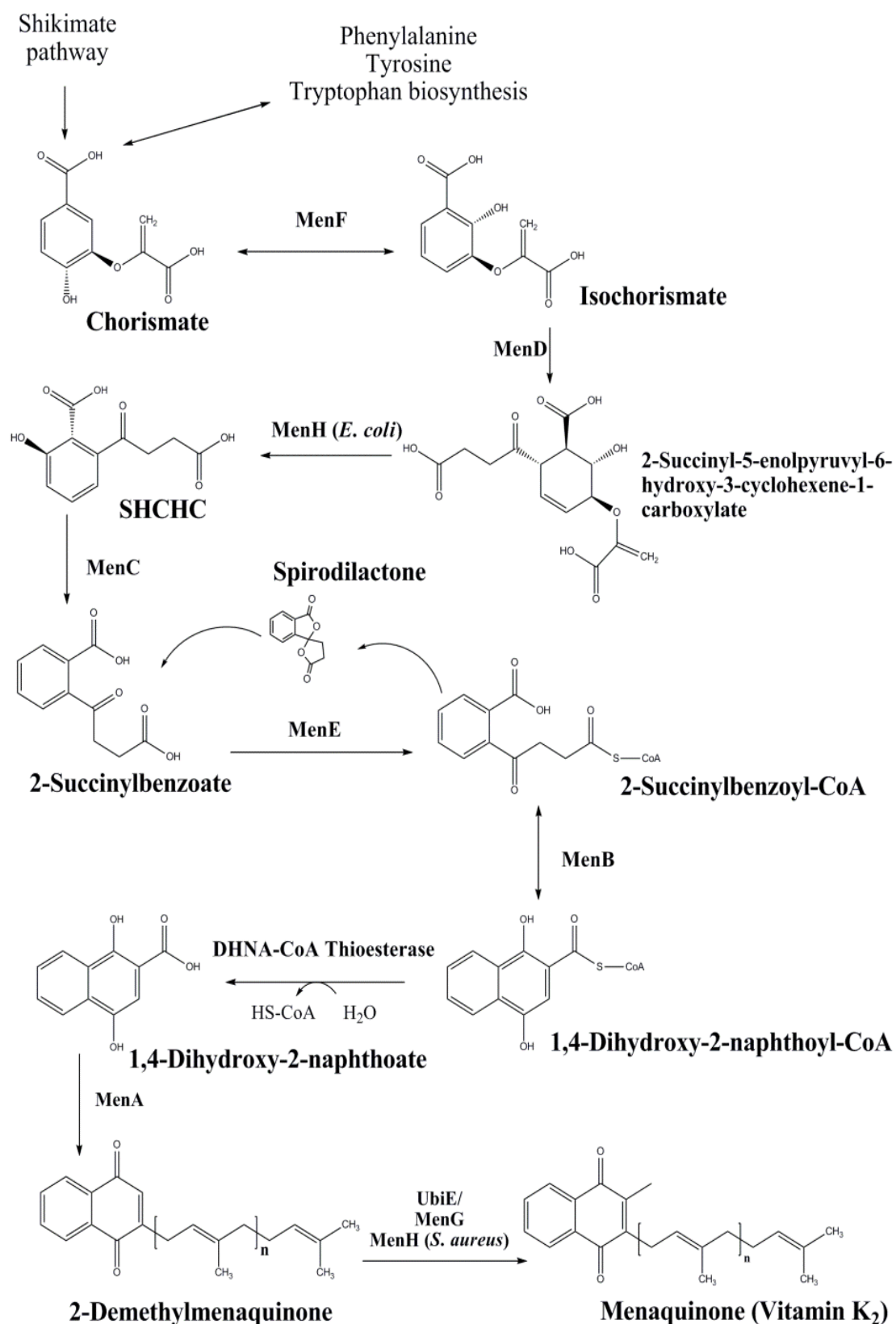


**Figure 4:** A classical overview of the menaquinone pathway. The figure was created by the ChemDraw program (PerkinElmer Inc.) based on the KEGG pathway [216].

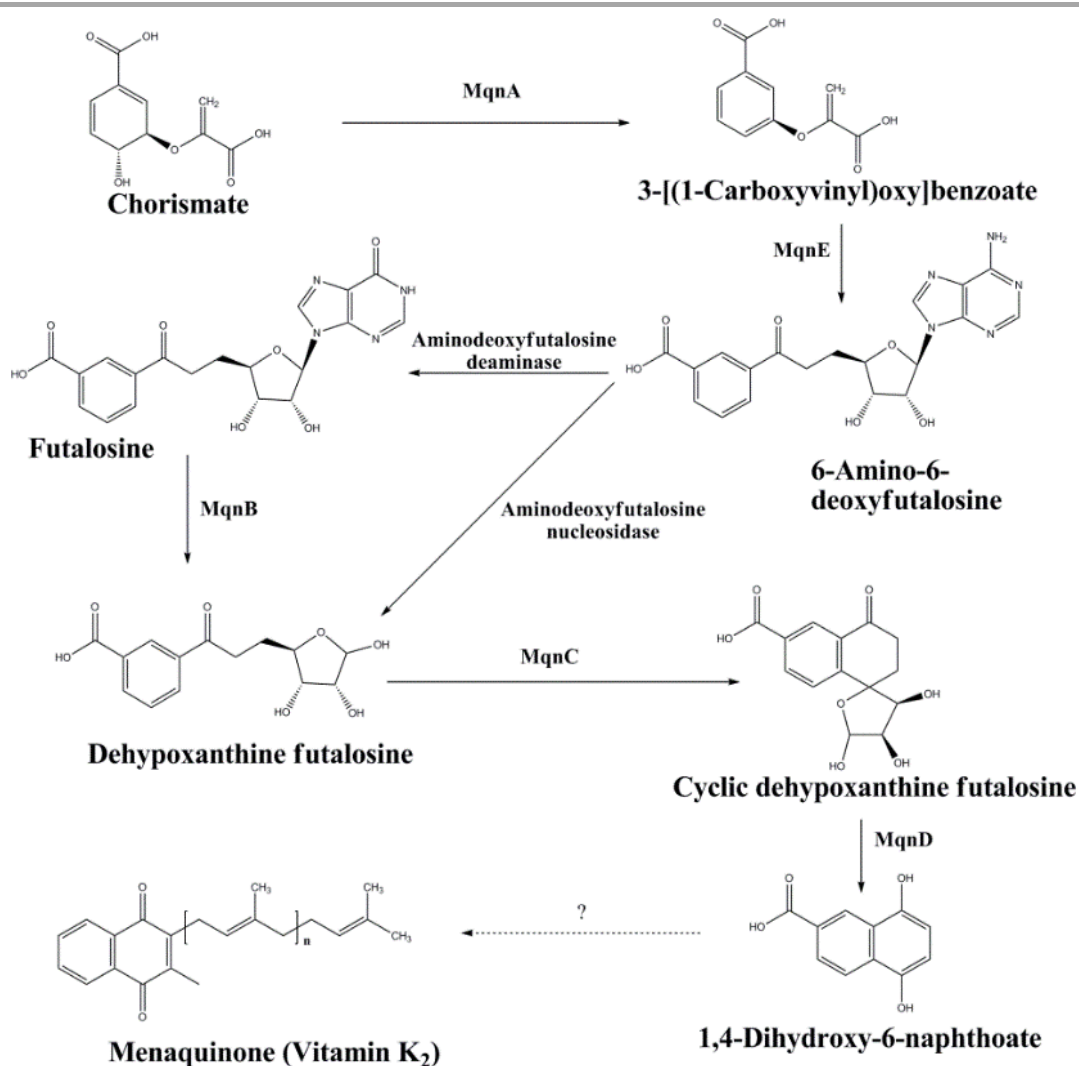


**Figure 5:** The alternative menaquinone production in bacteria, the futilosine pathway. The figure was created by the ChemDraw program (PerkinElmer Inc.) based on the KeGG pathway [216].

Intelligently designed drugs often require the knowledge of the protein structure. To date, crystal structures of Men enzymes have been reported for MenB [208], MenD [217], MenE [218], MenF [219], MenH [205], UbiE [220] and DHNA-CoA thioesterase [221,222]. Recently, Matarlo and collaborators [223] demonstrated the importance of the protein structure knowledge in drug design. Based on the crystal structure of *E. coli* MenE (OBS-CoA synthetase), several acyl-AMS (acyl-adenosyl mono phosphate) [5'-O-(N-acylsulfamoyl)adenosine] analogs were designed and tested regarding the ability to inhibit bacterial growth and OSB binding. The authors reported the OSB-AMS binds tightly in MenE of *S. aureus*, *M. tuberculosis* and *E. coli* in low concentrations and has a potent inhibition activity against MRSA. Furthermore, the effect of OSB-AMS on menaquinone levels of *S. aureus* was investigated. The treatment of MRSA with OSB-

AMS showed a direct interference upon menaquinone biosynthesis, indicated by decreasing levels of MQ<sub>7</sub>, MQ<sub>8</sub> and MQ<sub>9</sub>. A novel inhibitor for MenE with antimicrobial activity was discovered, demonstrating that the menaquinone pathway is a promising drug target for antibacterial drug development to treat MRSA infections.

---

### 3. Aim of this work

*Staphylococcus aureus* is one of the most common causative agents hospital infections. In Europe, more than 4.5 million episodes of hospital-acquired infections are observed and 175.000 patients die per year. Selective drug pressure has led to the emergence of Methicillin Resistant *S. aureus* (MRSA). MRSA resistance is observed practically for all developed antibiotic drugs and this highlights the necessity for the discovery of novel antimicrobials interfering with specific pathways of the bacterium.

One of these pathways is the vitamin K<sub>2</sub> biosynthesis in *S. aureus*, which is absent in humans and depends exclusively on food intake to cover its needs. Recently, inhibitors aimed at one of the menaquinone biosynthesis enzymes have been designed and demonstrated to be effective against bacterial growth. Targeting pathways absent in humans is important to avoid side-effects of the antimicrobial drug in the host, allowing it to specifically target the bacteria.

The menaquinone biosynthesis pathway is widely studied in *E. coli*, as well as in *M. tuberculosis*, but only a few surveys regarding protein structural information of the involved enzymes are available for *S. aureus*.

In this work, a structure-based investigation targeting the enzyme 4-hydroxybenzoyl coenzyme A thioesterase (DHNA-CoA thioesterase) of the vitamin K<sub>2</sub> metabolism of *S. aureus* is focused. The relationship of site-directed mutagenesis of selected residues in the biological function of the DHNA-CoA thioesterase was investigated as well. The evidence obtained from the protein architecture and the knowledge of the active site may be used for structure-based drug design. With the information of the active site arrangement, designed inhibitors should be addressed. Inhibition of the enzyme activity would interfere directly in the menaquinone biosynthesis pathway and consequently, disturb the bacterium growth.

Furthermore, the first characterizations of the isochorismate synthase (MenF) and demethylmenaquinone methyltransferase (UbiE/MenH) also involved in the menaquinone biosynthesis pathway should be addressed.



---

## 4. Material and Methods

### 4.1. Instrumentation and Chemicals

#### 4.1.1. Instrumentation

##### Beamlines

###### P14

EMBL (European Molecular Biology Laboratory, DESY, Hamburg, Germany)

Source: storage ring PETRAIII

Focal spot: 5 x 5  $\mu\text{m}^2$  up to 300 x 300  $\mu\text{m}^2$

Wavelength: 0.976262 / 0.976300 Å

Detector: Pilatus 6M

###### P13

EMBL (European Molecular Biology Laboratory, DESY, Hamburg, Germany)

Source: storage ring PETRAIII

Focal spot: 4 x 9  $\mu\text{m}^2$  up to 300 x 300  $\mu\text{m}^2$

Wavelength: 0.976262 / 0.976300 Å

Detector: Pilatus 6M

##### Rotating anode

University of Hamburg

Source: Rigaku RU 200 X-ray generator

Wavelength: Cu  $K\alpha$  = 1.5418 Å

Detector: MAR300 image plate

##### Agarose gel electrophoresis:

PerfectBlue<sup>TM</sup> Mini S (Peqlab, Germany)

##### Gel caster

PowerPac 200 (Bio-Rad, Germany)

##### Power supply

PerfectBlue<sup>TM</sup> Mini S (Peqlab, Germany)

##### Electrophoresis unit

##### CD spectrometer

J-815 (Jasco, UK)

##### UV transilluminator

Gel iX Imager (INTAS Science Imaging Instruments, Germany)

##### Balance

TE3102S (Sartorius, Germany)

##### DLS instrumentation

SpectroSize 300 (XtalConcepts, Germany)

<b>Centrifuges</b>	5415R/5804R/5810R (Eppendorf, Germany)	MinispinPlus
	Multifuge X3R (Thermo Fisher Scientific, Germany)	
<b>Crystal imaging</b>	Digital Sight DS-L3 (Nikon, Japan)	
	CrystalScore (Diversified Scientific Inc., US)	
	Microscope SZX12 (Olympus, Japan)	
<b>ELISA microplate reader</b>	TECAN GENios; XFLUOR4 Version: V 4.40 (MTX Lab Systems, Inc, USA)	
<b>FPLC machine</b>	ÄKTA Purifier P-901 (GE Healthcare, UK)	
<b>Incubator 37 °C</b>	Heraeus B6120 (Heraeus, Germany)	
<b>Crystal plate incubator</b>	RUMED 3001 incubator (Rubarth, Germany)	
<b>Microbalance</b>	CP224S-0CE (Sartorius, Germany)	
<b>Microscopes</b>	Stereo microscope SZX12 (Olympus, Japan)	
	Axiovert 25 (Zeiss, Germany)	
<b>Micropipette</b>	Micropipette Research (Eppendorf, Germany)	
<b>Multichannel pipette</b>	Multichannel pipette ResearchPlus (Eppendorf, Germany)	
<b>Microwave</b>	NN-e202W (Panasonic, Japan)	
<b>Roller mixer</b>	Stuart Roller Mixer SRT9 (Stuart, UK)	
<b>Pipetting robots</b>	Honeybee 961 (Genomic Solutions, US)	
	Oryx4 (Douglas Instruments Ltd, UK)	
<b>pH-meter</b>	SevenEasy (Mettler Toledo, US)	
<b>SDS-PAGE:</b>	Four Gel Caster (SE275)	
	EV 231 (Peqlab, Germany)	
	SE260 Mighty Small II Deluxe Mini electrophoresis unit (Hoefer, US)	

<b>Spectrophotometer</b>	GeneQuant 1300 (GE Healthcare, UK) Nanodrop 2000c and NanoDrop Lite (Thermo Fisher Scientific, Germany) UVICON 933 (BIO-TEK Kontron Instruments, US)
<b>Stirrer</b>	VMS-A (VWR, US) MR 3001 (Heidolph, Germany)
<b>Thermocycler</b>	MyCycler Thermal Cycler™ (Bio-Rad, US)
<b>Thermomixer</b>	Thermomixer comfort (Eppendorf, Germany)
<b>UV-light source</b>	CrystalLIGHT 100 (Nabitec, Germany)
<b>Western blot transfer unit</b>	V20-SDB Semi-Dry Blotter Unit (SCIE-PLAS Ltd., UK)

#### 4.1.2. Bacterial strains and plasmids

##### 4.1.2.1. Bacterial strains

<i>BLR (DE3)</i>	Novagen (Merck), US	F- ompT hsdSB(rB- mB-) gal dcm (DE3) Δ(srl-recA)306::Tn10 (TetR)
<i>BL21(DE3)</i>	Life Technologies, Germany	B F- ompT gal dcm lon hsdSB(rB-mB-) λ(DE3 [lacI lacUV5-T7p07 ind1 sam7 nin5]) [malB+]K-12(λS)
<i>DH5α</i>	Life Technologies,	F- Φ80lacZΔM15 Δ(lacZYA-argF) U169 recA1 endA1
XL10-Gold	Agilent Technologies, US	Tetrdelta- ( <i>mcrA</i> )183 delta- ( <i>mcrCB-hsdSMR-mrr</i> )173 <i>endA1 supE44 thi-1 recA1 gyrA96 relA1 lac Hte</i> [F' <i>proAB lacIqZDM15 Tn10</i> (Tetr) Amy Camr]

##### 4.1.2.2. Plasmid and plasmid primer sequence

**Plasmid:** pASK-IBA3plus (IBA, Germany)

**Genetic features:** c-term Strep-tag, *tet*-promoter, f1 origin, and ampicillin resistance

<b>Primer Name:</b>	<b>Sequence 5'-3'</b>
IBA fwd	GAGTTATTTTACCACTCCCT
IBA rev	CGCAGTAGCGGTAAACG

### 4.1.3. Primer

**Table 3:** Primer sequences used for cloning and site-directed mutagenesis in 5' → 3'. Mutation sites are in bold for mutagenesis primers.

<i>Sa</i> DHNA IBA3-S	5'-GCGCGCGGTCTCGAATGATATATAGTATTACAGAAATAG-3'
<i>Sa</i> DHNA IBA3-AS	5'-GCGCGCGGTCTCAGCGCTTAAAGAATCAATACCATCCATTATC-3'
<i>Sa</i> MenF IBA3-S	5'-GCGCGCGGTCTCGAATGGCTACGGGCGTATTAGAGGACG-3'
<i>Sa</i> MenF IBA3-AS	5'-GCGCGCGGTCTCAGCGCTTGATTTCCCATTCATATCGACTCC-3'
<i>Sa</i> MenH IBA3-S	5'-GCGCGCGGTCTCGAATGGCCGACAATAAAGCAAATAAAG-3'
<i>Sa</i> MenH IBA3-AS	5'-GCGCGCGGTCTCAGCGCTATCACCTTTGGTATTATCTTTTTTC-3'
DHNA-D16A-S	5'-GCGCGTTATGCTGAAACTGCTAAGATGGGTGTAATTTATC-3'
DHNA-D16A-AS	5'-GATAAATTACACCCATCTTAG <b>C</b> AGTTTCAGCATAACGCGC-3'
DHNA-E31N-S	5'-GCAACTTGGTTT <b>A</b> ACGTTGCGCGGTTGG-3'
DHNA-E31N-AS	5'-CCAACCGCGCAACG <b>T</b> TAAACCAAGTTGC-3'

### 4.1.4. Buffers, solutions and consumables

All buffers and solutions were produced in deionized H<sub>2</sub>O. If not specified, pH was adjusted with HCl or NaOH. Plastic consumables were obtained from Sarstedt or Eppendorf.

**Agarose-Gel electrophoresis:**

TAE-buffer (50x)	2 M Tris, 950 mM Acetic acid, 50 mM EDTA
Loading dye (5x)	0.05 % (w/v) bromophenol blue, 0.35 % (w/v) Xylene cyanol, 1 mM EDTA, 60 % (w/v) glycerol
DNA Marker	Medium Range DNA Ladder (5000-100 bp) (Thermo Fisher Scientific, Germany)
Ethidium bromide staining solution	0.5 $\mu\text{g}\cdot\text{mL}^{-1}$ in 1x TAE buffer #E1510 (Sigma, Germany)

**DNA purification**

GeneJET Plasmid Miniprep Kit	#K0502 (Thermo Fisher Scientific, Germany)
GeneJET Gel Extraction Kit	# K0701 (Thermo Fisher Scientific, Germany)

**Enzymes and buffers:**

dNTP's mix	#R0181 (Thermo Fisher Scientific, Germany) Preparation of 2 mM dATP, dCTP, dGTP, dTTP each
Q5 High Fidelity DNA polymerase	#M0491G (New England Biolabs, Germany)
T4 ligase and buffer	#EL0014 (Thermo Fisher Scientific, Germany)
<i>XbaI</i>	#ER0681 (Thermo Fisher Scientific, Germany)
<i>BsaI</i>	#R0535S (New England BioLabs, US)
<i>HindIII</i>	#ER0501 (Thermo Fisher Scientific, Germany)
<i>DpnI</i>	#ER1701 (Thermo Fisher Scientific, Germany)
Anhydrotetracyclin	2 $\text{mg}\cdot\text{mL}^{-1}$ in DMF (N,N-Di-methyl-formamide)

**Strep-tactin sepharose regeneration:**

Strep-tactin regeneration buffer (10x)	10 mM HABA (IBA, Germany) (2-[4'-hydroxy-benzeneazo]benzoic acid) in buffer W
--	--

Buffer W	100 mM Tris-HCl pH 8.0, 150 mM NaCl
Sodium phosphate buffer	0.094 M NaH <sub>2</sub> PO <sub>4</sub> + 0.006 M Na <sub>2</sub> HPO <sub>4</sub> . pH 6.0, 150 mM NaCl
Buffer W + ATP/MgCl <sub>2</sub>	1x buffer W, 5 mM ATP, 10 mM MgCl <sub>2</sub>

### Chromatography buffers

Size exclusion	Equilibration buffer: 100 mM Tris/HCl buffer pH 6, 200 mM NaCl.
Mono Q (anionic exchange)	Start buffer: 20 mM Tris-HCl, pH 8.0 Elution buffer: 20 mM Tris-HCl + 1.0 M NaCl, pH 8.0
Mono S (cationic exchange)	Start buffer: 20 mM 2-[N-morpholino] ethanesulphonic acid (MES), pH 6.0 Elution buffer: 20 mM MES + 1.0 M NaCl, pH 6.0

### SDS-PAGE:

Stacking gel buffer	0.5 M Tris-HCl, pH 6.8
Separating gel buffer	1.5 M Tris-HCl, pH 8.8
APS solution	10 % (w/v) Ammonium peroxydisulfate
TEMED (Tetramethylethylenediamine)	~99 % (Sigma Aldrich, Germany)
SDS solution	10 % (w/v) sodium dodecyl sulfate
SDS-PAGE electrode buffer	25 mM Tris, 0.192 mM glycine, 0.1 % (w/v) SDS
SDS-PAGE sample buffer (5×)	95 mM Tris-HCl pH 6.8, 40 % (v/v) Glycerol, 3 % (w/v) SDS, 0.17 % (w/v) Bromophenol blue, 0.5 % (w/v) DTT
SDS-PAGE Marker	Unstained Protein Molecular Weight Marker #26610, Size range 14.4-114 kDa (Thermo Fisher Scientific, Germany)
Coomassie staining solution	25 % (v/v) 2-Propanol, 10 % (v/v) Acetic acid, 0.25 % (w/v) Coomassie brilliant blue G-250
Coomassie destaining solution	20 % (v/v) Acetic acid

### Western blot

Transfer buffer	25 mM Tris, 192 mM Glycin, 20 % (v/v) Isopropanol, pH 8.3
Marker	PageRuler Plus Prestained Protein Ladder #26619, 10-250 kDa (Thermo Fisher Scientific, Germany)
Nitrocellulose membrane	Roti®-NC, 0.2 µm (Carl Roth, Germany)
Phosphate saline buffer (PBS) 20x	50 mM Potassium chloride, 2.7 M NaCl 50 mM KH <sub>2</sub> PO <sub>4</sub> , 160 mM K <sub>2</sub> HPO <sub>4</sub>
BCIP solution	20 mg·mL <sup>-1</sup> (w/v) BCIP (5-bromo-4-chloro-3'-indolyphosphate) in dimethylformamide (DMF)
NBT solution	50 mg·mL <sup>-1</sup> NBT (nitro-blue tetrazolium) in 70 % DMF
Reaction buffer	100 mM Tris/HCl, 4 mM MgCl <sub>2</sub> , pH 9.5
First antibody	Murine Anti-Strep-tag II antibody, IgG1; #2-1507-001, 0.2 mg mL <sup>-1</sup> in PBS (IBA, Germany) final dilution: 1:2000
Second antibody	Goat anti-mouse IgG-AP conjugated, #A3562 (Sigma, Germany) final dilution: 1:30000
<b>In-gel trypsin digestion</b>	
Digestion buffer	50 mM ammonium bicarbonate (AmBiCa), 10% Acetonitrile (ACN)/H <sub>2</sub> O
Digestion solution	10 ng·µL <sup>-1</sup> Trypsin solution in digestion buffer
Swelling solution	100 mM AmBiCa
Shrinking solution	50 mM AmBiCa, 60% ACN/H <sub>2</sub> O
Peptide extraction solution	65% ACN/H <sub>2</sub> O, 5% Formic acid
DTT solution	10 mM dithiothreitol in swelling solution
IAA solution	50 mM iodacetamide in swelling solution

**Crystallization screens and chemicals:**

---

PCT™ Pre-Crystallization Test	Hampton Research, US
Classics Suite	Qiagen, Germany
JCSG-plus	Molecular Dimensions, UK
Morpheus	Molecular Dimensions, UK
PACT premier	Molecular Dimensions, UK
Stura Footprint Screen & MacroSol	Molecular Dimensions, UK
JBScreen Classic HTS II	Jena Bioscience, DE
<b>Enzymatic assay chemicals</b>	
Stearoyl Coenzyme A	Sigma Aldrich (Germany)
Crotonyl Coenzyme A	Sigma Aldrich (Germany)
5,5'-Dithiobis(2-nitrobenzoic acid) - DTNB	Sigma Aldrich (Germany)

## 4.2. Molecular Biology and Biochemical Procedures

### 4.2.1. Polymerase chain reaction (PCR)

The polymerase chain reaction (PCR) technique was performed, aimed at the amplification of the DNA fragment of a gene of interest to clone into an expression vector. The reaction was carried out in a PCR machine using the *Pfu* DNA polymerase recombinant isolated from the thermophilic bacterium *Pyrococcus furiosus* [224] or the Q5 High-Fidelity DNA Polymerase. The typical reaction was carried out by adding 1  $\mu\text{L}$  of diluted primers (0.1  $\mu\text{M}$  final concentration), 1  $\mu\text{L}$  of DNA template (approximately 100 ng) and 47  $\mu\text{L}$  of PCR supermix into PCR tubes. The PCR parameters are described in Table 4. Primer melting temperatures ( $T_m$ ) were calculated, omitting the non-binding part of the oligonucleotides used as primers using calculations and parameters from Breslauer *et al.* and Sugimoto *et al.* [250, 251].



**Table 4:** PCR protocol for the *Pfu* and the Q5 High-Fidelity DNA Polymerase reaction.

Step	Temperature [° C]	Time	Number of cycles
<b>Initial denaturation</b>	95	1-3 min	1x
<b>Denaturation</b>	95	30 s	} 25-35x
<b>Primer annealing</b>	Tm-5	30 s	
<b>Extension</b>	72	2 min/kb	
<b>Final extension</b>	72	5-15 min	1x
<b>Storage</b>	4-6	∞	hold

#### 4.2.2. Agarose gel electrophoresis

In an attempt to verify and purify the amplified or digested DNA fragments and vectors, agarose gel electrophoresis was applied. DNA molecule (negatively charged) migration from the cathode (negative) pole to the anode (positive) pole is induced by the application of an electric field. Migration also depends on the agarose concentration (pore size), size and conformation [225]. Agarose gels were produced by adding 1 % (w/v) agarose powder electrophoresis grade into 1x Tris-acetate-EDTA (TAE) electrophoresis buffer. Chambers and gel casts from Peqlab and a power supply from Bio-Rad were used. A gel run was performed by applying a voltage of 5 volts per cm to the gel. After the run, the gel was submitted to an ethidium bromide staining solution for 10-15 minutes and stained DNA was visualized using an ultraviolet (UV) transilluminator.

#### 4.2.3. Restriction digestion, template removal and dephosphorylation

All restriction digestions were performed according to the manufacturer's protocols. After PCR, the DNA template used for the amplification has removed from the mixture by digestion with *DpnI* restriction endonuclease. The digestion was performed by adding 1 µL (10 U) of *DpnI* to a 45 µL of the PCR reaction and incubated for 1 h at 37 °C. Afterwards, the digested fragments were purified using the GeneJet PCR purification kit. *BsaI* restriction digestions were performed in the CutSmart buffer. Double digestion reactions of *XbaI* and *HindIII* were performed in 1x Tango buffer with

*XbaI* and *HindIII* in a ratio of 1:2. To prevent recircularization and religation of the linearized cloning vectors, alkaline phosphatase was added twice and the reaction was performed after restriction digestions of vectors in the corresponding buffers for 1 h at 37 °C.

#### 4.2.4. Site-directed mutagenesis

Site-directed mutagenesis was performed by whole plasmid PCR amplification according to Edelheit *et al.* [226]. Briefly, the PCR was performed by amplification of the parental plasmid containing the original DNA in two separate tubes, adding the primer forward or the reverse. After PCR, the reaction product was combined into one single tube, denatured by heat to separate the recently synthesized DNA strand from the template and cooled down gradually to allow annealing of the complementary chains. The original DNA template was digested by adding restriction enzyme which recognizes the Gm6A<sup>TC</sup> site (methylated DNA) and as a final step, transformed into competent cells. For this reaction, Q5 High-fidelity DNA polymerase was used. The following Table 5 and Table 6 describes the components for the SDM and the temperature range after PCR.

**Table 5:** Site-directed mutagenesis components using Q5 High-fidelity DNA polymerase.

Component	Reaction 1	Reaction 2
DNA template	≈ 500 ng	≈ 500 ng
Q5 buffer (5x)	1x	1x
dNTP's	0.2 mM	0.2 mM
Forward primer	40 pmol	-
Reverse primer	-	40 pmol
Q5 High-fidelity DNA polymerase	1.25 U	1.25 U
Nuclease-free water	To 25 μL	To 25 μL

**Table 6:** Temperature graduation after site-directed mutagenesis PCR.

Step	Temperature (°C)	Time (minutes)
1	95	5
2	90	1
3	80	1
4	70	0.5
5	60	0.5
6	50	0.5
7	40	0.5
8	37	Hold ( $\infty$ )

#### 4.2.5. Ligation

After PCR, the amplified DNA fragment was ligated to the target vector. Both DNA and vector were digested with the appropriate restriction enzymes and ligated using T4-ligase. The reaction contained 1x ligase buffer, 1 U of T4 DNA ligase, 10-20 ng of cut vector DNA and insert DNA (ratio 1:5) in 20  $\mu$ L final volume. The sample was incubated at 14 °C overnight. Afterwards, T4 DNA ligase was inactivated by heat at 65 °C for 10 minutes. Some amount of the final reaction was added to a tube containing competent cells XL10Gold or DH5 $\alpha$  and the cells were transformed to amplify the plasmid DNA. Positive clones were identified by DNA Sanger sequencing.

#### 4.2.6. DNA purification, concentration determination and sequencing

Bacterial plasmid DNA was purified from a 5-10 mL bacterial culture using GeneJET Plasmid Miniprep Kit (Thermo Fisher Scientific, Germany). Gene fragments and digested vectors were separated by agarose gels and purified using GeneJET Gel Extraction Kits (Thermo Fisher Scientific, Germany). PCR products and processing DNA after restriction were purified with the same kit as well, according to the manufacturer's manual. Sanger sequencing (GATC Biotech AG) was used to analyze the sequence of purified DNA plasmids. The DNA concentration was determined by Nanodrop.

#### **4.2.7. Preparation of chemically competent cells**

*E. coli* cells were submitted to a treatment to confer chemical competence, according to Mandel and Higa and Chan *et al.* (2013) [227,228], with modifications. *E. coli* cells were inoculated and grown in 100 mL Luria Bertani, Lennox (LB) supplemented with specific selection antibiotics until an OD<sub>600</sub> of 0.6 – 0.8 was reached. The *E. coli* culture was cooled by incubation on ice for 10 minutes, centrifuged at 800 x g, 4 °C for 15 min, then the supernatant was discarded and the pellet cells resuspended in 10 mL of pre-cooled CaCl<sub>2</sub>-buffer containing 10% glycerol (v/v) and further incubated on ice for 30 min. After centrifugation (800 x g, 4 °C for 15 min), the pellet was resuspended in 2 mL CaCl<sub>2</sub>-buffer supplemented with 10% glycerol, separated into 50 µL aliquots, flash-frozen in liquid nitrogen and stored at –80 °C. Cell competency was tested by plating the cells into ampicillin, tetracycline, kanamycin and chloramphenicol LB plates.

#### **4.2.8. Transformation of chemically competent bacteria**

The plasmid DNA (1-100 ng) was added to a tube containing the chemically competent cells and incubated on ice for 30 min. Incorporation of the plasmid DNA into the *E. coli* cells was induced by heat shocking at 42 °C for 1 min and a further incubation of the mixture on ice for another 1 min. LB-medium (1 mL) was added to the mixture, incubated at 37 °C, 400 rpm for 1 h and, finally, 200 µL of grown cells was plated on LB-agar supplemented with corresponding antibiotics as a selective marker.

#### **4.2.9. *E. coli* glycerol stock preparation**

Transformed single colonies were grown until it reached the high log-phase and preserved by the addition of 20% (v/v) glycerol to the culture and stored at –80 °C.

#### **4.2.10. Bacterial plasmid and oligonucleotides**

The plasmid used in this work for recombinant gene expression in *E. coli* was constructed with the plasmid pASK-IBA 3 plus and therefore under the control of *tet*-promoter [259]. The promoter is induced by a non-inhibitory concentration (200 ng mL<sup>-1</sup>) of anhydrotetracycline (AHT). The oligonucleotides used for cloning are summarized in Table 3.

#### 4.2.11. Microbial growth media and selection antibiotics used for *E. coli* cultivation

For *E. coli* cells cultivation, the growth media as well as the antibiotic supplementation are listed in Table 7.

**Table 7:** Media growth and antibiotic supplementation for microbial growth.

Medium	Composition	
Luria Bertani, Lennox (LB)	10 g·L <sup>-1</sup> tryptone, 5 g·L <sup>-1</sup> NaCl, 5 g·L <sup>-1</sup> yeast extract	
LB-Agar	1.5 % (w/v) agar in LB	
Terrific Broth (TB)	12 g·L <sup>-1</sup> , tryptone, 4 mL·L <sup>-1</sup> glycerol, 24 g·L <sup>-1</sup> yeast extract, 72 mM K <sub>2</sub> HPO <sub>4</sub> , 17 mM KH <sub>2</sub> PO <sub>4</sub>	
Antibiotic	Preparation	Working concentration
Ampicillin	100 mg·mL <sup>-1</sup> in 50% ethanol (v/v)	100 µg·mL <sup>-1</sup>
Chloramphenicol	34 mg·mL <sup>-1</sup> in 100% ethanol	34 µg·mL <sup>-1</sup>
Kanamycin	10 mg·mL <sup>-1</sup> in deionized H <sub>2</sub> O	100 µg·mL <sup>-1</sup>
Tetracyclin	17 mg·mL <sup>-1</sup> in 70% ethanol (v/v)	17 µg·mL <sup>-1</sup>

#### 4.2.12. Preparation of cleared lysates

After harvesting, *E. coli* cell pellets were resuspended in buffer W (approx. 3-5 g wet weight per 15 mL buffer) supplemented with 100 µM PMSF protease inhibitor and triton X-100 to a final concentration of 0.01%. Cell disruption was carried out twice by sonication for 5 min pulsed at 30 kHz on ice with 5 min pauses in between to avoid heat production. To separate the soluble proteins from the cell debris, the lysate was centrifuged at 17105 x g, 4 °C for 60 min. For analysis on SDS-PAGE, a small amount of the cell debris pellet, as well as the supernatant, were resuspended in 50 µL 5x SDS-PAGE (final concentration 1x).

#### 4.2.13. Affinity chromatography, size exclusion chromatography and anionic/cationic exchange

The supernatant after the preparation of the cleared lysate (containing soluble proteins, as well as the Strep-tagged proteins) was applied to a Strep-Tactin Matrix

previously equilibrated with buffer W. The column was placed in a roller mixer for 30 min to allow the interaction of the Strep-tagged proteins to the column matrix. Afterwards, the column was washed twice with buffer W buffer (50 mL) and bounded protein was eluted with buffer W supplemented with 2.5 mM D-desthiobiotin. Affinity chromatography runs were performed with a gravity flow in cold room conditions.

Size exclusion chromatography runs were performed using an ÄKTA FPLC purification system (ÄKTA Purifier P-901; GE Healthcare, UK). A Superdex 200 Hi-Load 16/60 column from GE Healthcare was used in cold room conditions (4 °C). For evaluation, absorbance at 280 nm and 220 nm were monitored. Calculations for molecular mass from the retention volume were done by applying the calibration curve ( $y = -0.224\ln(x) + 3$ ,  $R^2 = 0.9723$ ) using the following proteins: aproptinin (6.5 kDa), ribonuclease (13.7 kDa), (carbonic anhydrase; 29 kDa; Sigma), ovalbumin (44 kDa), conalbumin (75 kDa), aldolase (158 kDa), ferritin (440 kDa) and Blue Dextran 2000 (GE Healthcare, calibration kit).

For the anionic exchange runs, the ÄKTA FPLC purification system (ÄKTA Purifier P-901; GE Healthcare, UK) was used. A Mono Q 5/50 GL column from GE Healthcare was used in cold room. The sample was dialyzed previously in buffer 20 mM Tris-HCl pH 8.0 and applied in the column also previously equilibrated with same buffer. The sample elution was performed using a linear gradient from 0-100% of elution buffer containing 20 mM Tris-HCl pH 8.0 added 1 M NaCl. The cationic exchange runs, using the Mono S 5/50 GL (GE Healthcare), was also performed using the ÄKTA FPLC purification system (ÄKTA Purifier P-901; GE Healthcare, UK). The sample and the column were previously equilibrated with 20 mM MES pH 6.0 and the protein fractions were eluted using the buffer 20 mM MES pH 6.0, 1 M NaCl in cold temperatures (4 °C).

#### **4.2.14. Precipitation with ammonium sulfate**

The ammonium sulfate (AS) precipitations were carried out according to Duong-Ly and Gabelli [229]. Briefly, the protein solution, recently eluted from the affinity chromatography, was divided into four parts containing 10 mL each. Afterwards, the amount of solid AS was added according to the Table 14 (appendix), to bring the eluted protein solution to a saturation of 10%, 20%, 30%, and 40%. The solution was allowed to stir for 30 min and centrifuged 16000 x g for 30 min at 4 °C. The supernatant was

submitted to a second round of precipitation by adding enough solid AS to reach a saturation of 20%, 30%, 40% and 50%. The AS was allowed to interact with this protein solution and, afterwards, centrifuged for 30 min, 16000 x g at 4 °C. The resultant supernatant of this process possess a 20-30%, 30-40%, 40-50% and 50-60% saturation. Samples were collected and the purity was visualized by SDS-PAGE.

#### 4.2.15. Strep-tactin matrix regeneration

After elution of the target protein, the Strep matrix was washed several times with five CVs (column volumes) of buffer W and three times with 1x Strep-tactin regeneration buffer. Afterwards, the matrix was washed with buffer W until the HABA solution was removed completely and the matrix turned white. It was subsequently and stored in 1x Strep-tactin buffer W.

#### 4.2.16. SDS-PAGE

To analyze the protein expression, as well as the purity, SDS-PAGEs were prepared and gel electrophoresis was performed according to Laemmli [230]. The components to prepare a 4% stacking gel and a 12% separating gel are listed in Table 8.

**Table 8:** Components for a 4% stacking and 12% separating gel preparation.

Component	Stacking gel (4%)	Separating gel (12%)
Acrylamide/Bisacrylamide Ratio 37,5 : 1	4%	12%
Separating gel buffer -	-	0.37 M
Stacking gel buffer	0.125 M	-
SDS	0.1% (w/v)	0.1% (w/v)
TEMED	0.1% (v/v)	0.1% (v/v)
APS	0.05% (w/v)	0.05% (w/v)

The protein samples were supplemented with 5x sample buffer (1x final concentration), denatured by incubation at 96 °C for 10 minutes, applied onto the gel

wells, mounted in a SE260 Mighty Small II Deluxe Mini electrophoresis unit and run by applying a current of 25 mA per gel until the bromophenol blue reached the end of the gel. A standard molecular weight (MW) marker was used for size determination (listed in the buffers and consumables section). The protein was stained via incubation of the gel in Coomassie blue staining solution according to Neuhoff and coworkers [231,232] with modifications, for 3 h and subsequently destained for adequate contrast.

### **4.2.17. Western blot**

Purified samples from the affinity chromatography were blotted to a nitrocellulose membrane using a semi-dry blotting apparatus for 1 h at 35 mA. Afterwards, the membrane was blocked at 4 °C overnight with 3% bovine serum albumin (BSA) (w/v) in phosphate saline buffer (PBS) and washed with 1x PBS containing 0.3% Tween 20 (v/v) and incubated with Murine Anti-Strep-tag II antibody, IgG1 (IBA, Germany) diluted to 1:2000 in 1x PBS containing 1% BSA and 0.03% Tween 20 in a cold room overnight. The second antibody (Goat anti-mouse IgG-AP conjugated, (Sigma, Germany) was added and incubated for 45 min at room temperature (RT). The membrane was washed three times with PBS and incubated with BCIP and NBT in reaction buffer until the band of tagged protein was revealed. The reaction was stopped by adding PBS buffer.

### **4.2.18. Thermal shift assay**

The thermal shift assay was carried out using the RUBIC buffer screen MD1-96 by the technician Ioana-Maria Nemptanu at the EMBL-Hamburg in order to verify stable buffer conditions for MenF. After affinity chromatography, MenF was dialyzed against 50 mM Tris-HCl pH 7.5, concentrated until 20 mM using the extinction coefficient of  $54445 \text{ M}^{-1}\cdot\text{cm}^{-1}$  given by the Protparam program of the Expasy website (<http://web.expasy.org/protparam/>). SYPRO orange dye was added to the protein sample in a ratio of 1:1, protein sample: dye, mixed with 21  $\mu\text{L}$  of buffer screen condition and the analysis was carried out in a Real Time qPCR machine. Data from the melting temperature curve were plotted using the Microsoft excel program.



#### 4.2.19. Protein quantification

Protein concentrations were determined by measuring specific absorbance at a wavelength of 280 nm according to the Lambert-Beer law-equation:  $A = \varepsilon l c$ , where  $A$  = absorbance (optical density),  $\varepsilon$  = molar absorption ( $\text{mol}\cdot\text{cm}^{-1}\cdot\text{dm}^{-3}$ ),  $l$  = length of the light path (cm) and  $c$  = concentration of solution.

Physicochemical properties of MenF, MenH and DHNA, such as molecular mass, theoretical isoelectric points as well as the extinction coefficient, were calculated by the ProtParam server of the Swiss Institute of Bioinformatics (SIB), ExPASy Bioinformatics Resources Portal (Table 9) [233].

**Table 9:** Physicochemical properties of MenF, MenH and *S. aureus* DHNA protein.

	MW (Da)	pI	Ex. coefficient
MenF	53306.24	5.20	54320
MenH	28669.0	8.58	32555
DHNA	19356.0	5.69	41370
DHNA-D16A	19312.0	5.97	41370
DHNA-E31N	19341.0	5.96	41370

#### 4.2.20. Dynamic light scattering (DLS)

In order to investigate the hydrodynamic radius (HR) of the proteins, as well as the dispersity in solution, DLS was used. Before each measurement, the samples were centrifuged at  $16.100 \times g$  for 60 min. For standard measurements, the SpectroSize 300, which measures 15  $\mu\text{L}$  sample in a quartz cuvette, was used. The DLS device uses a red light laser ( $\lambda = 690$  nm and power 10-50 mW) which applies insignificant energies to the sample and the sample temperature is monitored and stabilized.

#### 4.2.21. Circular dichroism (CD)

In order to evaluate the secondary structure and folding of proteins, circular dichroism (CD) proves to be a rapid and easy method. Briefly, CD can be defined as a different absorption of left-handed and right-handed circularly polarized light.

Asymmetric molecules interact with light and absorb right and left-handed circularly polarized light to diverse amounts, depending on the amides in the protein backbone (far UV) and aromatic groups (near UV). The recorded ellipticity is shown in Equation 1.

The  $\alpha$ -helices of the proteins absorb light in a negative zone at 222 nm and 208 nm and in a positive zone at 193 nm. Well-defined antiparallel  $\beta$ -pleated sheets ( $\beta$ -helices) of the proteins absorb light in a negative zone at 218 nm and positive zone at 195 nm, according to standard curves [234] (Figure 6).

$$\theta = \frac{180 \cdot \ln 10}{4\pi} (E_l - E_r)$$

**Equation 1:** Recorded ellipticity, where  $\theta$  is the observed ellipticity (degrees); the absorbance of right- and left-handed circular polarized light is reflected in  $E_r$  and  $E_l$ .

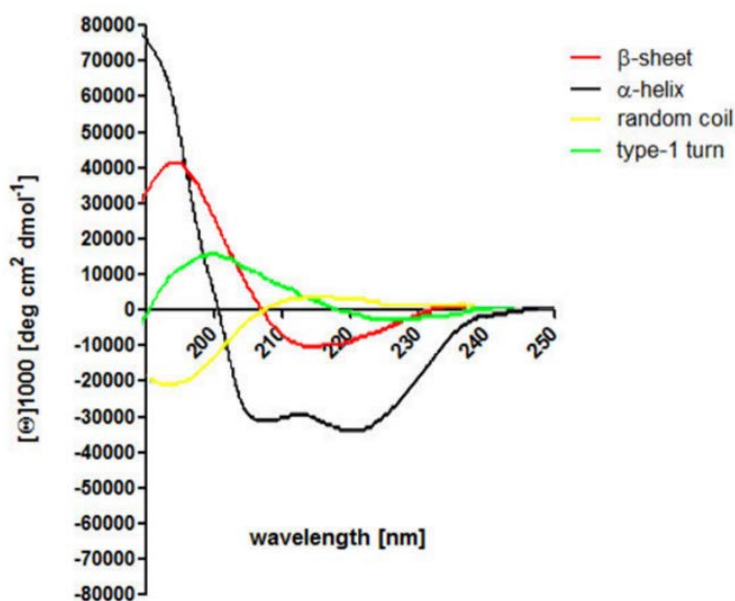


**Figure 6:** Standard curves for CD measurements determined by Yang and coworkers [234] plotted as  $\Theta \cdot 1000$  [ $\text{deg cm}^2 \text{dmol}^{-1}$ ], where  $\Theta$  is the molar ellipticity and [ $\text{deg cm}^2 \text{dmol}^{-1}$ ] is degrees per  $\text{M}^{-1} \cdot \text{m}^{-1}$ ).  $\beta$ -sheets are shown in red,  $\alpha$ -helices in black, random coil in yellow and turn structures (type-1) in green. The figure was generated with GraphPad Prism 5 version 5.01 for Windows (GraphPad Software, La Jolla California USA, [www.graphpad.com](http://www.graphpad.com)).

Protein samples were dialyzed in a low salt buffer and the measurements were performed in a 1 mm quartz cuvette scanning the near UV wavelength 190-260 nm using a CD spectrometer J-815 (Jasco, UK). To reach high accuracy, the general scanning speed was set to  $10 \text{ nm} \cdot \text{min}^{-1}$  and the spectral bandwidth was fixed to 1 nm.

---

The results were converted to molar ellipticity and plotted against the wavelength (Figure 6) by the software.

#### **4.2.22. MALDI-ToF Mass Spectrometry**

Mass spectrometry data collection and analysis were performed in the mass spectrometry facility in the Organic Chemistry Department of the University of Hamburg under the supervision of Dr. Maria Riedner. Protein samples from a SDS-PAGE gel stained with Coomassie blue were excised and subsequently destained by the addition of shrinking solution and swelling solution with an incubation of 5 min for each solution, according to Shevchenko and collaborators [235], with modifications. Cysteine reduction and alkylation were performed by the addition of dithiothreitol (DTT, final concentration 10 mM in swelling solution) for 10 min at 57 °C and iodoacetamide (IAA, final concentration 50 mM in swelling solution) for 30 min at RT. The supernatant was removed, shrinking solution added for 5 min and then the pieces of gel were dried in a speed vac. The trypsin digestion was carried out by adding digestion solution (barely covering the gel pieces) and 3x volume of trypsin solution for 30 min at 4 °C. Afterwards, the tube reaction was digested overnight at 37 °C. The digestion reaction was halted by adding 5% formic acid (FA) (final concentration), the digested solution was replaced with a new tube and to the gel pieces was added peptide extraction solution for 5 min. The supernatant was collected, replaced into the new tube containing the digested solution and 100% acetonitrile (ACN) was added to the gel pieces for 5 min. Henceforward, the supernatant was removed, added into the new tube and the extracted digestions were dried by speed-vac. The pellets were resolved in 50% ACN supplemented with 0.2% FA (final concentration) and samples were desalted by C18 zip tip. Results were analyzed using the mascot search (Matrix Science).

#### **4.2.23. Sample preparation for initial crystallization screening**

Initially, DHNA from *S. aureus* was purified using gravity flow affinity chromatography by the Strep-tag and was then applied to a size exclusion chromatography using the Superdex 200 HiLoad 16/60. In order to identify optimal concentrations for protein crystallization, the Pre-crystallization Test (Hampton Research, USA) was used according to the manufacturer's manual. Afterwards, the

protein was concentrated until it reaches  $10 \text{ mg}\cdot\text{mL}^{-1}$  and centrifuged to remove aggregations. The protein dispersity was monitored by DLS measurements.

Initial screenings were performed using the commercially available screens JCSG-plus (Molecular Dimensions, UK), Stura FootPrint & MacroSol (Molecular Dimensions, UK), JBScreen Classic HTS II (Jena Bioscience, DE) and Morpheus (Molecular Dimensions, UK). The pipetting robot Honeybee 961 (Genomic solutions, UK) was used to set up a screening plates in sitting drop format in an MRC 96-well sitting drop crystallization plate (Molecular Dimensions, UK). The drop size was 600 nL consisting of 300 nL of protein solution mixed with 300 nL of precipitant solution (1:1 ratio) and the reservoir was filled with 55  $\mu\text{L}$  of the precipitant solution. The plates were sealed and stored at 20 °C. The plates were monitored three-five days after the set up to identify crystallization hits.

#### **4.2.24. Optimization of the crystallization condition**

After identification of protein crystals in the commercially available screen, this condition was subsequently optimized by varying the type of the salt, as well as the salt concentration.

Conditions were optimized in MRC MAXI 48-well plate (Molecular Dimensions, UK) applying the sitting drop vapour diffusion technique. The total volume of the droplet size was 2  $\mu\text{L}$ , consisting of 1  $\mu\text{L}$  protein solution and 1  $\mu\text{L}$  precipitant solution and the reservoir was filled with 300  $\mu\text{L}$  of precipitant solution. In addition, automated pipetting was carried out by the Honeybee 961 (Genomic Solutions, USA) pipetting robot with droplets in the first well consisting of 0.5  $\mu\text{L}$  protein solution and 0.5 precipitant solution (50:50) and in the second well consisting of 0.5  $\mu\text{L}$  protein solution and 0.7 precipitant solution (60:40). In both optimizations, the reservoir solution consisted of 55  $\mu\text{L}$ . The influence of the temperature was tested and the plates were stored at 4 °C and 20 °C.

The initial condition provided some opportunities for optimization. Therefore, hanging drop vapour diffusion, seeding, as well as streak seeding techniques were considered.

For hanging drop vapour diffusion experiments, a Linbro plate (Jena Bioscience) was filled with 1 mL of the precipitant solution and sealed with a siliconized glass

---

coverslip containing a droplet with a total volume of 2  $\mu\text{L}$ , consisting of 1  $\mu\text{L}$  protein solution and 1  $\mu\text{L}$  precipitant.

Crystals obtained in the initial trial were used to produce a seedstock. Microseeding is a simple but efficient technique used to promote spontaneous nucleation and to optimize crystal quality. The seedstock was prepared initially by crushing the crystal in stabilizing solution using a crystal crusher. Afterwards, the seedstock was diluted to 1:10 – 1:1000 with the precipitant protein solution and used for both hanging drop and sitting drop vapour diffusion experiments. In addition to hanging drop experiments, seedstock was used to perform streaklines with a horse hair within droplets containing 1  $\mu\text{L}$  precipitant and 1  $\mu\text{L}$  protein solution.

In addition, crystallizations trials under oil were carried out using Terazaki's plates (Nunc, Denmark). The plates were previously treated with parafilm oil to cover all wells with oil. Afterwards, 1  $\mu\text{L}$  of precipitant and 1  $\mu\text{L}$  of protein solution were previously mixed and applied into the wells. The plates were stored at 20 °C and monitored every 3-5 days after crystallization setup.

#### **4.2.25. Soaking with platinum to obtain heavy atom derivatives**

In order to solve the phase problem, native crystals were soaked in a 10 fold molecular excess of a solution containing potassium tetrachloroplatinate (II) ( $\text{K}_2\text{PtCl}_4$ ) (1.25 mM final concentration). The compound was added to the crystallization drops 24 h before diffraction data measurement. After soaking, crystals were collected and placed in a cryoprotectant solution containing 15% glycerol directly prior to the diffraction data collection.

#### **4.2.26. Diffraction data collection**

Crystals obtained from the condition optimizations were used for a primary dataset collection to test crystal quality. Firstly, the cryoprotectant solutions were tested by flash frozen the loop in liquid nitrogen stream and checked for formation of ice rings. Secondly, before the data collection, the crystal was treated with a cryoprotectant solution consisting of the reservoir solution supplemented with 15% glycerol. Afterwards, the crystal was soaked in this solution for 20 seconds, mounted in a cryo nylon loops (Mounted CryoLoop, Hampton Research, US) and flash frozen in liquid

nitrogen. The dataset collection was carried out using the in-house rotating anode. Two pictures were collected, auto indexed and the strategy calculated to determine phi range for completeness was  $180^\circ$  using the iMOSFLM program [236]. The parameters for data collection consists of oscillation range of  $1^\circ$  (180 images in total), exposure time of 60 seconds and detector-to-crystal distance of 200.000 mm.

The beamline P13 (EMBL, Hamburg) at the PETRAIII synchrotron radiation source was used for data collection. All measurements were conducted under cryogenic conditions at 100 K in a liquid nitrogen stream. For cryoprotection, 15% glycerol was mixed with the precipitant solution of the obtained crystal conditions and 2  $\mu\text{l}$  was added to the crystal well. In general, the crystal mounting was carried out using nylon loops (Mounted CryoLoop, Hampton Research, US) and the crystals were flash frozen in liquid nitrogen. The data collection strategies was detector-to-crystal distance of 170.730 mm, exposure time of 0.0377440 seconds, wavelength of 1.033  $\text{\AA}$  and oscillation range of  $0.1^\circ$  collecting, in total, 3600 images.

The Beamline P14 (EMBL, Hamburg) at the PETRAIII synchrotron radiation source was used to collect diffraction data up to 2.0  $\text{\AA}$  for a heavy atom localization and subsequent phasing. A single-wavelength anomalous dispersion/diffraction (SAD) dataset from a single heavy-atom derivatized crystal was collected at a wavelength of 1.072  $\text{\AA}$  at 100 K using the anomalous scattering coefficient of platinum  $f'' -19.83$  and  $f' 8.34$  with 11.5622 KeV. The diffraction data collected included 7200 images of  $0.1^\circ$  rotation with 10% beam transmission and detector-to-crystal distance of 234.960 mm.

#### **4.2.27. Data processing and model building**

Data reduction from single-crystal diffraction experiments was performed with the XDS program package [237]. For scaling, AIMLESS [238] of the CCP4 software was applied. All data were selected and cut monitoring Rmerge,  $I/\sigma(I)$  and completeness in the following steps. To build a research model from the heavy atom derivatized crystal, scaled data were submitted to the EMBL-HH Automated Crystal Structure Determination Platform (Auto Rickshaw) [239,240]. Afterwards, the suitable search model provided by the Auto Rickshaw platform was used to perform a molecular replacement with DHNA native with MOLREP [241]. The model was manually revised using Coot [242] and refined with refmac5 [243].

#### 4.2.28. Model evaluation

Online tools, listed in Table 10, were used for structure model evaluation.

**Table 10:** Online tools frequently used for structure model evaluation.

<b>Tool</b>	<b>Application</b>	<b>Citation</b>
<b>Clustal Omega</b>	Primary sequence comparison	[244]
<b>Blast</b>	Sequence homology analysis	[245]
<b>PDBePISA</b>	Exploration of macromolecular interfaces	[246]
<b>eFold</b>	Comparison and 3D alignment of protein structures (C $\alpha$ -alignments)	[247]
<b>PDBsum</b>	Pictorial database of the content of each 3D structure	[248,249]

#### 4.2.29. Docking studies and peptide rational design

The docking studies, as well as the peptide rational design, were carried out with *Sa*DHNA dimer using the Bioluminate software from the Schrödinger suite (Schrödinger, LLC, USA). The peptides EGEYE and YGSDGR were designed and used for peptide docking with the Bioluminate tool. The third peptide (WRSMGR) was generated using the residue scanning tool prioritizing the ligand affinity. The docking parameter uses the Molecular Mechanics/Generalized Born Surface Area (MM/GBSA) method to calculate the free energy of the binding of ligands with the receptor [250].

#### 4.2.30. Thioesterase activity assays of DHNA

The thioesterase activity of *S. aureus* DHNA was measured according to Rodríguez-Guilbe and co-workers [251]. In a microplate ELISA reader, the formation of 2-nitro-5-thiobenzoate anion (TNB<sup>2-</sup>) by the reaction of thiolate anion (RS<sup>-</sup>) with Ellman's reagent (DTNB<sup>2-</sup>) and one mixed disulfide (R-S-TNB<sup>-</sup>) catalyzed by purified native *S. aureus* DHNA and mutants D16A and E31N C-terminally Strep-tagged was followed by monitoring the change in absorbance at 412 nm (extinction coefficient of 13.600 M<sup>-1</sup>·cm<sup>-1</sup>). The enzymatic assay was performed in a total volume of 200  $\mu$ l at

room temperature in 50 mM HEPES-K<sup>+</sup> buffer, pH 7.5 containing 10  $\mu$ M enzyme, 100  $\mu$ M stearyl-CoA (long chain) or 1 mM crotonyl-CoA (short chain) and 1 mM DTNB. The substrates were added after one hour of incubation and the results were analyzed using the Microsoft excel program.

Enzymatic assays were also carried out to evaluate the activity of designed inhibitors. The peptides pep1 EGEYE (623.23 Da), pep2 WRSMGR (792.39 Da) and pep3 YGSDG (654.28 Da) were kindly designed and synthesized by Dr. André Murad and Dr. Carlos Bloch from the National Centre for Genetic Resources and Biotechnology (EMBRAPA/Cenargen, Brasília-Brazil). The enzymatic assays were performed as described above, including 100  $\mu$ M of the respective peptides. All enzymatic assays were carried out in triplicates from separated protein purifications and separate expressions.



## 5. Results

The open read frame (ORF) of MenF, MenH and DHNA was amplified from Strep-tagged constructs by PCR. The reverse primer was encoded for a strep-tag (SAWHSPQFEK) and a stop codon after the tag. Fragment and an empty vector pASK-IBA 3 plus were digested with *BsaI* and ligated. After transformation of this construct into *E. coli* XL-10 gold or DH5 $\alpha$  cloning cells, the plasmid DNA was isolated and sequenced. The C-terminal tagged construct was used to transform the *E. coli* BLR (DE3) BL21 (DE3) and BL21 (DE3) star.

### 5.1. Recombinant expression, purification, physicochemical characterization and secondary structure estimation of MenF

Isochorismate synthase (MenF) Strep-tagged was initially expressed in the BLR (DE3) *E. coli* expression strain at 20 °C, 37 °C or 30 °C, however, the initial amount obtained of recombinant protein was not satisfactory. In order to optimize the expression, the pASK-IBA 3 plus expression vector containing the *menF* gene was used to transform the *E. coli* BL21 (DE3) Star strain. The sequence-based molecular weight (MW) prediction for the monomeric protein MenF, including the Strep-tag sequence, was 53306.24 Da. The expression carried out for 6 h at 30 °C in terrific broth media and inducing the culture starting with an OD<sub>600</sub> of 0.6-0.8 demonstrated to be more efficient for expressing MenF recombinant protein. Afterwards, a solubility test was performed by resuspending the cell pellet in buffer W. The recombinant expression of MenF in BL21 (DE3) Star, TB medium for 6 h at 30 °C resulted in satisfactory amounts of soluble protein, visualized in Figure 7. The clear cell lysate containing the soluble MenF was submitted to affinity chromatography and MenF was successfully eluted, together with some minor contaminants. Further washing steps with buffer W, together with buffer W supplemented with ATP/MgCl<sub>2</sub> demonstrated to be efficient for removing unspecific protein-protein interactions between MenF and *E. coli* protein contaminants (Figure 7).

Fresh samples were dialyzed in a low salt concentration buffer and secondary structure was performed using circular dichroism spectroscopy. Using a final concentration of 0.4 mg·mL<sup>-1</sup>, the MenF secondary structure content, 27% of  $\alpha$ -helix,

40% of  $\beta$ -sheets, 3 of turn and 30% to be random was determined, according to the Reed reference standard curve (Figure 8). The root-mean-square (RMS) value between the fitted curve (reference curve) and the MenF data was 4.9% using the Reeds reference curve [252].

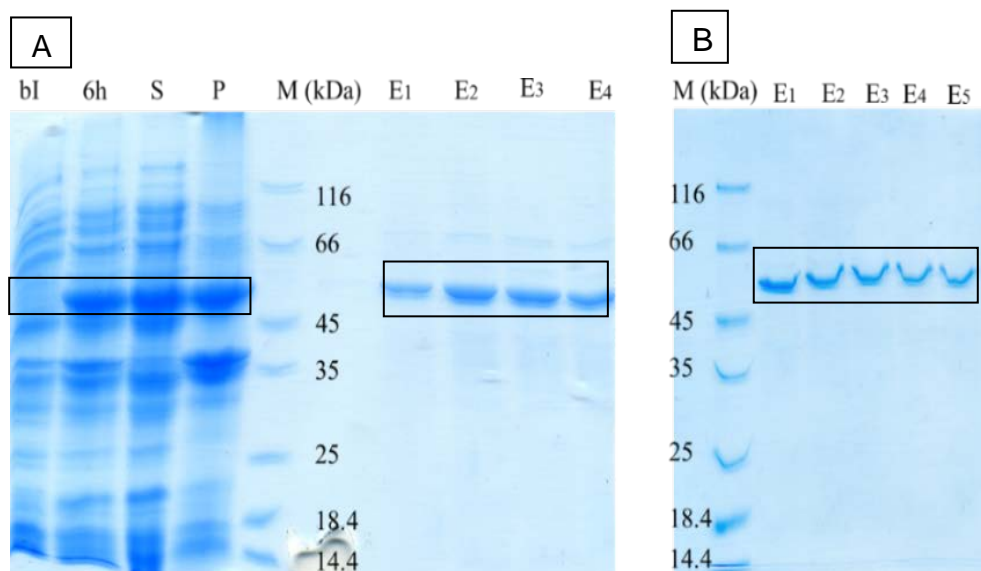


**Figure 7:** Recombinant expression profile and solubility of *S. aureus* MenF. A: from left to right: Expression profile of *S. aureus* MenF before induction (bI) and 6h (10  $\mu$ L) after induction, respectively. “S” = supernatant (soluble proteins) and “P” = pellet (insoluble proteins), M = molecular marker. E1-E4 protein eluted with D-desthiobiotin (black box). B: MenF after washes with buffer W supplemented with ATP/MgCl<sub>2</sub> (53.3 kDa). M = molecular marker in kDa, E1-5: elutions with D-desthiobiotin.

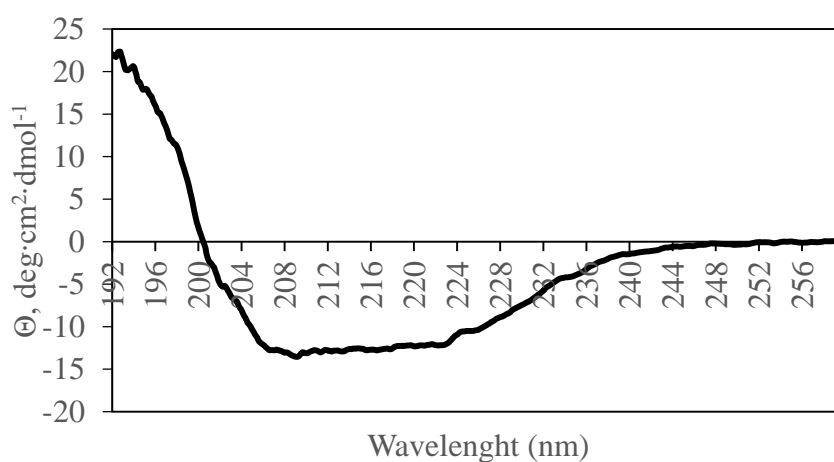


**Figure 8:** CD measurement of MenF protein solution. The figure was created using the Microsoft excel program.

Afterwards, MenF was dialyzed overnight into 100 mM Tris-HCl pH 6, 100 mM NaCl and submitted to further purification using the size exclusion chromatography. As

shown in Figure 9, MenF was mainly aggregated and most of the sample was collected in the void volume.

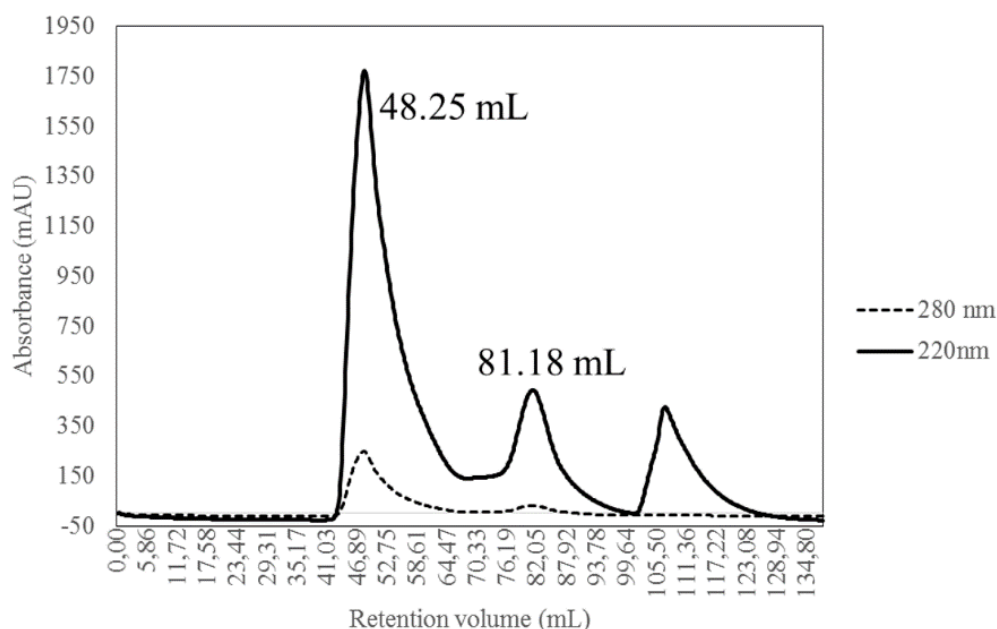


**Figure 9:** Size exclusion chromatography of *S. aureus* MenF protein. SaMenF was collected in the void volume, indicating that the protein sample was aggregated. The figure was created using the Microsoft excel program.

MenF eluted protein from the affinity chromatography was dialyzed against 100 mM Tris-HCl at pH ranging from 6 to 7.5, 150 mM NaCl and in 100 mM sodium phosphate buffer in the pH ranging from 6 to 7.4 in solution, concentrated to  $2 \text{ mg}\cdot\text{mL}^{-1}$  and the oligomerization state was analyzed using dynamic light scattering (DLS). As shown in Figure 10, MenF suspensions showed a high hydrodynamic radius (from 6.50 to 20 nm) for all buffers and pH conditions, indicating the sample was not stable in those buffer systems as well as not monodisperse and, thus, aggregated.

Since none of the buffer systems used demonstrated optimal conditions for MenF stability, thermal shift assays were performed. The RUBIC buffer screen involves different buffers, varying pHs as well as the influence of salt content on the protein folding. The SYPRO orange dye has an affinity to bind to hydrophobic patches of the protein. Rising temperatures induce protein unfolding and expose hydrophobic regions

of the protein, which can interact with the fluorophore (SYPRO orange) and, therefore, emit fluorescence.

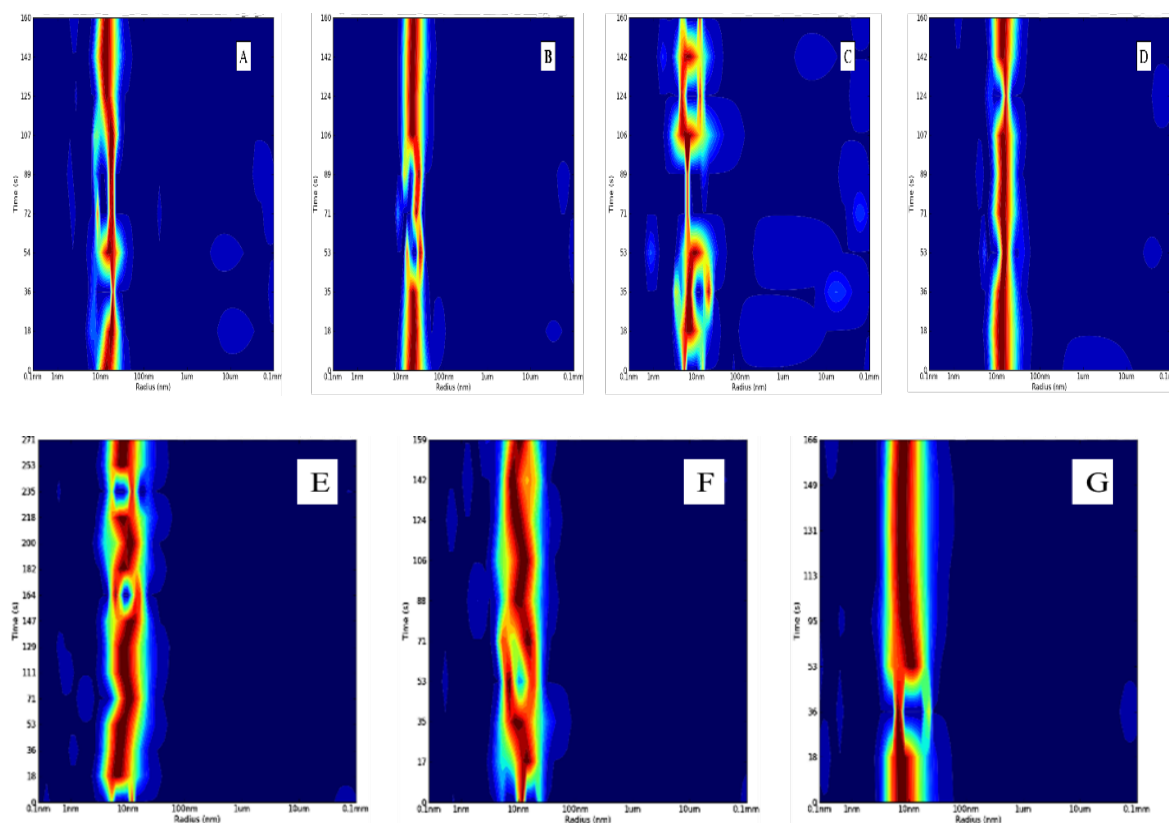


**Figure 10:** Dynamic Light Scattering for MenF in Tris-HCl buffer A: pH 6 (HD =  $7.6 \pm 0.8$  nm and  $16 \pm 2.2$ ). B: pH 6.5 (HD =  $20.8 \pm 0.8$  nm). C: pH 7.0 (HD =  $6.0 \pm 1.1$  nm,  $6.5 \pm 1.2$  nm,  $14.1 \pm 2.3$  nm). D: pH 7.5 (HD =  $15 \pm 1$  nm. Sodium phosphate buffer E: pH 6 (HD =  $8.1 \pm 1.5$  nm,  $8.6 \pm 1.6$  nm). F pH 7.0 (HD =  $10 \pm 1.65$  nm,  $11.5 \pm 2.6$  nm). G: pH 7.4 (HD =  $8.1 \pm 0.4$  nm).

As expected, for a stable sample, the signal given by the fluorophore starts to increase with increasing temperature, a situation that did not occur for the MenF protein sample. High fluorescence signals emitted by the SYPRO orange dye during the first cycles indicated that the MenF protein was already denatured before the test began. In addition, the MenF protein was not well behaved during these conditions and none of the buffer systems used in this assay resulted in satisfactory stabilization for the MenF protein (Figure 11 and Figure 12). Once all the strategies failed to produce stable MenF protein samples, the MenF protein was identified to be not suitable for further characterizations, as well as for crystallization trials.

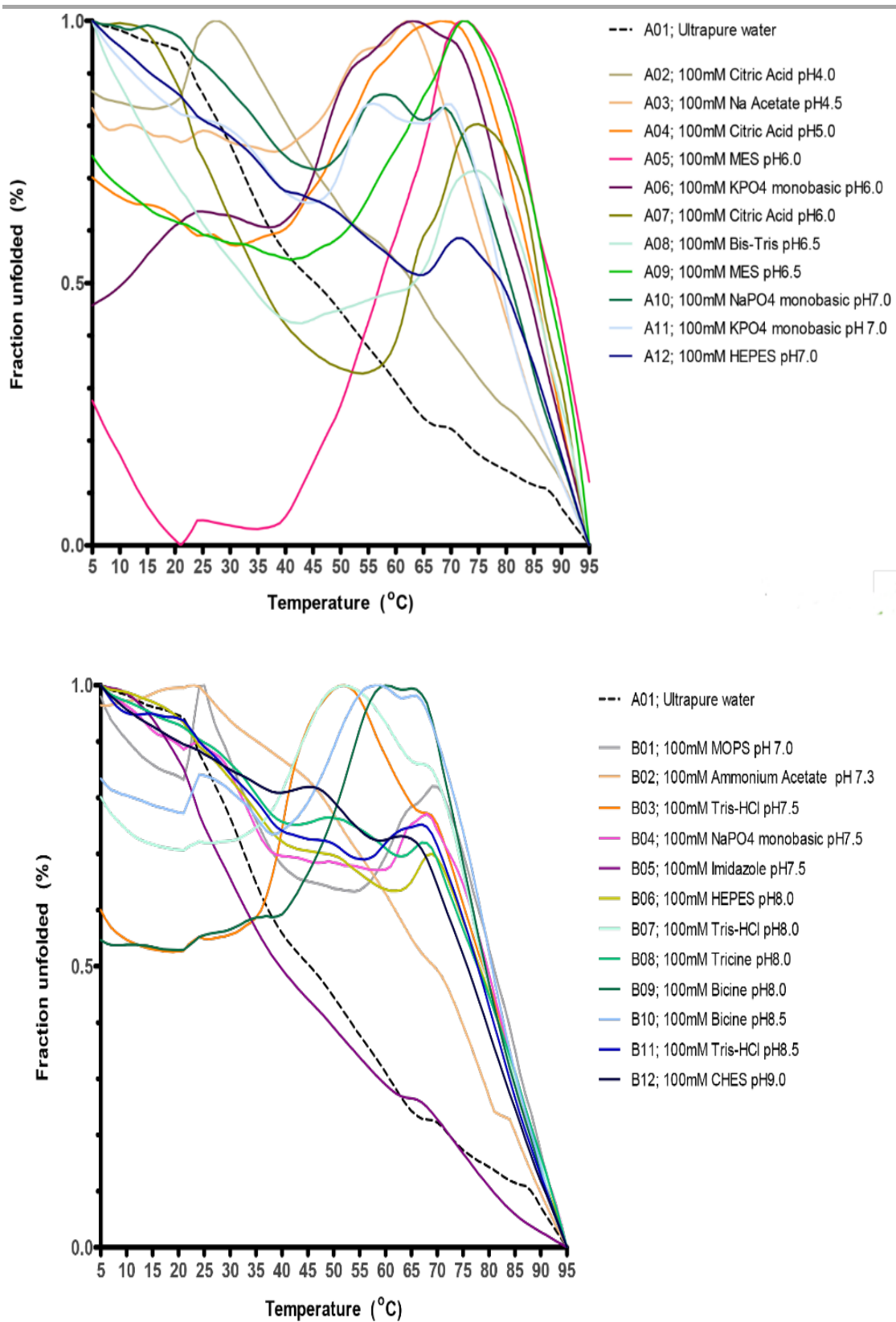


**Figure 11:** Thermofluor shift assays for MenF in different buffer systems and pH ranges using the Rubic screen buffer MD1-96. The control consists MenF sample mixed with ultrapure water.

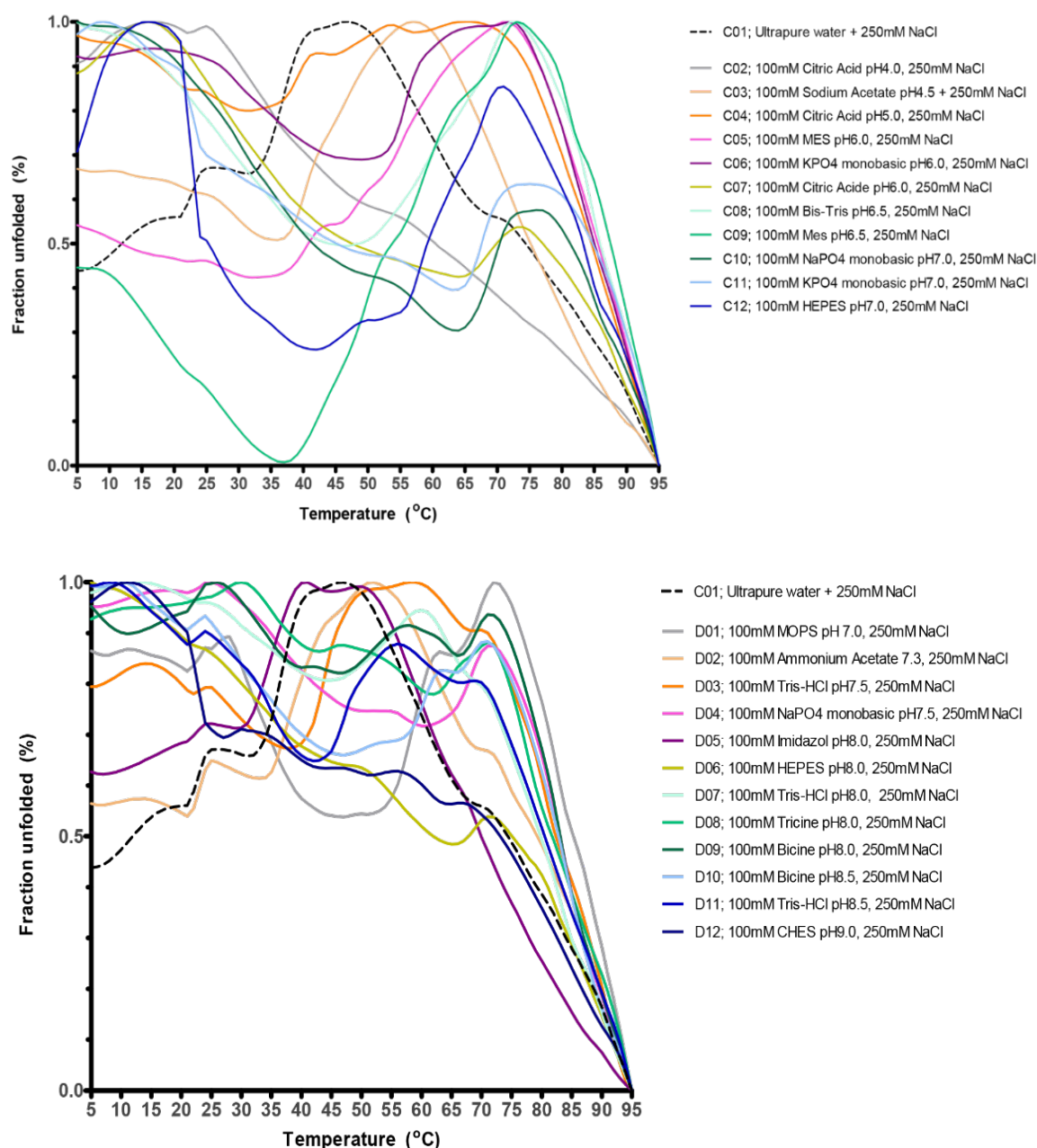


**Figure 12:** Thermofluor shift assays for MenF in different buffer systems with salt additive in pH ranges using the Rubic screen buffer MD1-96. The control consists MenF mixed with ultrapure water.

## 5.2. MenF sequence alignment and prediction model

Sequence alignment with the homolog structure from the NCBI/BLAST search performed with Clustal Omega showed a sequence identity of 29% (Figure 13). The *S. aureus* MenF and the *E. coli* MenF (PDB entry 3BZN) N-terminal sequence demonstrated to be significantly different. This low homology observed for the N-terminal region is also reflected in the predicted structural model, which the N-terminal

for all models showing different secondary structures (Figure 14). The CD measurements of *SaMenF* indicated high contents of random structures (30%). This result is confirmed via the predicted model, which shows several random loops.

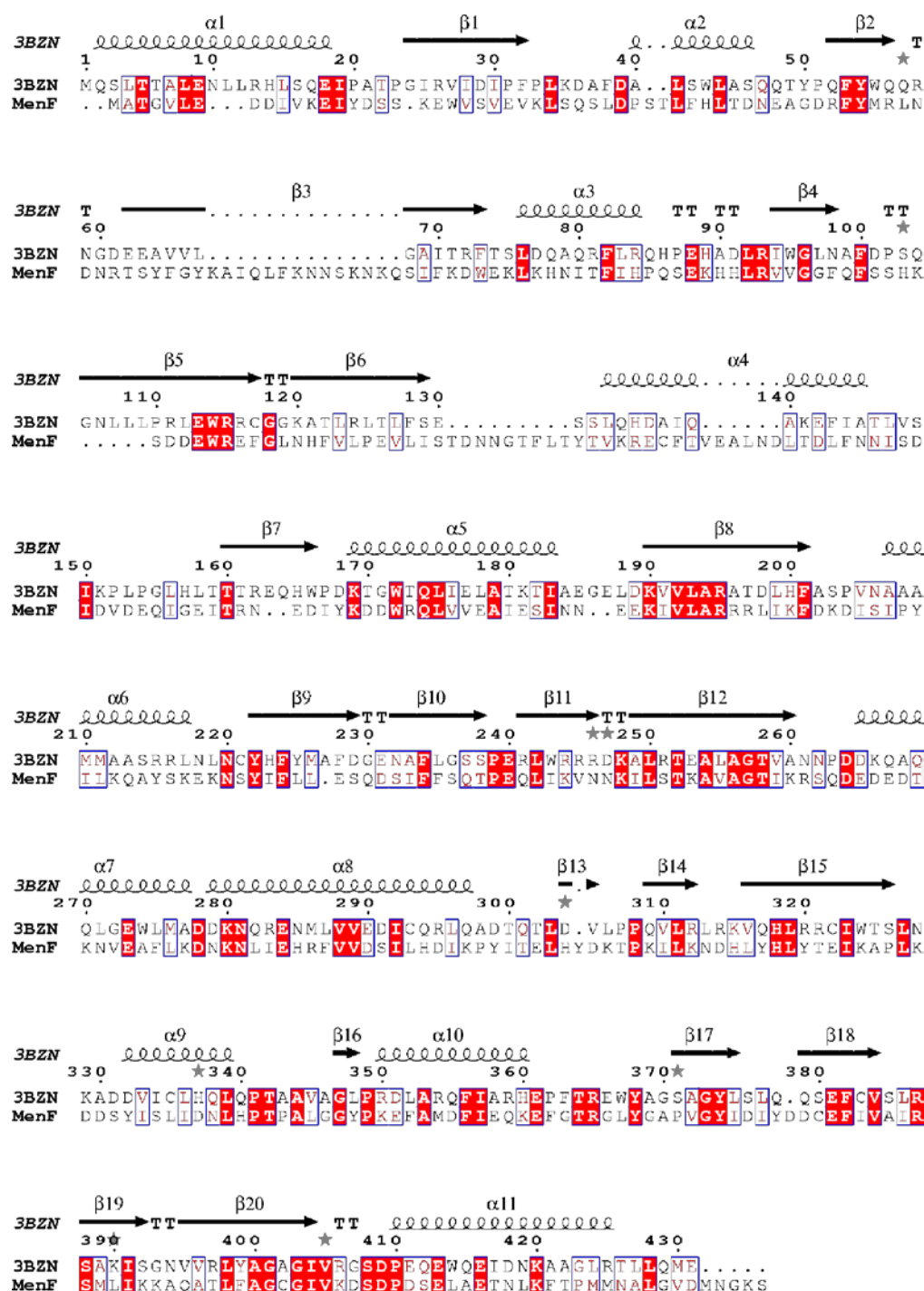


**Figure 13:** Protein sequence alignment of MenF and *E. coli* Menaquinone-Specific Isochorismate Synthase (PDB entry 3BZN). Identical residues are highlighted in red boxes, similar physico-chemical properties residues in blue boxes. A dashed line indicates disordered regions. The multiple sequence alignment was performed using ClustalOmega (<http://www.ebi.ac.uk/Tools/msa/clustalo/>) and ESPript (<http://esprict.ibcp.fr/ESPript/cgi-bin/ESPript.cgi>).

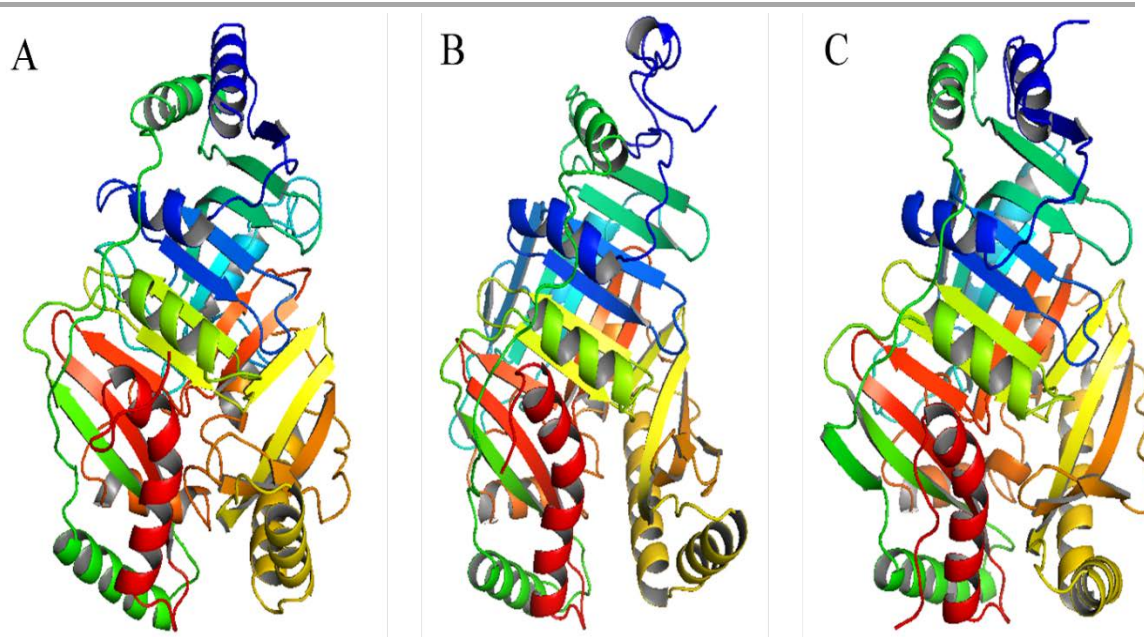


**Figure 14:** Predicted structure models for MenF given by A: IntFOLD [253], B:Phyre2 [254] and C: RaptorX [255]. All predicted structures were created using the *E. coli* Menaquinone-Specific Isochorismate Synthase (PDB entry 3BZN) crystal structure as template. Secondary structure is colored using rainbow spectrum from N-terminus (blue) to C-terminus (red). The figure was created with The PyMOL Molecular Graphics System, Version 1.7.4 Schrödinger, LLC.

### 5.3. Recombinant expression, purification and physicochemical characterization of MenH

Demethylmenaquinone methyltransferase (MenH) C-terminal Strep-tagged was expressed in BLR (DE3) *E. coli* expression strain in TB medium at 30 °C for 6 h with success and demonstrated to be a soluble protein in these conditions. The cell lysate was applied to a Strep-tag matrix to obtain pure samples of MenH protein. During the first solubility test, a modified buffer W containing 300 mM NaCl was used for cell disruption. After protein elution, the MenH protein solutions demonstrated precipitation, a situation that was reversed by decreasing the amount of salt used in buffer W to 100 mM NaCl. Additionally, the MenH protein showed to be sensitive regarding temperature, therefore, affinity chromatography steps were carried out at room temperature. As shown in Figure 15 (A-C), satisfactory amounts of MenH were expressed and eluted after the addition of D-desthiobiotin. The sequence-based molecular weight (MW) prediction for the monomeric protein MenH was 28669.0 Da.

In order to remove unspecific *E. coli* protein interactions, several washing steps were carried out. After applying the clear cell lysate onto the column and before the



elution steps, buffer W supplemented with ATP/MgCl<sub>2</sub> was added to the empty column as a first washing step, the protein as eluted and samples were collected to verify purity on SDS-PAGE (Figure 15 D). This wash step was not enough to remove all *E. coli* protein contaminants. Afterwards, a second wash step was carried out by adding to the column buffer W supplemented with ATP/MgCl<sub>2</sub> and afterwards with buffer W with 0.5% of CHAPS added, a non-denaturant zwitterion surfactant. As shown in the Figure 15 E, this extra washing step was important to remove around 90% of the *E. coli* protein contaminants. In addition, Western blot against the Strep-tag was also performed to confirm the presence of MenH protein after expression and purification (Figure 15 F).

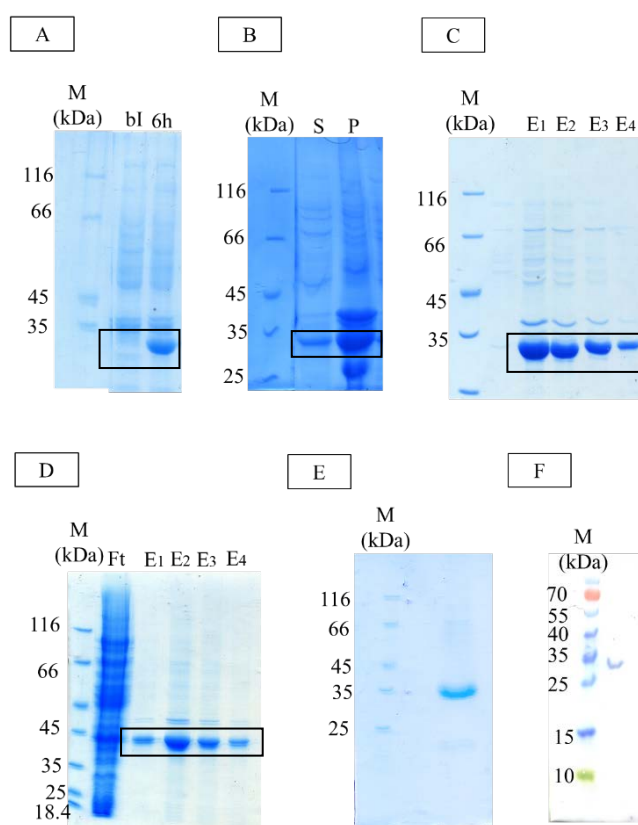


**Figure 15:** Recombinant expression profile, solubility and affinity chromatography purification of *S. aureus* MenH. A: Expression profile of *S. aureus* MenH before induction (bl) and 6h, respectively. B: solubility test “S” = Soluble proteins and “P” = Insoluble proteins). C: Eluted MenH after the addition of D-desthiobiotin (E1-E4 protein elution, 28.6 kDa). D: MenH eluted with D-desthiobiotin and after the ATP/MgCl<sub>2</sub> wash step. E: MenH after the CHAPS washing steps. F: MenH Western blot (28.6 kDa). M = molecular marker in kDa.

Subsequently, MenH was concentrated to 5 mg·mL<sup>-1</sup> using the extinction coefficient of 32555 M<sup>-1</sup>·cm<sup>-1</sup> given by the ProtParam (ExPASy Bioinformatics Resources Portal) website (<http://web.expasy.org/protparam/>) and the purity was

verified once more with SDS-PAGE. Unfortunately, after concentration, the same contaminants observed in the first wash step were visualized in this sample, together with MenH (Figure 16 A). Further purification strategies, such as cationic and anionic exchange chromatography were applied using the Mono S HR 5x50 GL and Mono Q 5x50 GL. However, this purification strategy failed to separate MenH from all impurities, which no protein interacted with the matrix was observed to both the anionic and the cationic exchange matrixes. For all samples, MenH, as well as all impurities, were collected in the void volume of the column (Figure 16 B and C).

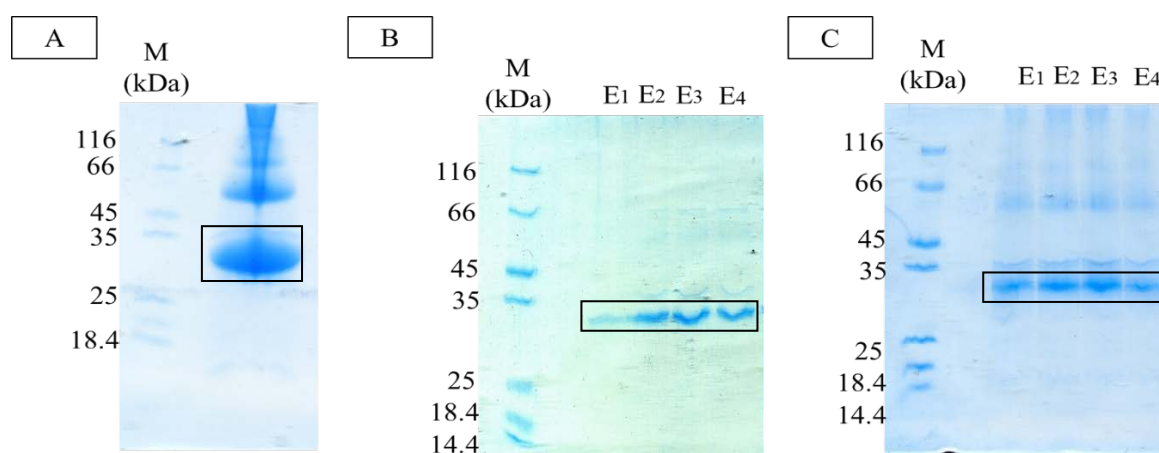


**Figure 16:** MenH purification. A: MenH sample after additional washing steps with ATP/MgCL<sub>2</sub> - CHAPS and concentration to 5 mg·mL<sup>-1</sup>. B and C: MenH after cationic (Mono S) and anionic (Mono Q) exchange chromatography, respectively. E1-4 indicate protein elution (black box, 28.6 kDa) and M indicates molecular marker, in kDa.

Once the anionic and cationic exchange columns failed, protein precipitation with ammonium sulfate (10-50% saturation) was performed as another strategy in an attempt to remove the *E. coli* impurities. Ammonium sulfate (AS) precipitation explores the relationship between solubility and ionic strength in the protein solution in a process known as “salting out”. For some proteins, with the increase of the ionic strength (e.g. salt concentration) the solubility of the protein starts to decrease and it therefore precipitates [229]. Thus, ammonium sulfate corresponding to desired salt saturation point was added into the MenH protein solution and, afterwards, the sample was centrifuged and applied in an SDS-PAGE. However, this strategy also failed and MenH, as well as all impurities, were precipitated in one single fraction (Figure 17).

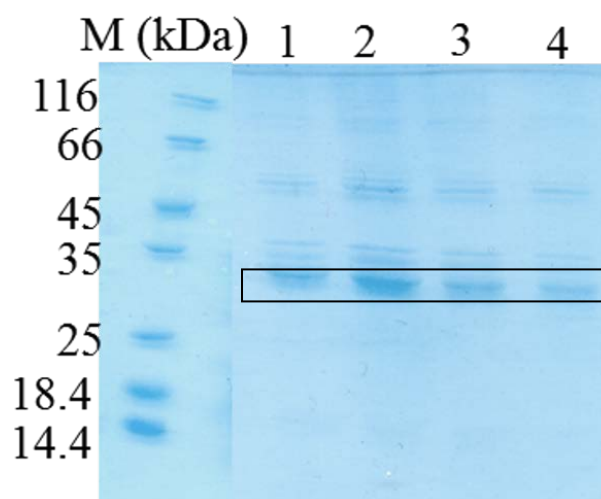
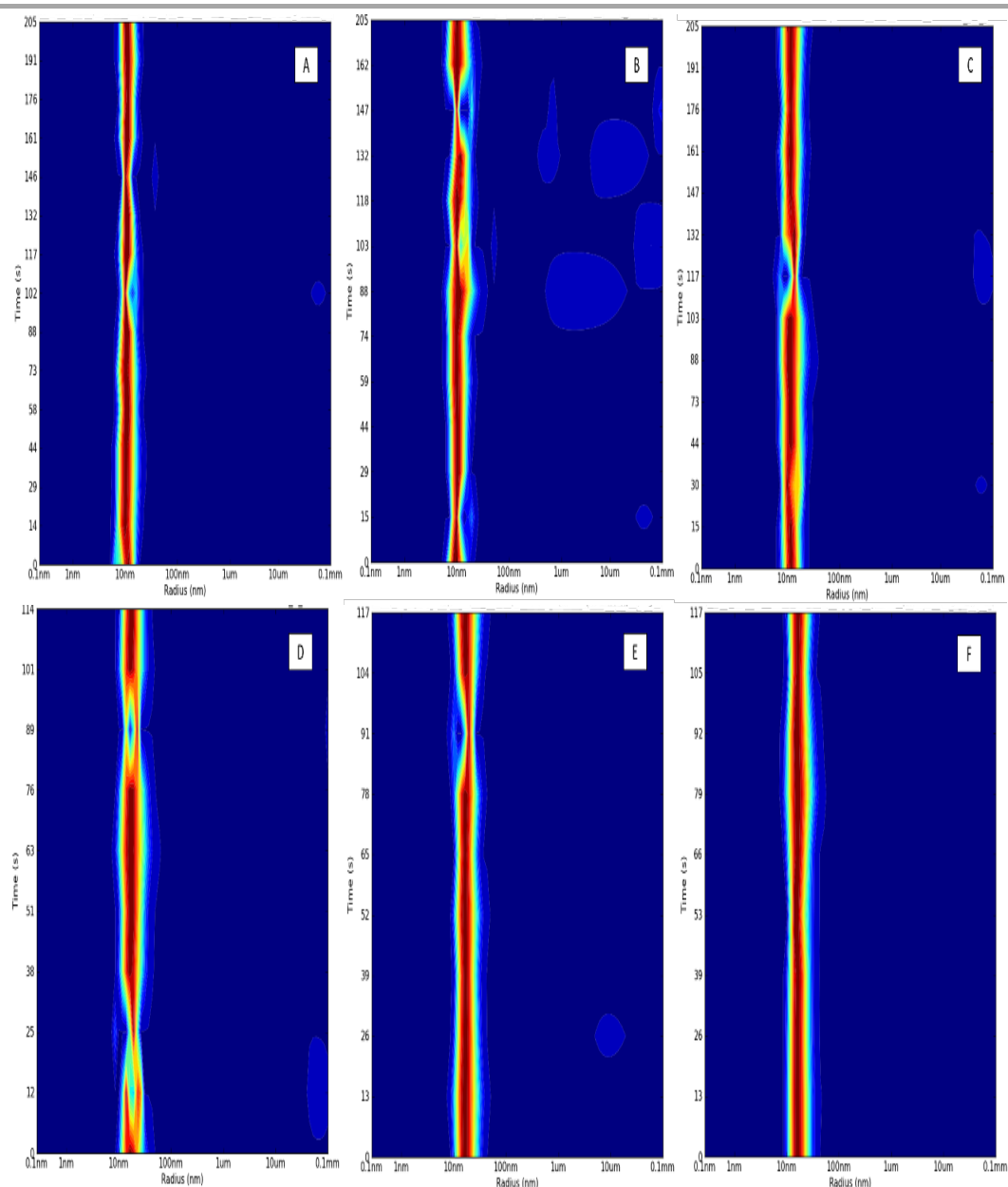


**Figure 17:** Ammonium sulfate precipitation of MenH. 1: 10-20%, 2: 20-30%, 3: 30-40% and 4: 40-50% ammonium sulfate saturation.

After affinity chromatography, followed by ATP/MgCl<sub>2</sub> – CHAPS washing steps, MenH was also evaluated regarding protein stability as well as monodispersity using DLS. Despite MenH demonstrating a high hydrodynamic radius (from 11 to 18 nm), the sample showed to be monodisperse in all buffer systems tested and the lowest hydrodynamic radius (HR) was observed for 100 mM K<sub>2</sub>HPO<sub>4</sub> pH 9.14, 100 mM NaCl with a hydrodynamic radius of  $11.8 \pm 1$  nm.

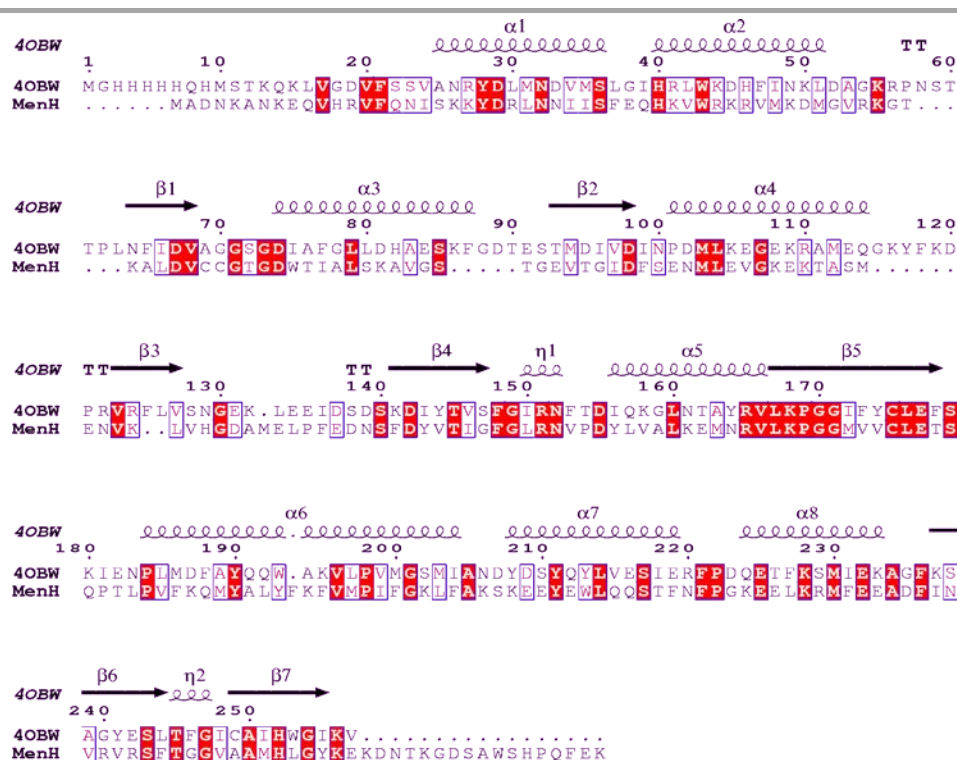
#### 5.4. MenH sequence alignment and predicted model

In order to investigate the differentiation of MenH as well as to produce a structure prediction, MenH protein sequence was submitted to the Protein Model Portal at the Expasy website ([http://www.proteinmodelportal.org/?pid=modelling\\_interactive](http://www.proteinmodelportal.org/?pid=modelling_interactive)). *Saccharomyces cerevisiae* Coq5 (S-adenosyl methionine (SAM)-dependent methyltransferase, PDB entry 4OBW) was the only homologous structure found for MenH. The overall sequence alignment is shown in Figure 19 and the structure prediction is shown in Figure 20. *S. cerevisiae* Coq5 shares a sequence identity of 30% (BLAST research using the Protein Data Bank database - [http://blast.ncbi.nlm.nih.gov/Blast.cgi?PROGRAM=blastp&PAGE\\_TYPE=BlastSearch&LINK\\_LOC=blasthome](http://blast.ncbi.nlm.nih.gov/Blast.cgi?PROGRAM=blastp&PAGE_TYPE=BlastSearch&LINK_LOC=blasthome)).

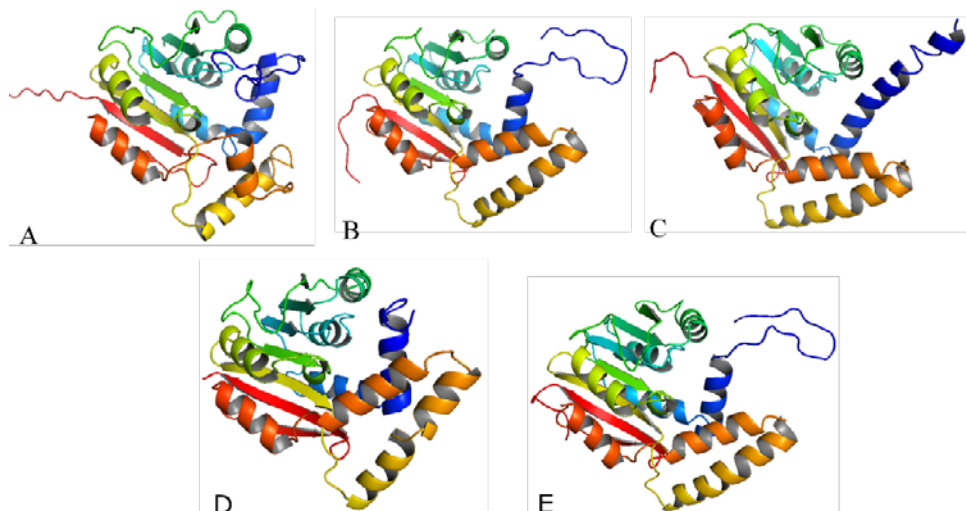


**Figure 18:** DLS of MenH in the different buffer system. A: 100 mM  $\text{Na}_2\text{HPO}_4$  pH 9.0, 100 mM NaCl HR =  $12.2 \pm 1.5$  nm. K. B: 100 mM CHES pH 9.5, 100 mM NaCl HR =  $11.8 \pm 1$  nm. C:  $\text{K}_2\text{HPO}_4$  pH 10, 100 mM NaCl HR =  $12.8 \pm 2$  nm. D: potassium phosphate pH 6.0, 100 mM NaCl HR =  $17.4 \pm 2$  nm. E: potassium phosphate pH 7.0, 100 mM NaCl HR =  $17.6 \pm 1.0$  nm. F:  $\text{K}_2\text{HPO}_4$  pH 8, 100 mM NaCl HR =  $17.6 \pm 1$  nm.

Predicted models for the monomer obtained by different programs display similar structures and MenH presents a mix of  $\alpha/\beta$  topology with disordered N- and C-terminals for some models.



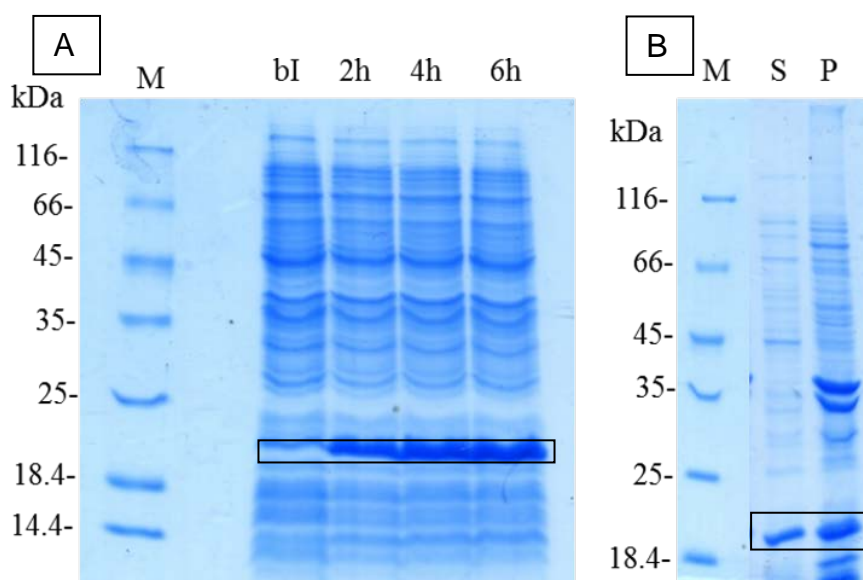
**Figure 19:** Protein sequence alignment of MenH and *S. cerevisiae* Coq5 (S-adenosyl methionine (SAM)-dependent methyltransferase, PDB entry 4OBW). Identical residues are highlighted in red boxes, similar physicochemical properties residues in blue boxes. A dashed line indicates disordered regions. The multiple sequence alignment was performed using ClustalOmega (<http://www.ebi.ac.uk/Tools/msa/clustalo/>) and ESPript (<http://esprict.ibcp.fr/ESPript/cgi-bin/ESPript.cgi>).



**Figure 20:** Predicted structure model for MenH given by A: HHpredB [256], B: intFOLD [253], C: iTASSER [257], D: M4T [258] and E: RaptorX [255]. All predicted structures were created using the *S. cerevisiae* Coq5 (PDB entry 4OBW) crystal structure. Secondary structure is colored using rainbow spectrum from N-terminus (blue) to C-terminus (red). The figure was created with the PyMOL Molecular Graphics System, Version 1.7.4 Schrödinger, LLC.

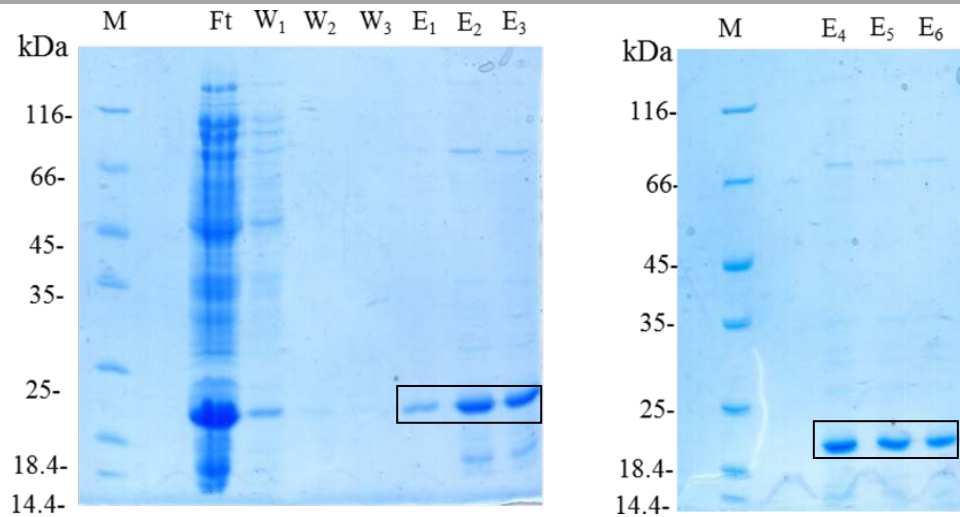
### 5.5. Recombinant expression, purification, physicochemical characterization and secondary structure estimation of DHNA-CoA thioesterase

DHNA Strep-tagged was successfully expressed using the *E. coli* expression cell BL21 DE3 at 30 °C for 6 hours in terrific broth media starting with and OD<sub>600</sub> of 0.6-0.8. After expression, the cell pellet was resuspended in buffer W for solubility tests, according to standard procedures described previously in Material and Methods. The heterologous expression profile, as well as the solubility of *S. aureus* DHNA, are shown in Figure 21.



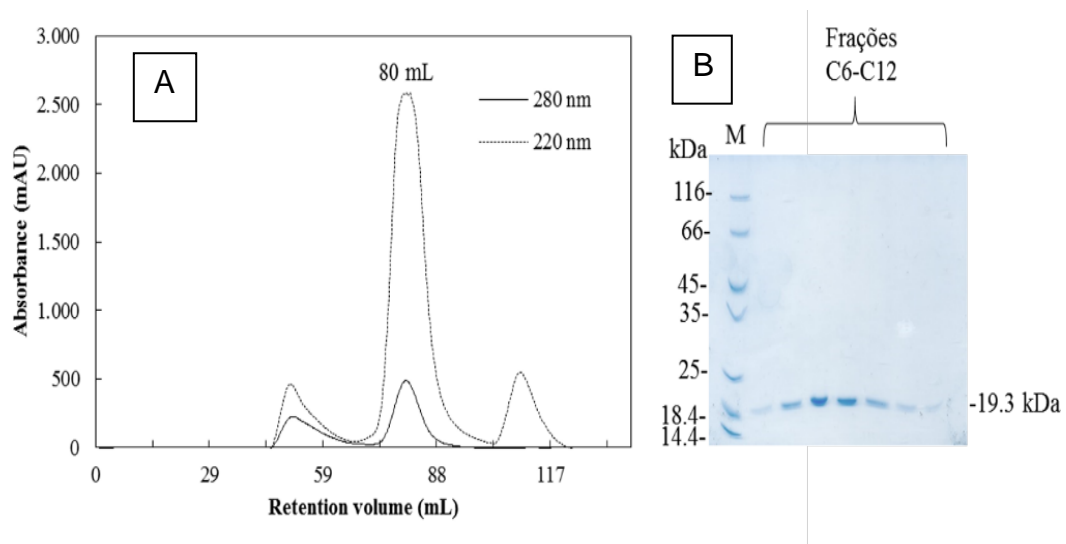
**Figure 21:** Recombinant expression profile and solubility of *S. aureus* DHNA. A: Expression profile of *S. aureus* DHNA before induction (bI) and after 2-6h (10  $\mu$ L), respectively. B: Solubility profile of *S. aureus* after expression, “S” = supernatant (soluble proteins) and “P” = pellet (insoluble proteins), M = molecular marker, in kDa. DHNA (black box, 19.3 kDa).

Once it was possible to observe the presence of soluble *S. aureus* DHNA thioesterase in the supernatant, the cleared cell lysate was submitted to affinity chromatography in a one-step Strep-Tactin matrix, in order to obtain a pure solution containing only *S. aureus* DHNA. *S. aureus* DHNA was purified, as well as some unspecific proteins impurities (Figure 22). The sequence-based molecular weight (MW) prediction for the monomeric protein DHNA was 19356.0 Da.



**Figure 22:** Cleared cell lysate submitted to affinity chromatography in a Strep-Tactin matrix. Ft - Flow through, W1-3 – wash step 1-3, E1-6 – elution step (DHNA in black box, 19.3 kDa), M – molecular marker.

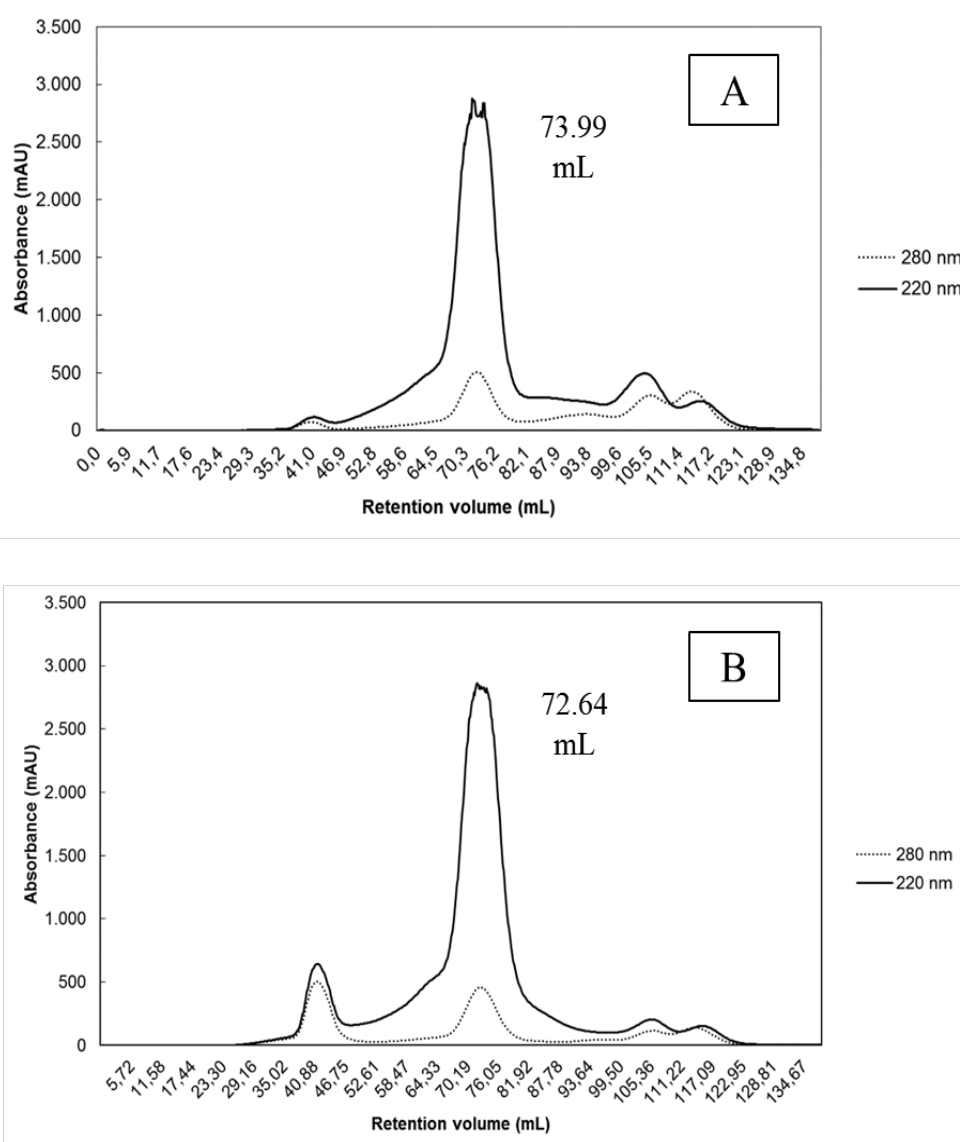
The protein eluted from the affinity chromatography was submitted to a buffer exchange in 100 mM Tris/HCl buffer pH 6, 100 mM NaCl, concentrated and applied to a size exclusion chromatography exchange. According to the calibration curve, DHNA eluted corresponds to a tetramer (Figure 23).



**Figure 23:** Affinity chromatography of *S. aureus* DHNA. A: Chromatogram profile of DHNA, which was eluted with 80 mL corresponding to a tetramer and B: SDS of the collected fractions, confirming cleanness of the sample.

In addition, mutations of DHNA, D16A and E31N, were prepared and purified by affinity chromatography, following the established protocol for native DHNA. Both mutations were dialyzed in 100 mM Tris/HCl buffer pH 6, 100 mM NaCl and applied to a size exclusion chromatography exchange previously equilibrated with 100 mM Tris/HCl buffer pH 6, 200 mM NaCl. As expected, both mutations were eluted as a tetramer (Figure 24).

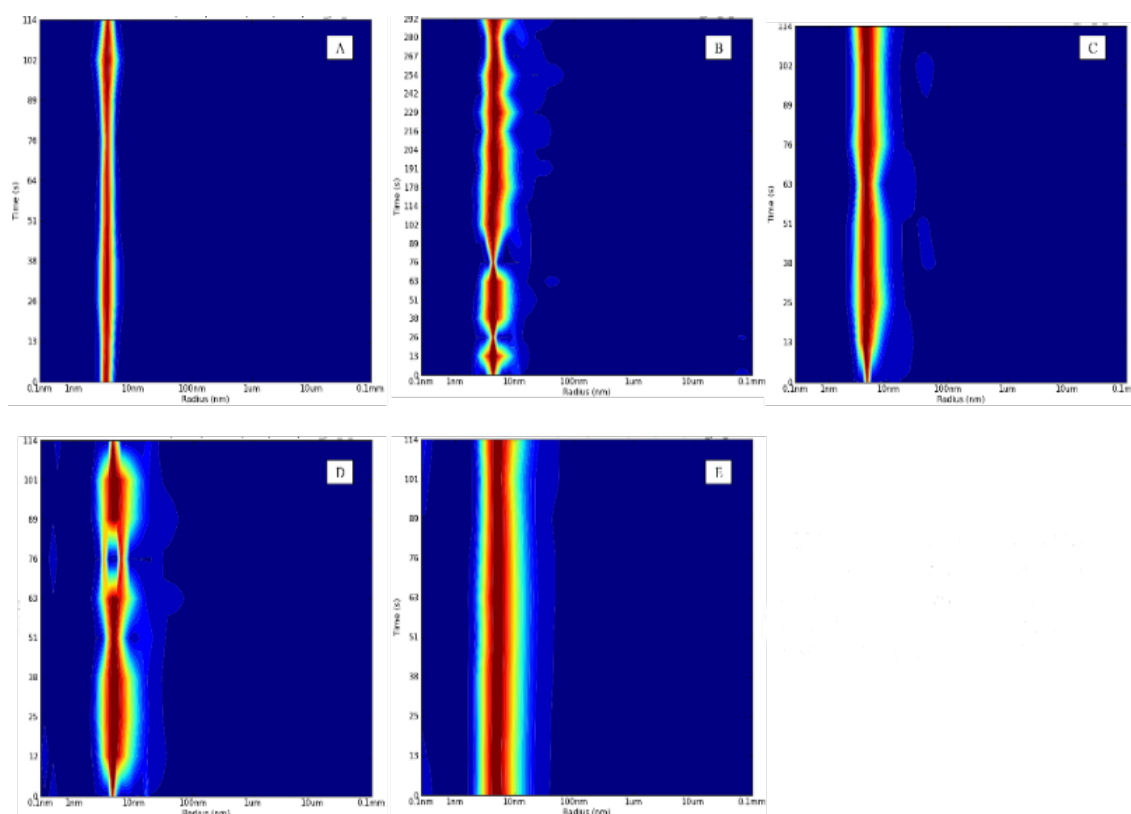
All fractions corresponding to the tetramer after size exclusion were pooled and submitted to buffer exchange in 100 mM Sodium phosphate buffer pH ranging from 6-8, 150 mM NaCl to investigate the influence of pH on the *S. aureus* DHNA oligomerization state and stability.



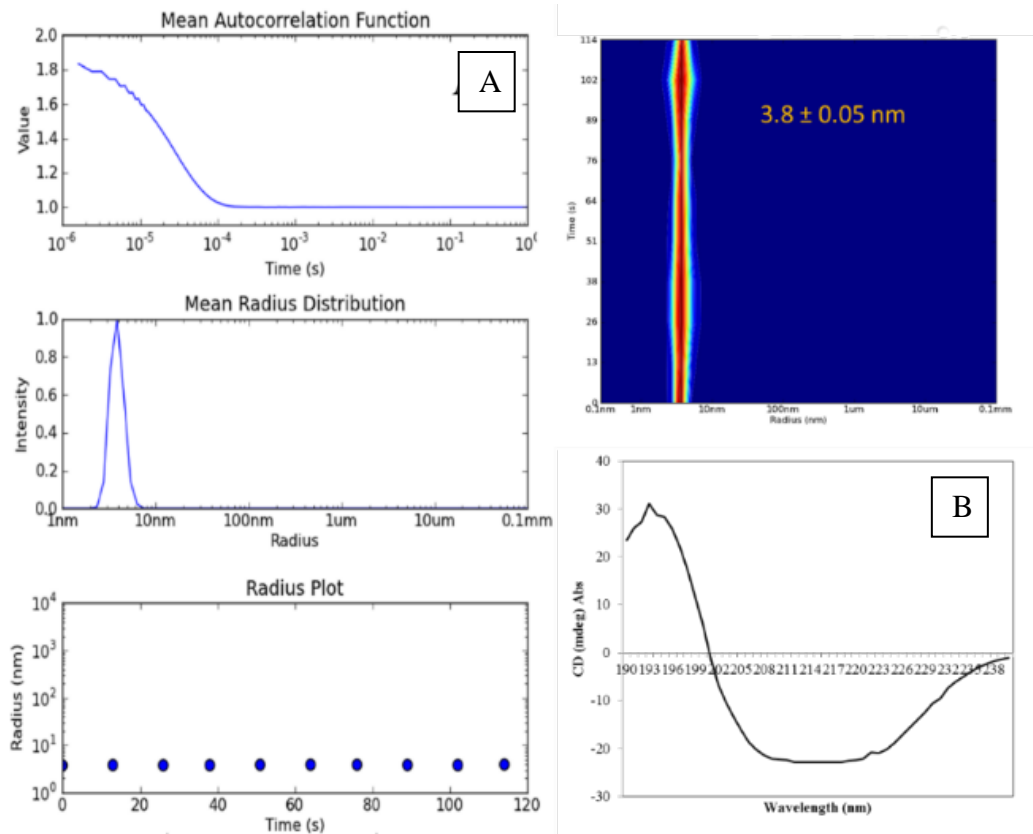
**Figure 24:** Affinity chromatography of *S. aureus* DHNA mutants. A: Chromatogram profile of D16A, eluted with 74 mL and B E31N variant, eluted with 72.6 mL. In both chromatographs, DHNA mutants correspond to a tetramer.



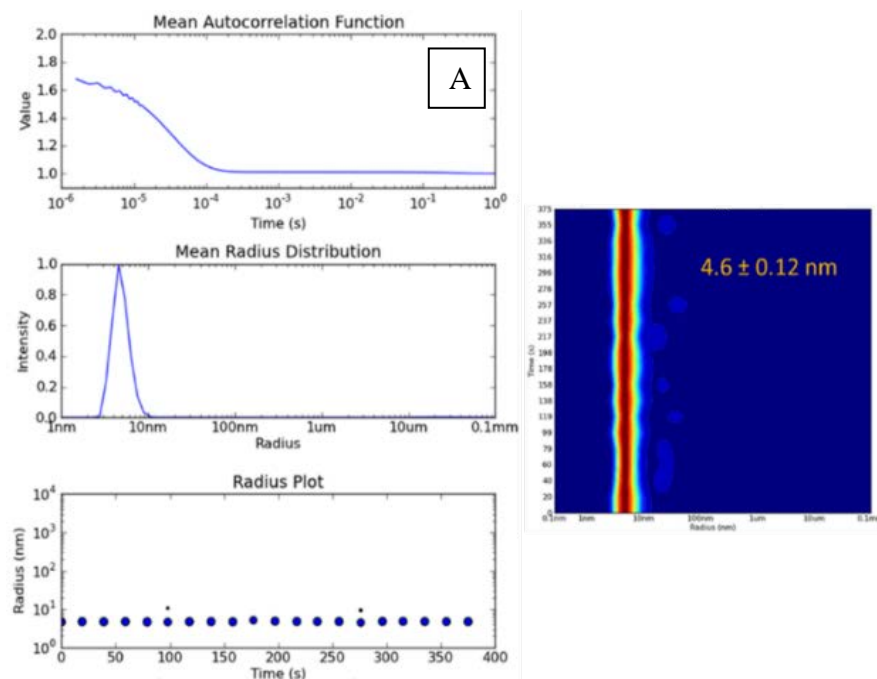
The native sample was concentrated to  $2 \text{ mg}\cdot\text{mL}^{-1}$  and the dispersity of the protein in solution was analyzed using dynamic light scattering (DLS). Among all pHs, pH 6.0 demonstrated the oligomeric state of a tetramer (70.75 kDa) and a hydrodynamic radius of 3.8 nm in a sample solution corresponding to  $2 \text{ mg}\cdot\text{mL}^{-1}$  (Figure 25). The same sample was analyzed using CD spectroscopy to verify the secondary structure. *S. aureus* DHNA thioesterase, according to Yang's reference [234,259], demonstrated to be composed of 50%  $\beta$ -sheets, 22%  $\alpha$ -helices, 4% turns and 24% other structures (Figure 26). Samples of the native, DHNA-D16A and DHNA-E31N mutants were also concentrated up to  $13 \text{ mg}\cdot\text{mL}^{-1}$  and  $10 \text{ mg}\cdot\text{mL}^{-1}$ , respectively, and the dispersity of the protein in solution was observed. Native and mutated versions of DHNA thioesterase showed similar hydrodynamic radius (Figure 27). This result indicates that *Sa*DHNA thioesterase is stable at high concentrations and a mutation on D16A does not affect the stability of the enzyme.



**Figure 25:** Dynamic Light Scattering of *Sa*DHNA-CoA thioesterase in pH A: 6.0 HR:  $3.8 \pm 0.1 \text{ nm}$ , B: 6.5 HR:  $4.8 \pm 0.2 \text{ nm}$ , C: 7.0 HR:  $4.6 \pm 0.1 \text{ nm}$ , D: 7.5 HR:  $5.3 \pm 1 \text{ nm}$  and E: 8.0 HR:  $5.6 \pm 0.2 \text{ nm}$ . With the increase of pH the hydrodynamic radius and molecular weight also increase, indicating that in high pH there is a direct interference in the protein stability.



**Figure 26:** Dynamic Light Scattering of SaDHNA-CoA thioesterase. A: Detailed DLS measurements in pH 6 and B: CD spectrum of *S. aureus* DHNA thioesterase. The folding state of *S. aureus* DHNA thioesterase was monitored in far the UV spectrum (190-260 nm) at 20 °C. All 10 measurements were accumulated.



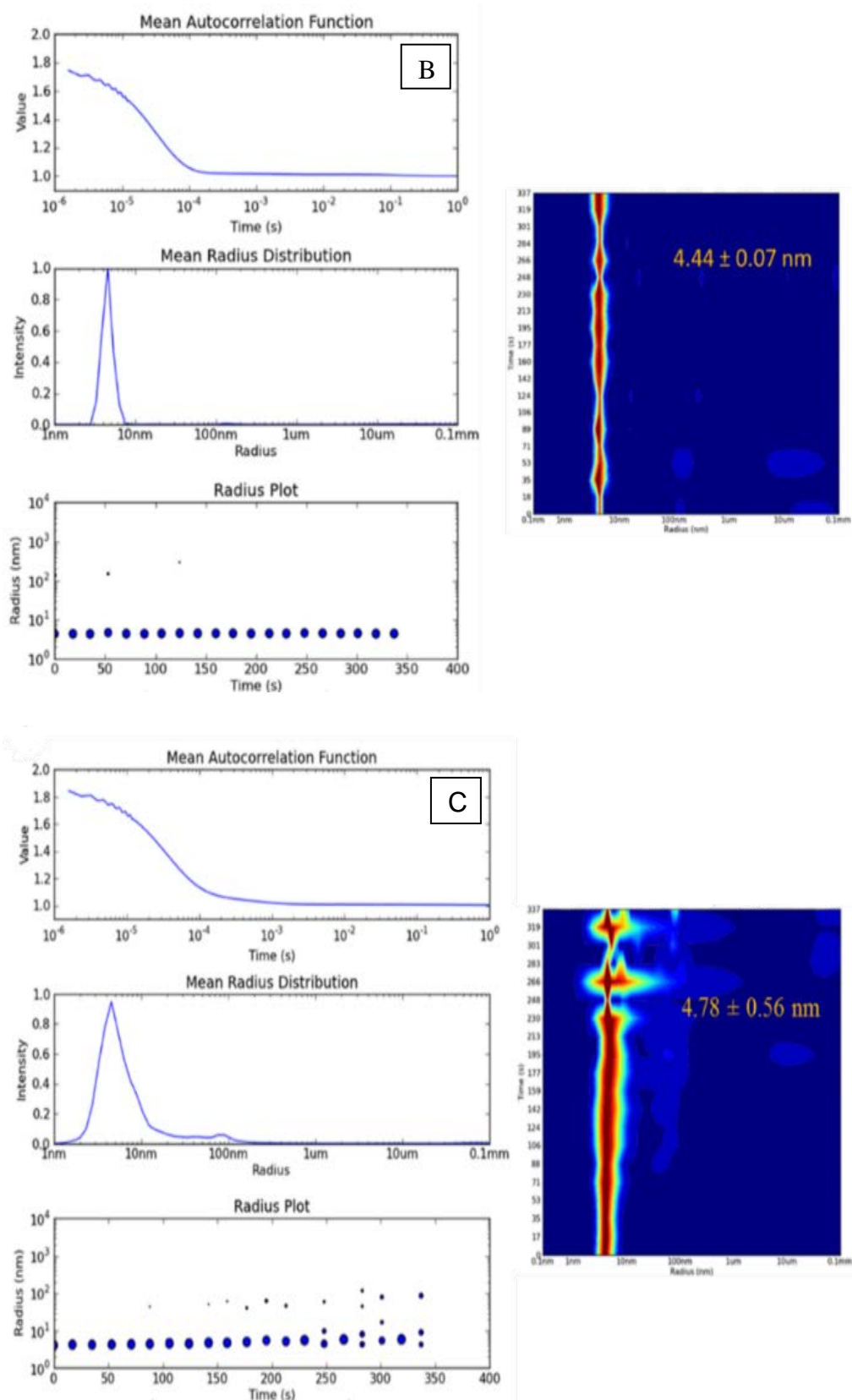


**Figure 27:** Dynamic Light Scattering of native and variants of *S. aureus* DHNA thioesterase. A: Native enzyme at a concentration of  $13 \text{ mg mL}^{-1}$  ( $\text{HD} = 4.6 \pm 0.1 \text{ nm}$ ), B: D16A mutation enzyme at a concentration of  $10 \text{ mg mL}^{-1}$  ( $\text{HD} = 4.44 \pm 0.1 \text{ nm}$ ) and C: E31N mutation enzyme at a concentration of  $10 \text{ mg mL}^{-1}$  ( $\text{HD} = 4.8 \pm 0.6 \text{ nm}$ ).

## 5.6. Crystallization experiments of *S. aureus* native DHNA, D16A and E31N variants

Despite all the efforts in order to produce large quantities of expressed protein, due to purification issues and protein instability, MenF and MenH were not suitable for further characterizations and crystallization experiments.

Initial crystallization screening of DHNA was carried out with DHNA Strep-tagged purified via Strep-tactin matrix and dialyzed against 100 mM Sodium phosphate pH 6 and 150 mM NaCl buffer overnight. Dispersity of the protein solution was checked by DLS prior to crystallization experiments: 15  $\mu$ L of protein solution were filled into an optical cuvette.

The stable *S. aureus* DHNA protein solution was concentrated to 10 mg·mL<sup>-1</sup> using a centrifugal filter device with a cut-off of 3.000 Da (Millipore, USA) and submitted to crystallization using commercially available crystallization kits. In total, 384 conditions were tested applying the JCSG-plus, Stura FootPrint & MacroSol, JBScreen Classic HTS II and Morpheus screening kits.

After 3-5 days sea urchin shaped protein crystals were observed in the C1-C3 Stura FootPrint & MacroSol conditions of 100 mM HEPES pH 8.2, 30-60% (v/v) PEG 550 MME. However, the crystals grown were too small to X-ray analysis.

A condition which initial crystals was further optimized by varying the pH of the buffer, as well as adding different lithium sulfate and ammonium sulfate salt concentrations in 48-well MRC plates. Varying the salt concentrations (0.25-2M), X-ray suitable crystals grew in the presence of 1 M lithium sulfate. Single and large crystals of native *S. aureus* DHNA thioesterase were obtained in a condition containing 100 mM HEPES pH 7.0, 1 M lithium sulfate at 20 °C in a sitting drop, vapor diffusion setup after one week (Figure 28 A-E). Native protein crystals had dimensions of 0.4 x 0.2 x 0.05 mm<sup>3</sup>. Experiments performed using hanging drop vapour diffusion and microseeding were ineffective to produce DHNA protein crystals.

Further crystallization experiments with DHNA variants were carried out in order to analyze the influence of single mutations on the protein activity and stability. The native DHNA construct was used as a template in an SDM PCR reaction.

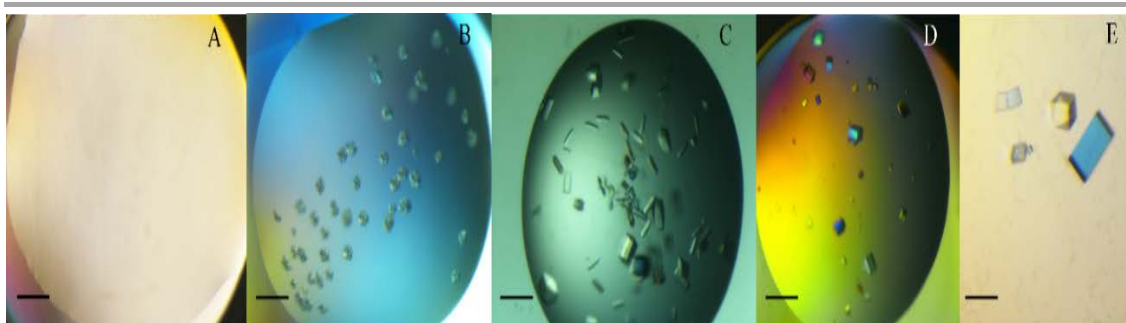


**Figure 28:** Crystals of *S. aureus* DHNA. A: Initial crystallization drop B: protein crystals applying from Stura FootPrint & MacroSol 100 mM HEPES pH 8.2, 30-60% (v/v) PEG 550 MM. C: Crystals achieved after manual conditions optimization (1:1 protein: precipitant) containing 100 mM HEPES pH 7.0, 1 M lithium sulfate. D: DHNA crystals obtained at pH 8.5. E: DHNA crystals obtained at pH 7.0 in detail. Protein concentration in all conditions was  $10 \text{ mg}\cdot\text{mL}^{-1}$ . Scale bar corresponds to 0.1 mm.

Mutagenic studies revealed that the solubility of D16A and E31N mutants did not decrease, in comparison to native DHNA. Both mutants could be concentrated up to  $18 \text{ mg}\cdot\text{mL}^{-1}$ . On the other hand, the E31N stability decreased in comparison to native DHNA.

The DHNA-D16A mutant demonstrated an outstanding stability. Purified protein samples continue to be suitable for crystallization for weeks after protein purification. Using similar crystallization conditions established for native DHNA, the D16A protein was successfully crystallized. In addition, the influence of pH on the crystal quality was also verified. Several protein crystals were obtained at pH 7.5, 8.2 and 8.5. Higher pHs than pH 8.5 were not suitable to obtain protein crystals, once none crystals were observed in pH 9. It is noteworthy that with increasing pH, the size of the crystals tended to be smaller and the crystals turned out to be more fragile to manipulation. The largest DHNA-D16A crystal was observed at pH 7.0 and possessed the following dimensions  $0.1 \times 0.2 \times 0.03 \text{ mm}^3$  (Figure 29 A-D).

Furthermore, DHNA-E31N was also crystallized in a condition containing 100 mM HEPES pH ranging from 7.0 to 8.5, 1 M lithium sulfate at  $20 \text{ }^\circ\text{C}$  in a sitting drop, vapor diffusion setup and crystals appeared after one week (Figure 30 A-C). Likewise, as for the native and D16A variant, the largest DHNA-E31N protein crystal was observed in a condition containing mother liquor at pH 7.0.

In order to obtain detailed information regarding the active site and since no detectable activity was observed for the E31N variant, co-crystallization trials with the substrate were performed. DHNA-E31N protein was mixed with the substrate stearyl-

CoA in a molar ratio of 1:5 (protein solution: substrate) and submitted to protein crystallization, using the same conditions described above. After two weeks, DHNA-E31N protein crystals were obtained for all different pH (7.5 to 8.5), except for pH 7.0 (Figure 30 D-F).

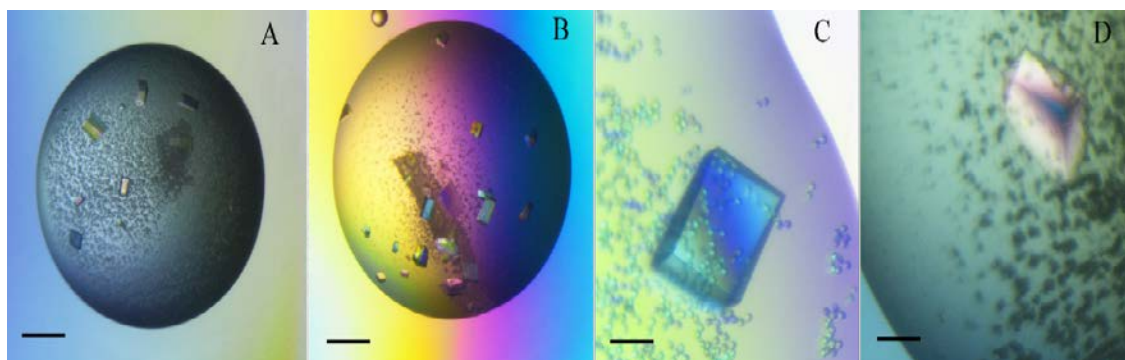


**Figure 29:** Crystals from *S. aureus* DHNA-D16A. A: Protein crystals obtained at pH 7.0 using the same condition used to crystallize native DHNA (reservoir solution 100 mM HEPES pH 7.0, 1 M lithium sulfate, 1:1 protein: precipitant). B: D16A protein crystals obtained at pH 8.5. C: DHNA-D16A protein crystal at pH 7.0, 1 M lithium sulfate. D: DHNA crystal obtained in pH 8.5. The protein concentration in all conditions was  $10 \text{ mg}\cdot\text{mL}^{-1}$ . Scale bar corresponds to 0.1 mm.

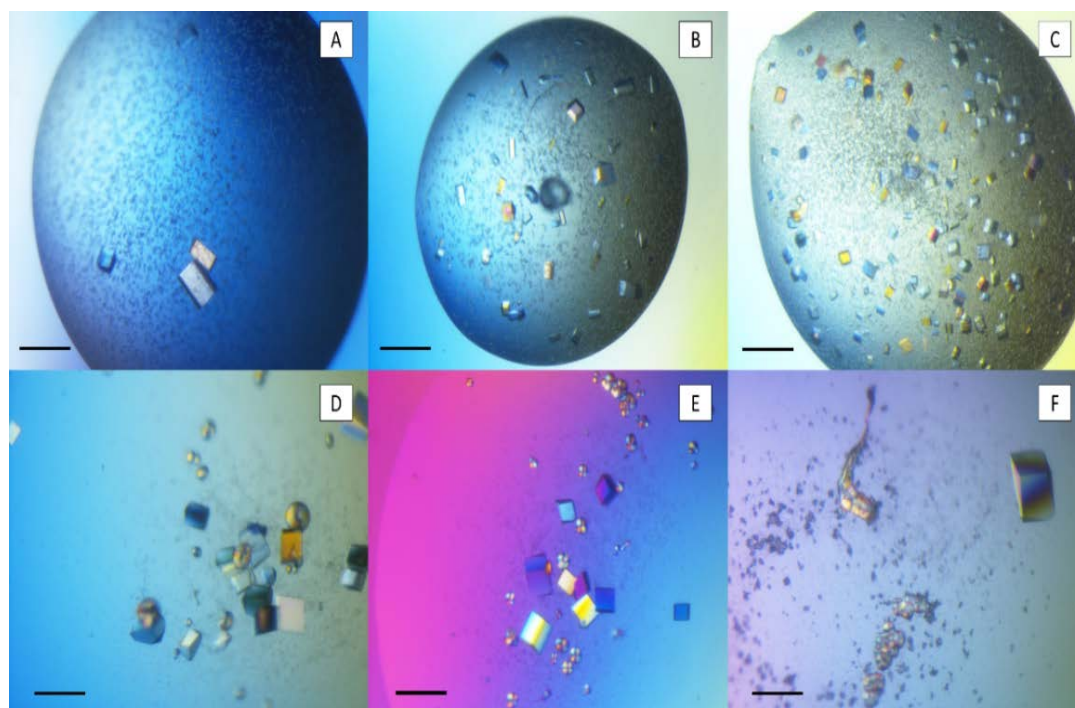


**Figure 30:** Protein crystals of DHNA-E31N mutant obtained using the sitting drop vapour diffusion technique in condition 1 M lithium sulfate, 100 mM HEPES. A: pH 7.5, B: pH 8.2 and C: pH 8.5. D-F are DHNA-E31N protein crystals obtained after incubation with 1 mM Stearoyl-CoA in pH 7.5, 8.2 and 8.5, respectively. The protein concentration in all conditions was  $10 \text{ mg mL}^{-1}$ . Scale bar corresponds to 0.1 mm.

## 5.7. Diffraction data collection, data processing and model building of *S. aureus* DHNA

An *S. aureus* native DHNA data set was collected at 100 K at the Petra III P14 EMBL beamline. Before data collection, a *Sa*DHNA crystal drop was complemented with 15 % (v/v) glycerol. Diffraction data were collected up to 1.3 Å resolution using the oscillation method (0.1 degrees) and indexed, integrated and scaled with XDS from a single crystal. Data were cut to 1.5 Å monitoring  $R_{\text{merge}}$  and  $I/\sigma$ . Diffraction data from the soaked DHNA-Pt crystal were collected to 2.0 Å resolution using the oscillation method (0.1 degrees), indexed, integrated and scaled in the same way as for the DHNA native dataset. The *Sa*DHNA crystal belongs to the monoclinic space group  $P2_1$  with unit cell dimensions of  $a = 53.46$  Å,  $b = 90.47$  Å,  $c = 75.12$  Å and  $\beta = 92.0^\circ$ . The Matthews coefficient was calculated to be  $2.36$  Å<sup>3</sup> Dalton<sup>-1</sup>, corresponding to a solvent content of 47.9 % with four molecules in the asymmetric unit. The final model, after molecular replacement using native DHNA, has an  $R_{\text{work}}$  of 14.97 % and a  $R_{\text{free}}$  of 17.85 % and 373 water molecules. The model shows a good geometry and only one Ramachandran outlier (Aspartic acid, position 115). The following Table 11 summarizes the data collection, processing and refinement statistics of *S. aureus* DHNA.

**Table 11:** Data collection and refinement statistics from *S. aureus* DHNA.

	Native DHNA <sup>a</sup>	DHNA-Pt <sup>a</sup>
Beamline	P13 Petra III	P14 Petra III
Detector	Pilatus 6M	Pilatus 6M
Wavelength (Å)	1.0332	1.072
Temperature (K)	100	100
Oscillation range (°)	0.1	0.1
Crystal-to-detector distance (mm)	170.32	236.16
Exposure time (s)	0.037704	0.037704
<b>Data-integration statistics</b>		
Space-group	$P2_1$	$P2_1$
Unit-cell parameters a, b, c (Å)	53.46, 90.47, 75.12,	55.20, 90.90, 74.80
$\beta$ (°)	92.09	90.8
Resolution range (Å)	57.02-1.5 (1.58-1.5)	55.29-2.00 (2.10-2.0)
Total no. of reflections	771011	680773
No. of unique reflections	113731	97013
Multiplicity	6.8 (6.9)	6.9 (6.6)
Completeness (%)	99.6 (99.9)	98.2 (98.4)
$R_{\text{merge}}^b$	0.04 (0.267)	0.111 (0.864)
Mean $I/\sigma$ (I)	26.1 (6.4)	16.6 (2.8)

Mosaicity	0.072	0.085
Molecules in the unit cell	4	
V <sub>m</sub> (Å <sup>3</sup> Da <sup>-1</sup> )	2.36	
Protein atoms	5685	
Average B-factor (Å <sup>2</sup> )	20.0	
Solvent content (%)	47.9	
Water molecules	373	
<b>Refinement and model building statistics</b>		
R <sub>work</sub> (%) <sup>a</sup>	14.97/16.84	
R <sub>free</sub> (%) <sup>b</sup>	17.85/19.25	
Ramachandran plot		
Favoured regions (%)	98.55	
Allowed regions (%)	1.27	
Residues in disallowed regions	0.18	
RMS Bonds length (Å)	0.0259	
RMS Angles (°)	2.265	

<sup>a</sup>: values in parentheses are for the highest resolution shell

<sup>b</sup>:  $R_{\text{merge}} = \frac{\sum_{hkl} \sum_i |I_i(hkl) - [I(hkl)]|}{\sum_{hkl} \sum_i I_i(hkl)}$ , where  $[I(hkl)]$  is the mean intensity of the observations  $I_i(hkl)$  of reflection  $hkl$ .

## 5.8. *S. aureus* DHNA: Structure analysis

The structure of DHNA is formed by the gathering of four identical subunits, (A=B=C=D) arranged out of two dimers, frequently referred as “dimer of dimers”. Amino acid residues 150-155 from subunits A and C, as well as the Strep-tag sequence (amino acids 156-165) in subunits B and D were disordered, consequently were omitted from the final model (Figure 31). Using the PBEQ solver [260] the electrostatic potential and solvation energy was calculated for a *Sa*DHNA tetramer by solving the Poisson-Boltzmann equation (Figure 32). The result shows that *Sa*DHNA electrostatic free energy ( $\Delta G^{\text{elec}}$ ) was  $-9516.320 \text{ kcal}\cdot\text{mol}^{-1}$  and for the monomer was  $-2676.08 \text{ kcal}\cdot\text{mol}^{-1}$ . The  $\Delta\Delta^{\text{elec}}$  of  $6.840 \text{ kcal}\cdot\text{mol}^{-1}$  shows that a significant stability towards the tetramer formation in solution.

Belonging to the 4-hydroxybenzoyl Coenzyme A thioesterase class I, each monomer of DHNA adopts a “Hotdog” fold, which comprises a long four-turn alpha helix ( $\alpha_2$ ) formed by His23-Ile38 surrounded by five-stranded antiparallel  $\beta$ -sheets (strands  $\beta_1$  to  $\beta_5$ ) and one parallel  $\beta$ -sheet  $\beta_6$  in the order 6-1-3-4-5-2 formed by Ile145-Glu147, Met1-Ile8, Val74-Ser84, Arg87-Phe95, Ala102-Leu109, Thr58-Tyr64, respectively. Three short helices  $\alpha_1$  (Tyr12-Glu14),  $\alpha_3$  (Tyr45-Gln51) and  $\alpha_4$  (Leu122-Tyr125), two beta-hairpin (Lys73-Tyr83 and Arg87-Phe95), four beta bulges (Val89-



Glu81-Lys82, Ile94-Ala102-Thr103, Glu102-Thr58-Asp59 and Asn96-Gly99-Glu100), eight beta turns (four type I, one type II, two type IV and one type VIII) and one gamma turn complete the structure, represented in Figure 33.

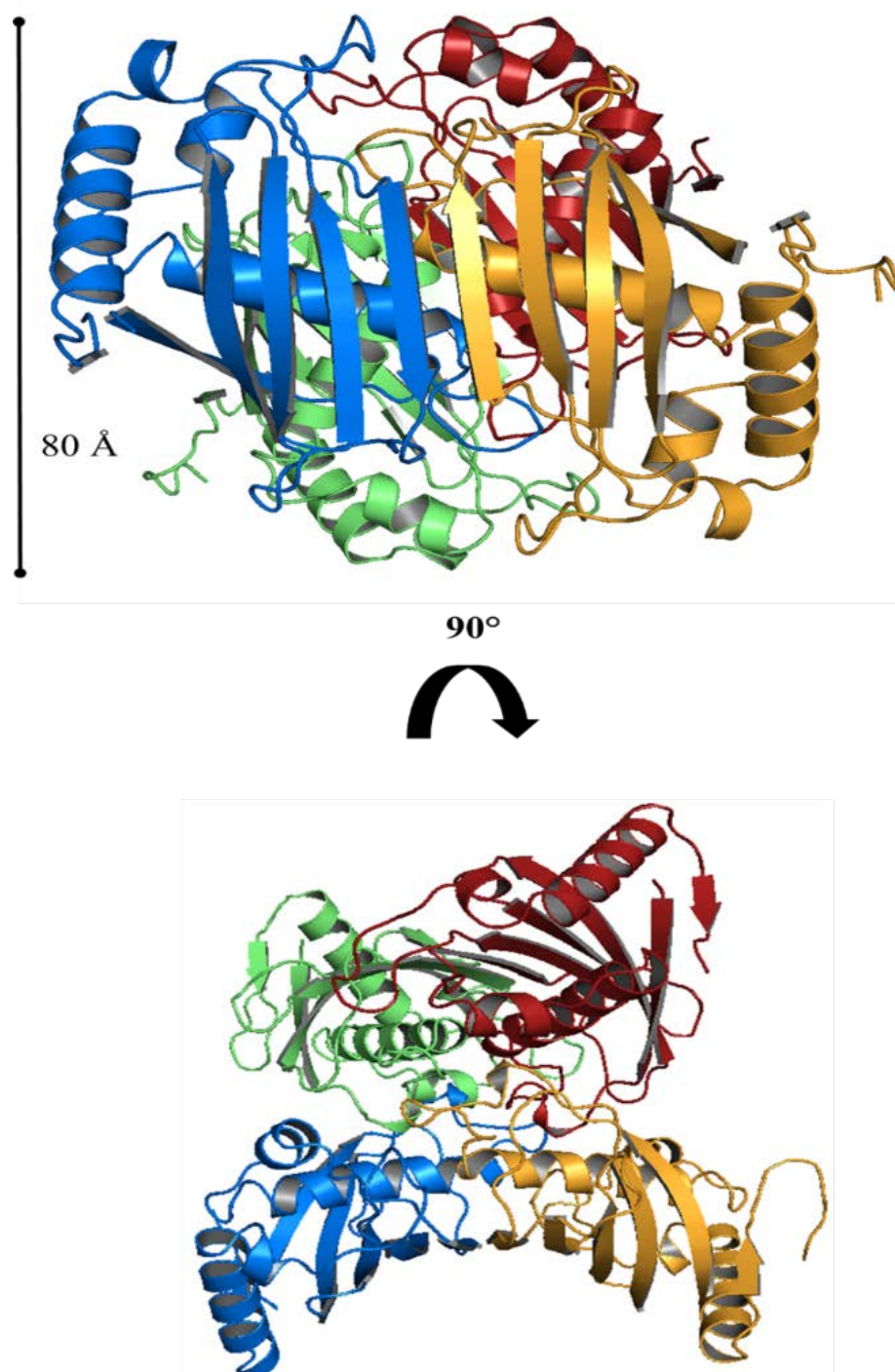


**Figure 31:** Ribbon representation of the *Sa*DHNA structure refined to 1.5 Å resolution. DHNA comprises four identical monomers, indicated by four different colors. The subunits A-D are represented in colors orange, blue, light green and dark red, respectively. The figure was created with the PyMOL Molecular Graphics System, Version 1.7.4 Schrödinger, LLC.

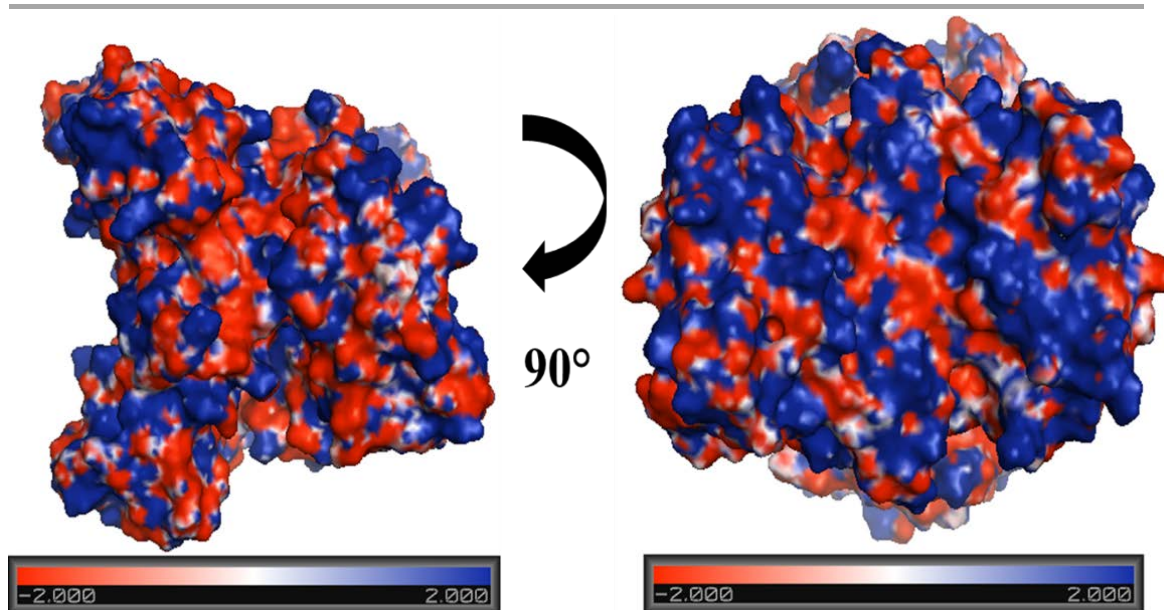


**Figure 32:** Surface charge representation for *Sa*DHNA. Residues positively charged are colored as red, negatively charged in blue and uncharged residues in grey. The figure was generated using Pymol PyMOL Molecular Graphics System, Version 1.7.4 Schrödinger, LLC.

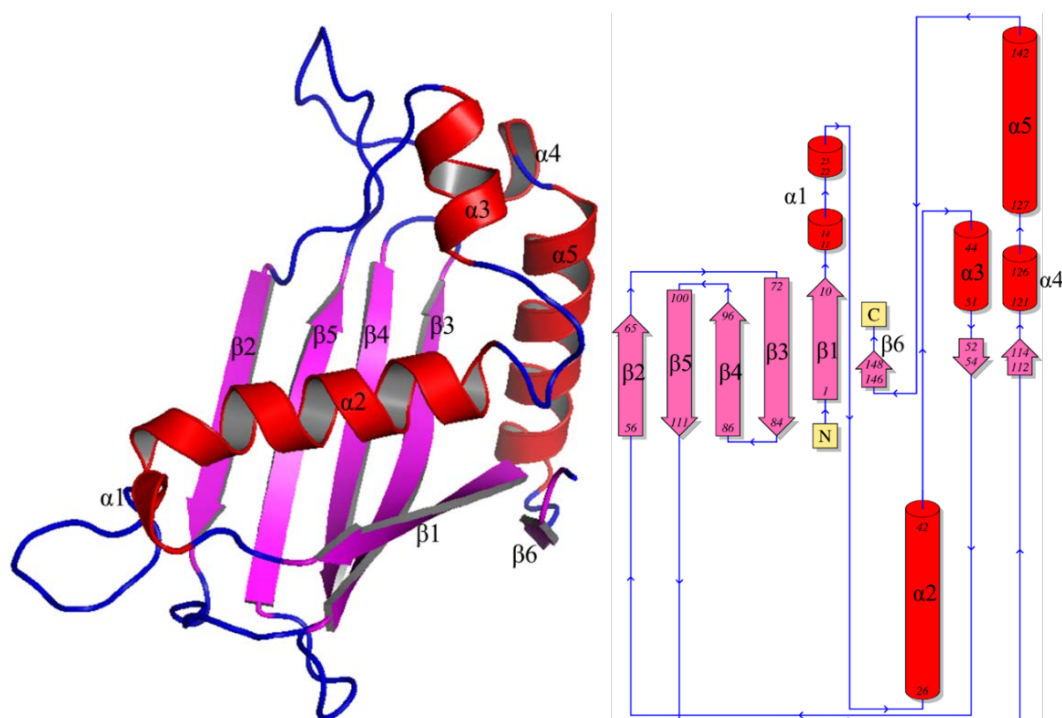


**Figure 33:** Ribbon illustration of the monomer structure of *Sa*DHNA and topology. The secondary structure of the *Sa*DHNA monomer cartoon illustration is shown (left); magenta is used for  $\beta$ -strands, red for  $\alpha$ -helix and blue for turns and loops. The respective domains are annotated and the topology plot of the HotDog-fold domain (right) is illustrated using the same colors. The figure was created with the PyMOL Molecular Graphics System, Version 1.7.4 Schrödinger, LLC. The topology figure was prepared with PDBsum [249].

Two monomers of DHNA assemble to produce the dimer stabilized by a netting of hydrogen bonds between  $\beta$ -strands  $\beta 2$  of each monomer with the main  $\alpha$ -helix ( $\alpha 2$ ) facing the other dimer. Atoms located on the  $\beta$ -strands  $\beta 2$  are responsible for the formation of nine hydrogen bonds. The H-bonds are mediated by the residues Thy58, Asp59, Asn61 and Asn63 of one monomer with amino acid residues Tyr64, Asn63, Asn61 and Asp59 from the corresponding monomer, in which each one contributes with one H-bond. Further residues Leu60, Val62 from one monomer and Val62, Leu60 from the corresponding monomer contribute with two H-bonds. This net of hydrogen bonds produces a 12-stranded antiparallel  $\beta$ -sheet (Figure 34).

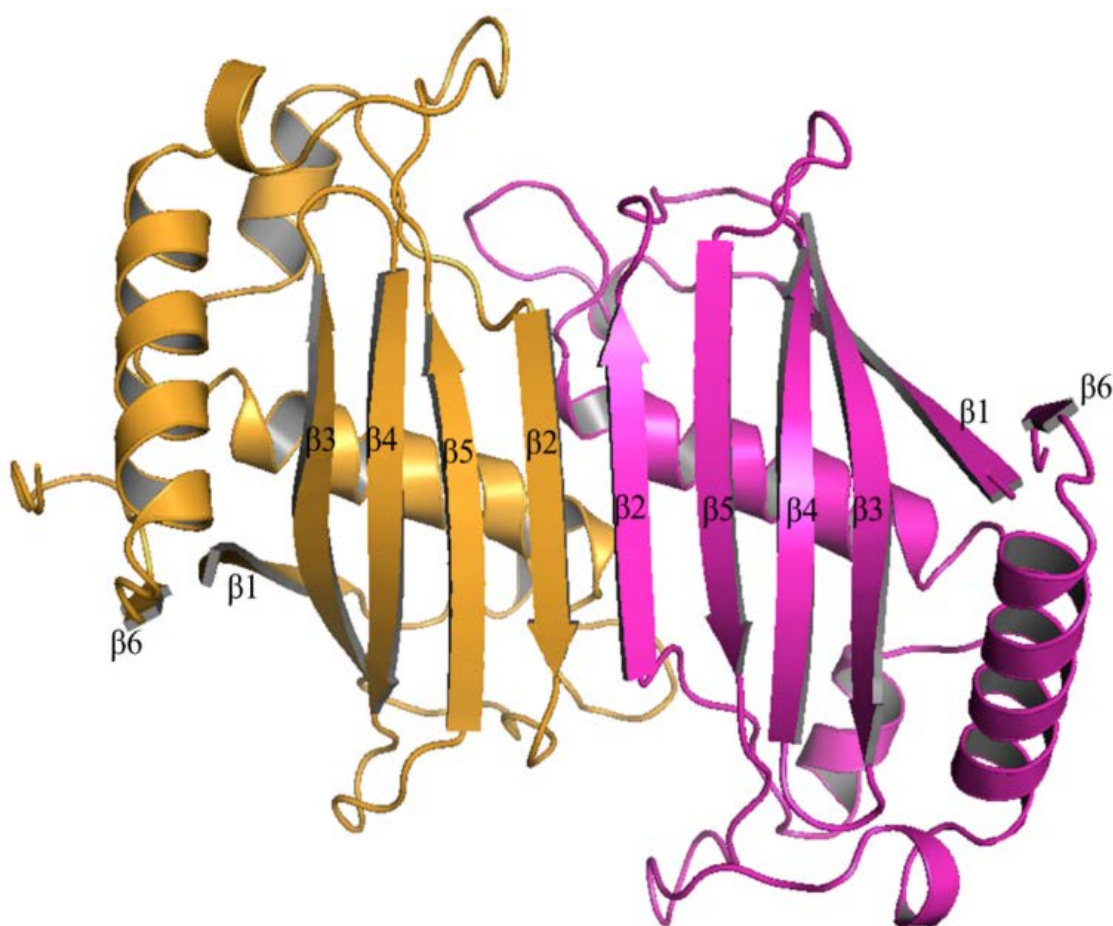


**Figure 34:** Dimerization of SaDHNA-CoA thioesterase. Hydrogen bonds formed between two monomers are responsible for the stabilization of the dimer, forming a continuous beta-sheet.

Four hydrogen bonds stabilize the interaction between monomer A-B (or C-D)  $\alpha 1$  to  $\alpha 3$ , involving the amino acid residues Lys17, Glu31, Try22 and Glu49 from one monomer and Glu49, Try22, Glu31 and Lys17 from the corresponding monomer. In

addition, two salt bridges between Lys17-Glu49 and Glu49-Lys17 complete the interaction. Between the monomers A and C, there are two hydrogen bonds responsible for the interaction involving the amino acids Thr15, Lys17 from one monomer and Lys17, Thr15 from the equivalent monomer. Among the monomers A and D, the residues Try12, Glu14, Arg11, from one monomer and Glu49, Arg11, Glu14, from the corresponding monomer are responsible for the formation of three hydrogen bonds. Between monomers B and C there is a formation of four hydrogen bonds involving Arg11, Glu14, Tyr12, Glu49 from one monomer and Glu14, Arg11, Glu49, Tyr12 from the corresponding monomer. Between the monomers B and D, there are three hydrogen bonds among the amino acid residues Met18, Lys17, Thr15 of one monomer and Tyr12, Thr15, Lys17 from the corresponding monomer. In addition, two salt bridges between Glu14 and Arg11 from one monomer and Arg11 and Glu14 of the equivalent monomer as well as hydrophobic interaction complete the stabilization (Figure 35).

In general, 38 amino acid residues are involved and situated in the interface of each monomer of the homotetramer (Table 12). The average value for the area buried involving 22/21 amino acid residues of each monomer in the A-B or the equivalent C-D (23/20) interface is  $1060 \text{ \AA}^2$ , corresponding to 11% of the total surface of  $23366.402 \text{ \AA}^2$  of the monomer. The buried surface of all monomers is  $8653 \text{ \AA}^2$ , corresponding to 33% of the total surface area of  $65484.656 \text{ \AA}^2$  of the homotetramer. In Table 12, the interface interactions of DHNA are summarized.

**Table 12:** Summary of interface data of *S. aureus* DHNA structure

Chains	No. of interface residues	Interface area ( $\text{\AA}^2$ )	No. of hydrogen bonds	No. of non-bounded contacts	No. of salt bridges
A-B	22:21	1051:1070	13	119	2
C-D	23:20	1056:1063	13	133	2
A-C	7:7	431:433	2	50	-
B-D	7:8	424:422	3	51	-
A-D	8:8	612:624	3	43	2
B-C	9:10	612:607	4	44	2

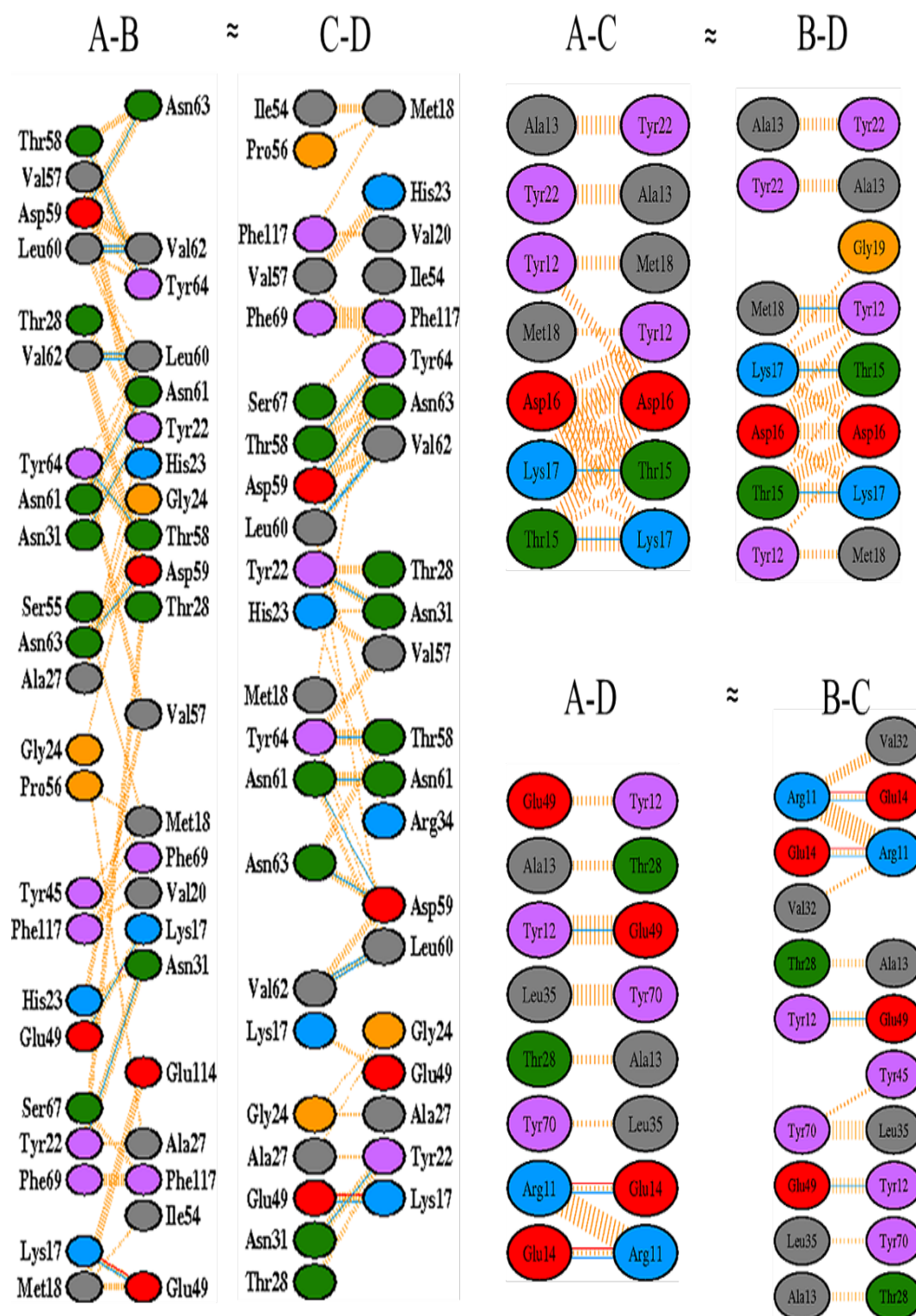


**Figure 35:** Schematic of non-covalent interactions within the *SaDHNA* tetramer, analyzed by PDBsum [248]. On top of every column, the respective interface is indicated with the letters for the amino acid chains. Based on symmetry:  $A-B \approx C-D$  and  $A-C \approx B-D$ . Amino acids are represented as ovals, whereas positively charged residues (H, K, R) are depicted in blue, negatively charged residues (D, E) in red, neutral (S, T, N, Q) in green, aliphatic residues (A, V, L, I, M) in grey, aromatic residues (F, Y, W) in purple and P and G in orange. Interactions are highlighted with dashed orange lines for non-bonded interactions, red lines for salt bridge interactions and blue lines for hydrogen bonds.

## 5.9. 4-Hydroxybenzoyl CoA thioesterase structure comparison

In an attempt to investigate the differentiation of DHNA thioesterase, a protein sequence comparison analysis between *S. aureus* DHNA and other thioesterases to *Pseudomonas* sp. CBS-3 (PDB entry 1LO7, RMSD: 1.8Å), *Photobacterium profundum* (PDB entry 3R87, RMSD: 2.0Å) and a hypothetical protein with possible thioesterase function from *Thermus thermophilus* (PDB entry 1Z54; RMSD: 1.2 Å) homologs was performed.

The overall sequence alignment is shown in Figure 36 and the structure comparison is shown in Figure 37. *Pseudomonas* sp. CBS-3 4-hydroxybenzoyl CoA thioesterase (4-HBT) has a sequence identity of 21%, *P. profundum* shares a 25% identity and *T. thermophilus* 27% ([http://blast.ncbi.nlm.nih.gov/Blast.cgi?PROGRAM=blastp&PAGE\\_TYPE=BlastSearch&LINK\\_LOC=blasthome](http://blast.ncbi.nlm.nih.gov/Blast.cgi?PROGRAM=blastp&PAGE_TYPE=BlastSearch&LINK_LOC=blasthome)). The residue Asp16 (numeration according to *Sa*DHNA), is well conserved in those proteins. The residue Trp47 in *Ps*HBT is substituted by Tyr45 in *S. aureus* DHNA, as well as Asp32 with Glu31, a conservative replacement.

Despite the low identity among all thioesterases, the secondary structures are well conserved and only slight differences between structures were observed, as shown in Figure 37. In comparison between *S. aureus* DHNA and TT1821 hypothetical protein from *T. thermophilus* (light pink), a longer loop between residues 112-118 is observed in *S. aureus* DHNA, as well as the existence of an extra parallel  $\beta$ -strand ( $\beta_6$ ), which comprises the amino acid residues 140-155. Regarding the *Pseudomonas* 4-HBT structure (cyan), *Ps*HBT has a longer loop, comprising the residues between 102-107 and the antiparallel  $\beta$ -strand  $\beta_6$  (residues 126-130) interacts with  $\beta$ -strand  $\beta_5$ , whereas in *S. aureus* DHNA this  $\beta$ -strand  $\beta_6$  (residues 138-155) interacts with  $\beta$ -strand  $\beta_1$ . Finally, the *P. profundum* Orf6 structure has an elongated three turn- $\alpha_2$  (corresponding to  $\alpha_3$  in *S. aureus* DHNA) and  $\alpha_4$  (*S. aureus* DHNA) as well as the residues 136-155, corresponding to  $\beta$ -strand  $\beta_6$ , were absent.

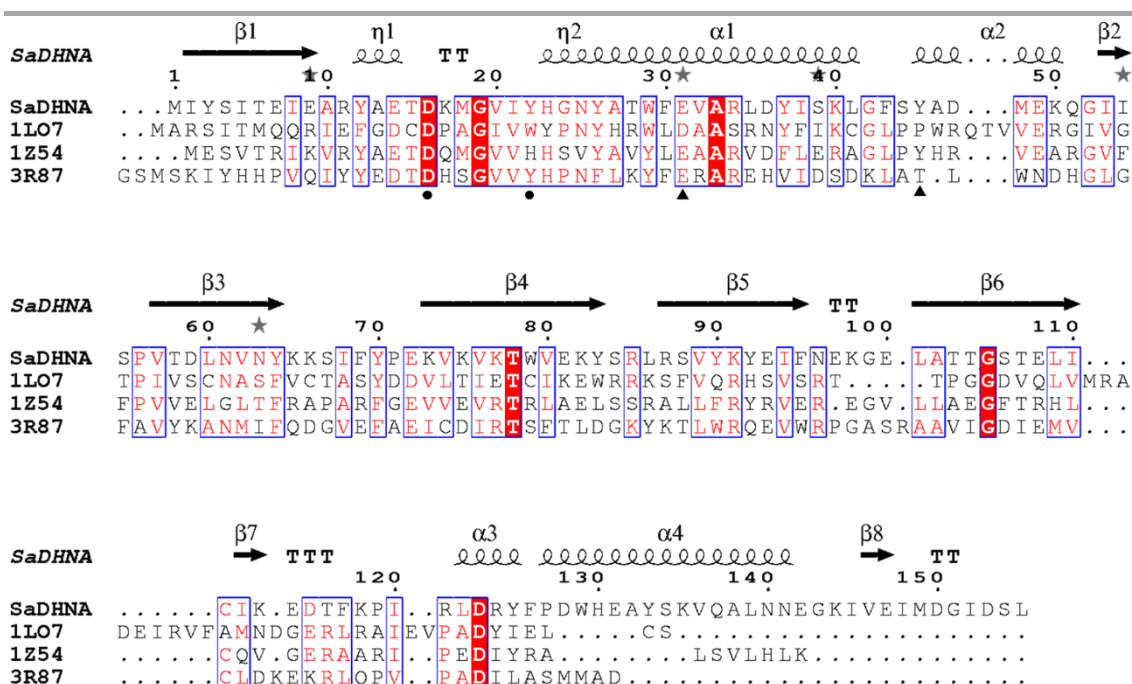


**Figure 36:** A multiple sequence alignment was performed using ClustalOmega, representation was generated with ESPrit [261]. Identical residues are highlighted in red boxes, similar physicochemical properties residues in blue boxes. A dashed line indicates disordered regions. The black circles below the sequence indicate the residues responsible for the activity and triangles represent residues, which stabilize the substrate binding. *Pseudomonas* sp. CBS-3 (PDB entry 1LO7), *Photobacterium profundum* (PDB entry 3R87), and a hypothetical thioesterase from *Thermus thermophilus* (PDB entry 1Z54).

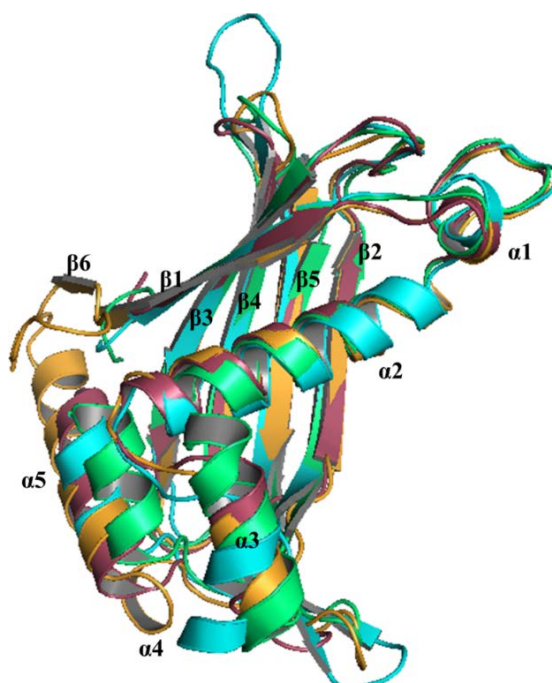


**Figure 37:** 4-Hydroxybenzoyl CoA thioesterase structure comparison. Structure comparison between *S. aureus* DHNA thioesterase (orange) with *Thermus thermophilus* hypothetical thioesterase TT1821 (light pink), *Pseudomonas* sp. CBS-3 4-HBT (cyan) and *Photobacterium profundum* Orf6 thioesterase (green). The figure was created with the PyMOL Molecular Graphics System, Version 1.7.4 Schrödinger, LLC.

### 5.10. Putative active site of *S. aureus* DHNA and thioesterase activity

In order to obtain detailed information about the location of the putative active site of DHNA, the coordinates of DHNA were superimposed with the coordinates from the mutated *Pseudomonas* sp. 4-Hydroxybenzoyl CoA thioesterase - *PsHBT*, (PDB 1LO9) in complex with the substrate 4-hydroxybenzoyl-CoA. The putative active sites of DHNA in the interface region between two monomers in the quaternary structure of a homotetramer, resulting in four active sites, as shown in Figure 38.

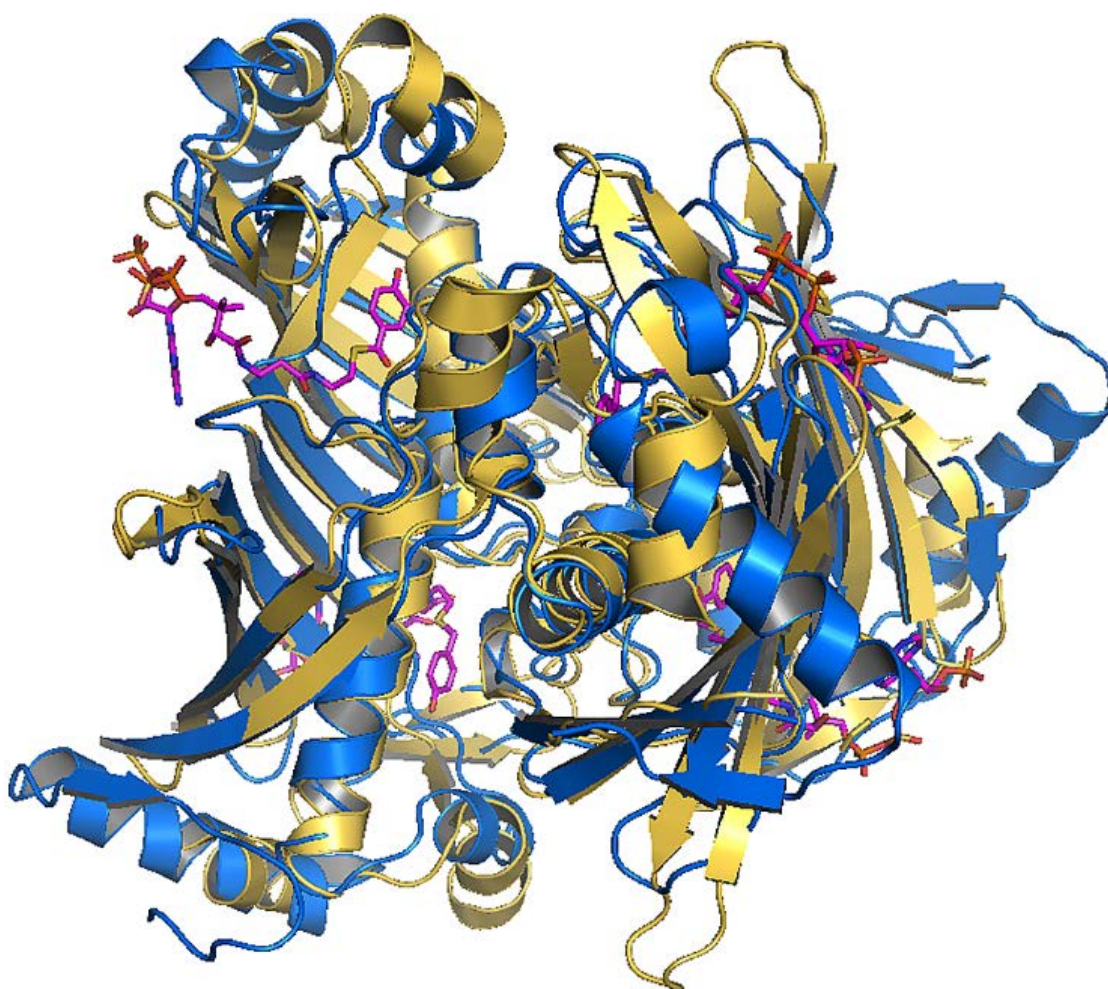


**Figure 38:** Structural comparison of *Pseudomonas* 4-HBT active site (PDB entry 1LO7) with DHNA-CoA thioesterase of *S. aureus*. Ribbon illustrations of the tetramers of *PsHTE* (yellow) superimposed with DHNA-CoA thioesterase (blue). The substrate 4-hydroxybenzoyl-CoA superimposed with the structure of *PsHTE* (PDB entry 1LO9) is represented by sticks and colored by atoms (carbon, magenta; yellow, sulfur; nitrogen, blue; oxygen, red). The figure was created with the PyMOL Molecular Graphics System, Version 1.7.4 Schrödinger, LLC.



Surface analysis, solvent access, as well as docking studies, had identified the presence of four long tunnels connecting both subunits, possessing mainly a hydrophobic nature and involving the residues Tyr45 from the  $\alpha$ 3, Val57 from  $\beta$ 2, Val80 and Tyr83 from  $\beta$ 3, as well as Cys111, Ile120 and Leu121 from  $\beta$ 5- $\alpha$ 4 connecting loop (Figure 39). This connecting tunnel might be related to the substrate preferences of DHNA-CoA during the thioesterase activity.

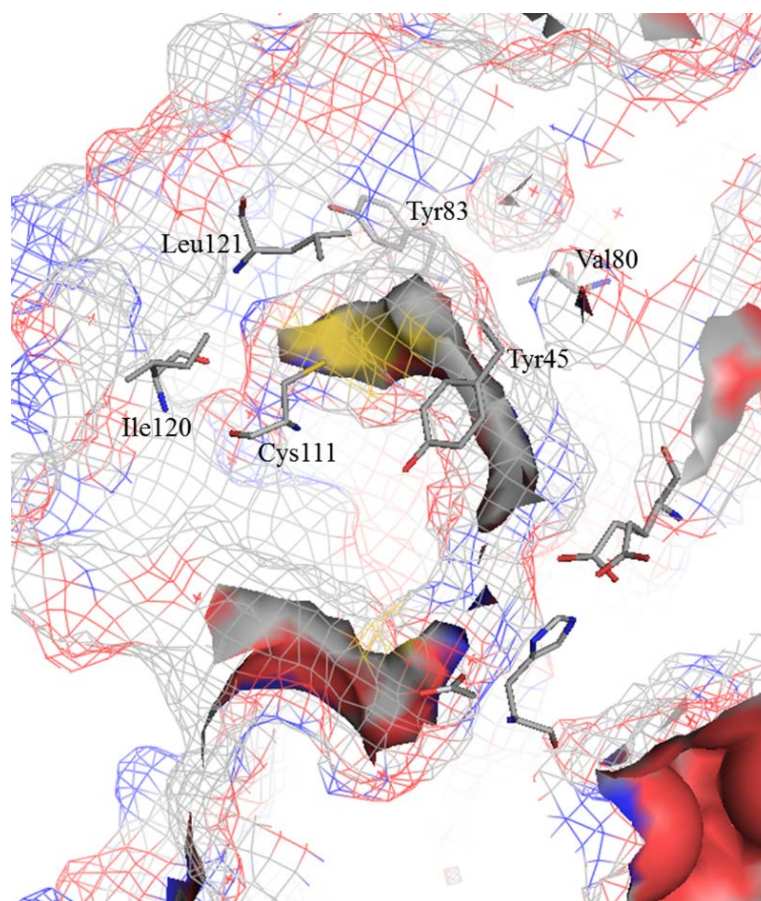


**Figure 39:** Schematic view of the surface and solvent accessibility binding pocket of *S. aureus* DHNA. The residues involved in the catalytic active site, as well as responsible for the hydrophobicity of the long tunnel are displayed as sticks, colored as carbon: gray, blue. Nitrogen, red; oxygen, yellow; Sulfur. The surface generated for the active site highlights the limits of the binding pocket with blue for positive charges, red for negative charge and gray for uncharged residues. The figure was created with the PyMOL Molecular Graphics System, Version 1.7.4 Schrödinger, LLC.

The binding of the ligand is mediated by interaction with the amino acid residue Tyr45 and Glu31 from one monomer and Asp16 and His23 from the corresponding monomer, all located in the interface region, as shown in Figure 40. The binding of the 4-hydroxybenzoyl CoA substrate inside the binding pocket is mainly stabilized by

hydrogen bonds formed between the hydroxyl group of the aromatic moiety of the ligand and the benzoyl ring hydroxyl group of the amino acid residue Tyr45, as well as through the carbonyl carbon group of the amino acid Glu31, mediated by a water molecule. In Figure 40, it is possible to observe the position occupied by the BCA substrate in the tunnel formed by two monomers of *Sa*DHNA.

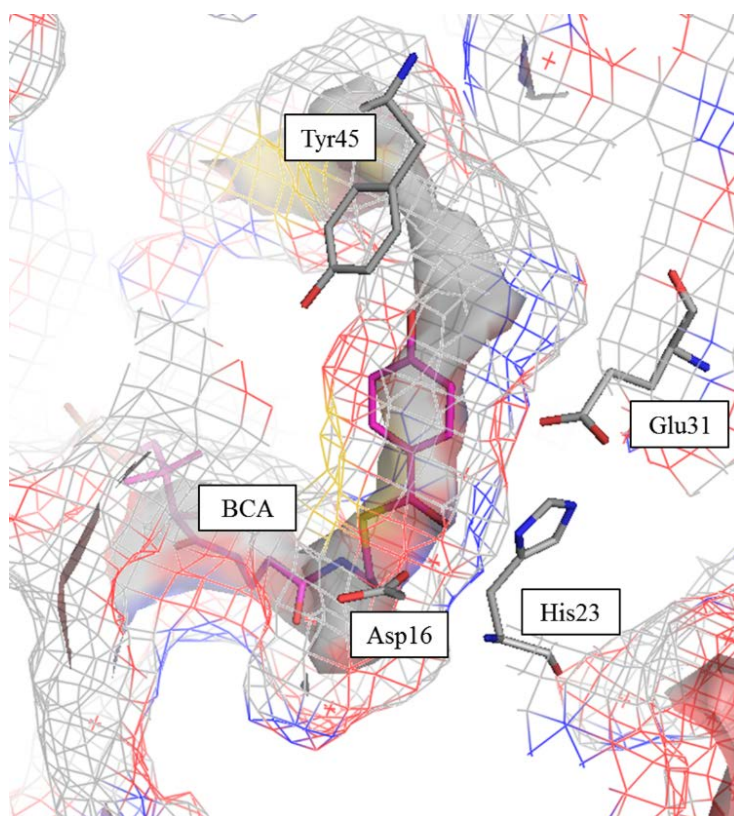


**Figure 40:** Superposition of the substrate 4-hydroxybenzoyl-CoA from the structure of *P<sub>s</sub>*HTE (PDB entry 1LO9) is represented by sticks and colored by atom (carbon, magenta; yellow, sulfur; nitrogen, blue; oxygen, red). The figure was created with The PyMOL Molecular Graphics System, Version 1.7.4 Schrödinger, LLC.

The position of the benzoyl ring hydroxyl group of the substrate interacts with the hydroxyl of the aromatic ring side chain of Tyr45 from one monomer and the  $\alpha$ -helix N-terminus of the backbone amide NH of His23 from the corresponding subunit through hydrogen bonds. The nucleotide is positioned in a cavity located on the surface of one monomer and the remaining part of the ligand is situated in a deep cleft formed by the subunit-subunit interface. The thioester carbonyl group of the substrate is located at the end of  $\alpha_2$ , which forms a hydrogen bond with His23, as well as with the imidazole ring of the side chain within 3.6 and 2.5 Å distance, respectively. The side

chain of Asp16 points in the direction of the carbonyl carbon of the substrate with 3.9 Å distance (Figure 41).

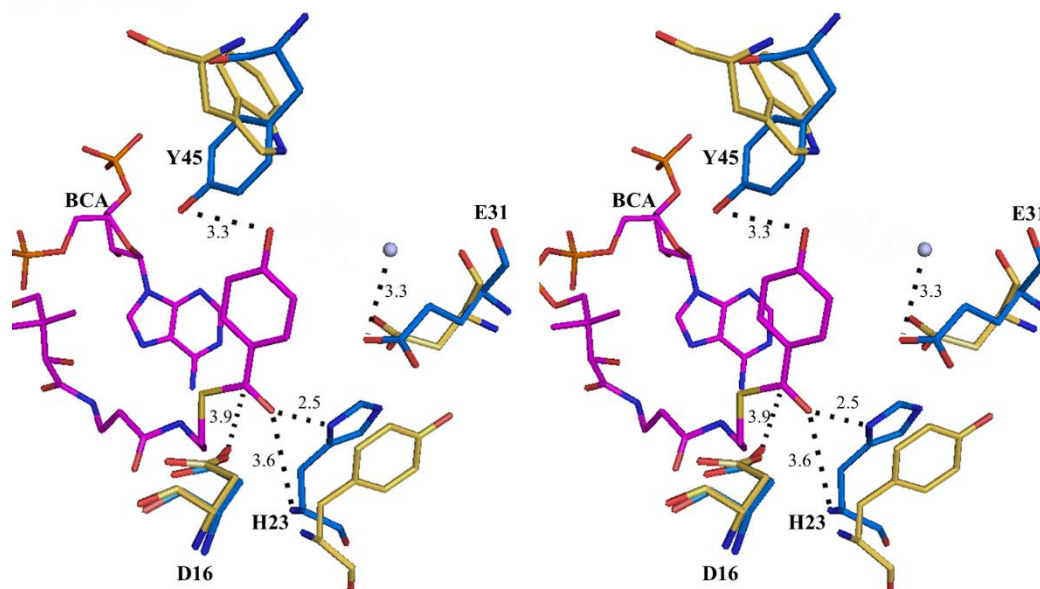


**Figure 41:** Stereo diagram (wall-eye) of the active site in stick representation of *Sa*DHNA and *Ps*HBT (PDB entry: 1LO9). The dimer of *Sa*DHNA is superimposed with the *Ps*HBT dimer, the structure of *Ps*HBT is displayed in yellow, *Sa*DHNA in blue and the active site residues are highlighted by stick representation; the ligand BCA is displayed in magenta and a water molecule in light gray. The catalytic residues are displayed as sticks, other active site residues as lines with oxygen atoms in red, carbon in the respective chain color, nitrogen in blue, and sulfur in yellow. Labels indicate the respective *Sa*DHNA residues, hydrogen bonds are represented as dashed lines and numbers show the hydrogen bond length, in Å.

The thioesterase, in general, shows different behavior regarding the substrate preferences. Therefore, in order to investigate the substrate preferences for DHNA, the thioesterase activity was performed against stearoyl-CoA and crotonyl-CoA. As demonstrated in Table 13, for the native DHNA, the long acyl chain stearoyl-CoA (C<sub>18:0</sub>) demonstrated to be a more active substrate, indicating high levels of free thiol identified by the DTNB reagent. On the other hand, short chain crotonyl-CoA, (C<sub>4:1</sub>) has lower specificity for thiol hydrolysis by the DHNA since low amounts of free thiol were recognized by the DTNB. This result might indicate that the hydrolysis rate may decrease with decreasing chain length.

According to structure superimposition studies performed using the *Ps*HBT (PDB 1LO9) structure coordinates, it was hypothesized that the residue D16 might be essential for the thioesterase activity. Thus, in order to verify the importance of the amino acid residues D16 and E31 on the thioesterase activity, site-directed mutagenesis

(SDM) towards both residues were performed and the aspartic residue was mutated to alanine and glutamic acid was changed to asparagine (Figure 42). Thioesterase assays were carried out using the same conditions used for the native enzyme. The DHNA-D16A mutation, with the putative site carboxylate group removed, showed an enormous decrease in the hydrolysis rate, in comparison with the native DHNA, demonstrated by the small amounts of free thiol detected in the solution. Regarding to the second variant, E31N, no detectable activity was observed, indicating that this residue also might be important for the activity.

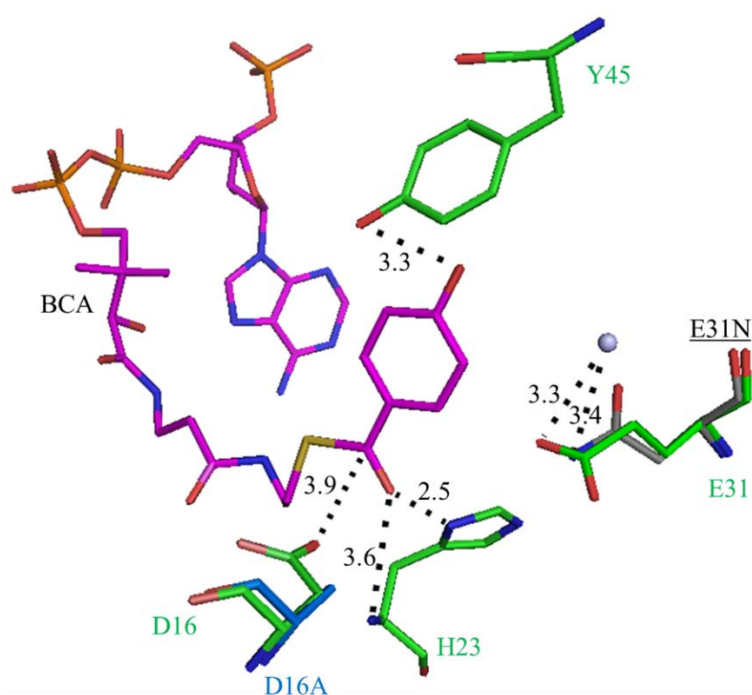


**Figure 42:** Diagram of the active site in stick representation of *SaDHNA* variants using *PsHBT* coordinates (PDB entry: 1LO9). *SaDHNA* native in green, D16A in blue and E31N in gray and the active site residues are highlighted by stick representation; the ligand BCA is displayed in magenta. Carbon is in the respective chain color, nitrogen in blue, and sulfur in yellow. Labels indicate the respective *SaDHNA* residues, hydrogen bonds are represented as dashed lines and numbers show the hydrogen bond length, in Å.

Once a substantial decrease in the thioesterase activity was observed for the D16A mutant, a third variant, D16A-E31N was prepared using the SDM technique to completely inactivate the enzyme activity. However, during affinity chromatography purification with the double mutant D16A-E31N, protein precipitation was observed. Different strategies, such as changes in the chromatography temperature and buffer

composition, as well as changes in the buffer pH were not effective to avoid protein precipitation. The double mutations D16A-E31N demonstrated unstable protein, and thus investigations towards this mutation were not carried out.

**Table 13:** Enzymatic assay for native DHNA and the variants D16A and E31N against short (C<sub>4:1</sub>) and long acyl-CoA chain (C<sub>18:0</sub>). Calculated values are in nMol TNB min<sup>-1</sup>·(mg protein)<sup>-1</sup>.

	Crotonyl-CoA		Stearoyl-CoA	
	Uncatalysed	Catalyzed	Uncatalyzed	Catalyzed
Native DHNA	0.1±0.0021	0.27±0.002	0.15±0,0026	128±0.054
DHNA-D16A	-	-	0.1±0.002	0.8±0.02
DHNA-E31N	-	-	0.13±0,0014	ND

### 5.11. Designed peptides and thioesterase inhibition

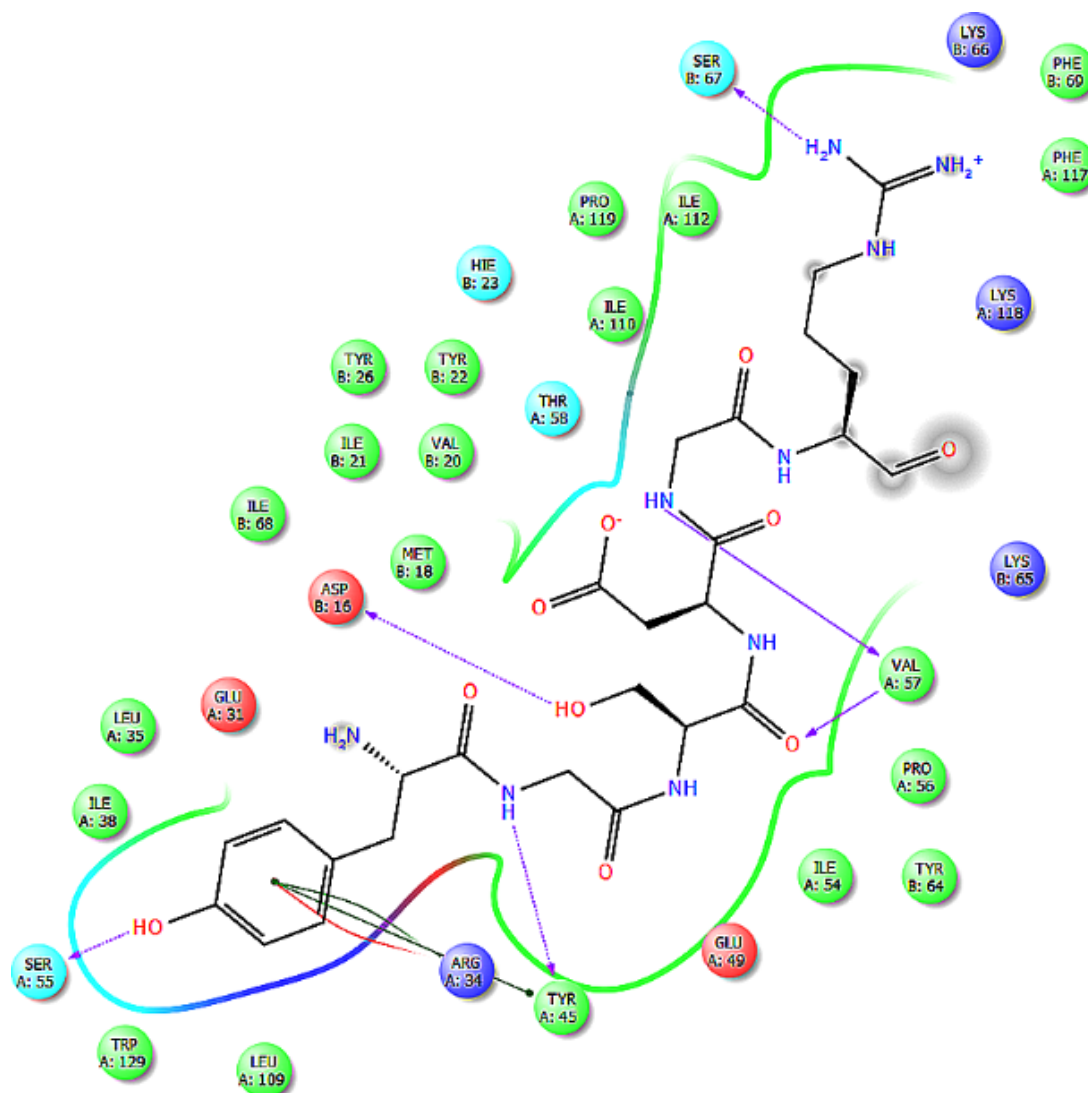
The protein structure obtained for *Sa*DHNA thioesterase was also used for docking studies, in order to discover possible thioesterase inhibitors. The docking analysis identified two binding sites at the protein surface and in the predicted binding site. The peptides EGEYE and YGSDGR showed the smallest Optimized Potentials for Liquid Simulations (OPLS) force field (potential energy OPLS2005  $-1927.27$  kcal·mol<sup>-1</sup> and  $-1583.93$  kcal·mol<sup>-1</sup>, respectively). One more peptide (WRSMGR) was designed after a residue scanning (single mutations of peptide residues to determine the lowest energetic state) of the YGSDGR peptide have a potential energy OPLS2005  $-1590$  kcal·mol<sup>-1</sup>.

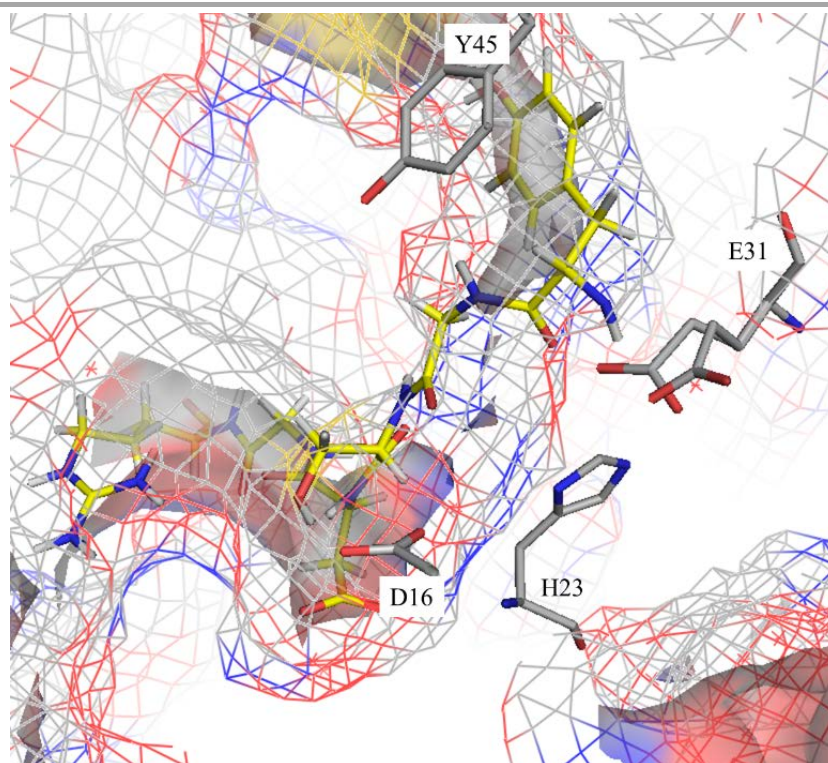
The peptide YGSDGR (Figure 43), with a molecular weight of 654.28 Da and a pI of 3.8 was designed and predicted to bind inside the active site with a  $\Delta G_{\text{bind}}$  of  $-81.0$  kcal·mol<sup>-1</sup>. In general, the stability is mediated mainly through six hydrogen bonds formed between the designed peptide and residues present in the active site. The benzoyl ring of the tyrosine (peptide) has non-covalent  $\pi$ -stacking interactions with the benzoyl ring of Try45, as well as with the side chain of Ser55 through a hydrogen bond. The residues important for the substrate binding and activity, Glu31 and D16, respectively, are predicted to interact with the amide of the peptide backbone and with the side chain of serine (peptide) via hydrogen bonds as well.

The second peptide, WRSMGR, has a molecular weight of 792.39 Da and a pI of 12 (Figure 44). Likewise as for the previous peptide, WRSMGR was designed and

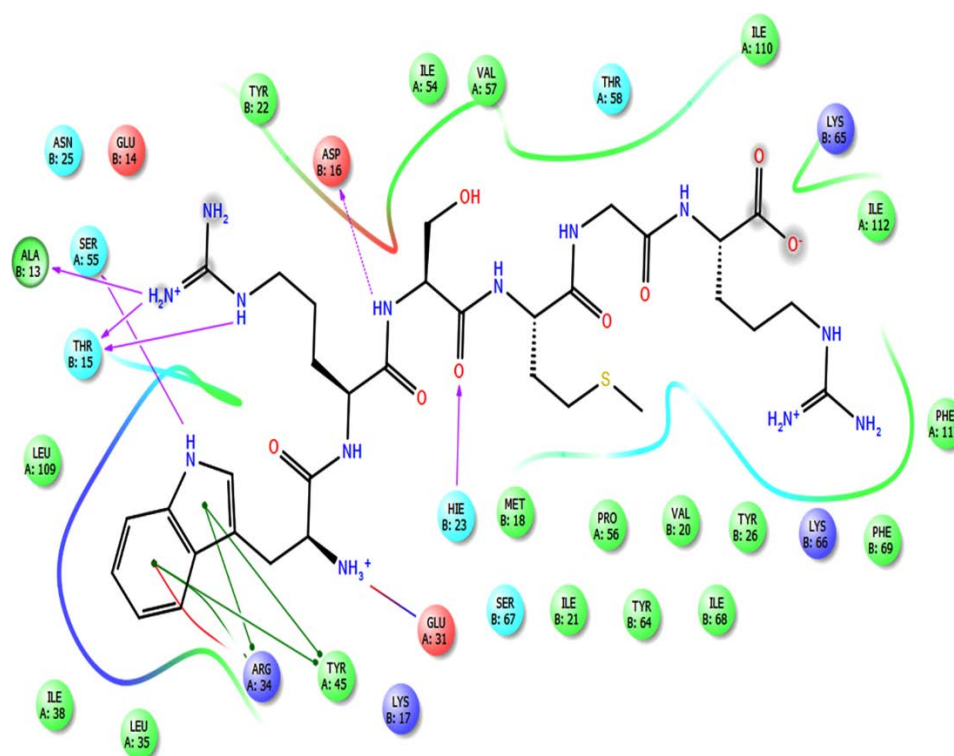
predicted to bind inside the active site as well, with an  $\Delta G_{\text{bind}}$  of  $-76.3 \text{ kcal}\cdot\text{mol}^{-1}$ . The indole ring of the tryptophan (peptide) is stabilized by non-covalent  $\pi$ -stacking interactions with the benzoyl ring of Try45, as well as by six hydrogen bonds. The residues, Glu31 and Asp16 are predicted to interact with the amide from the peptide backbone. In addition, His23 is also involved in the interaction with the serine (peptide) carbonyl group of the peptide backbone via hydrogen bond.

The third peptide EGEYE (623.23 Da, pI 3.67), on the other hand, was predicted to interact not with the binding site residues but with residues present on the surface of *Sa*DHNA, close to the binding site entrance, with an  $\Delta G_{\text{bind}}$  of  $-41.3 \text{ kcal}\cdot\text{mol}^{-1}$ . The interactions involve seven hydrogen bonds, as well as hydrophobic interactions between residues localized on connecting loops  $\beta 2$ - $\beta 3$ ,  $\beta 4$ - $\beta 5$  and  $\beta 5$ - $\alpha 3$  (Figure 45).





**Figure 43:** The interaction of YGSDGR peptide according to the *S. aureus* DHNA thioesterase structure. The predicted interaction (top) and visualization inside of the tunnel of the active site (bottom). Peptide molecules are shown in yellow sticks and residues involved in the interaction are shown in balls colored as pink: negatively charged, purple: positively charged, green: hydrophobic, cyan: polar, magenta arrows indicate hydrogen bonds and green arrow indicate  $\pi$ -stacking interactions. The figure was created with Maestro Molecular Modeling Interface Version 10.1.013, Schrödinger, LLC and the PyMOL Molecular Graphics System, Version 1.7.4 Schrödinger, LLC.



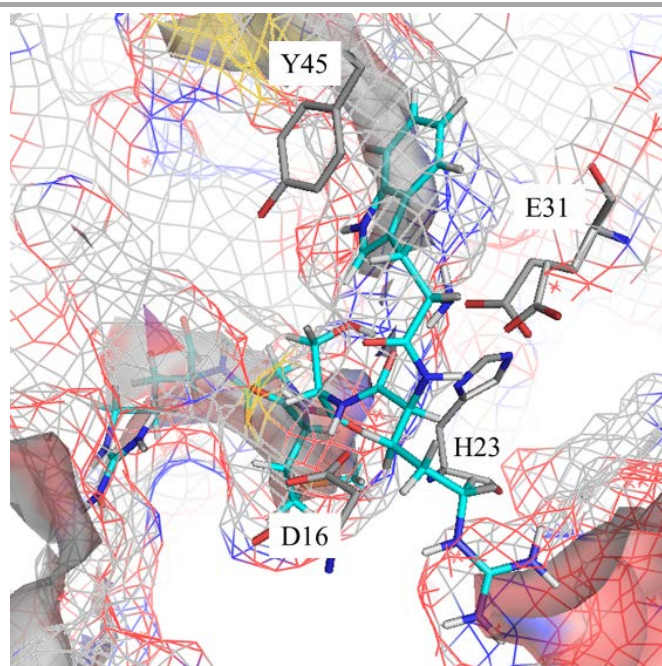


**Figure 44** Interaction of the designed peptide WRSMGR according to the *S. aureus* DHNA thioesterase structure. The predicted interaction (top) and visualization inside of the tunnel of the active site (bottom). Peptide molecules are shown in cyan sticks and residues involved in the interaction are shown as balls, colored as pink: negatively charged, purple: positively charged, green: hydrophobic, cyan: polar, magenta arrows indicate hydrogen bonds and green arrow indicate  $\pi$ -stacking interactions. The figure was created with Maestro Molecular Modeling Interface Version 10.1.013, Schrödinger, LLC and The PyMOL Molecular Graphics System, Version 1.7.4 Schrödinger, LLC.

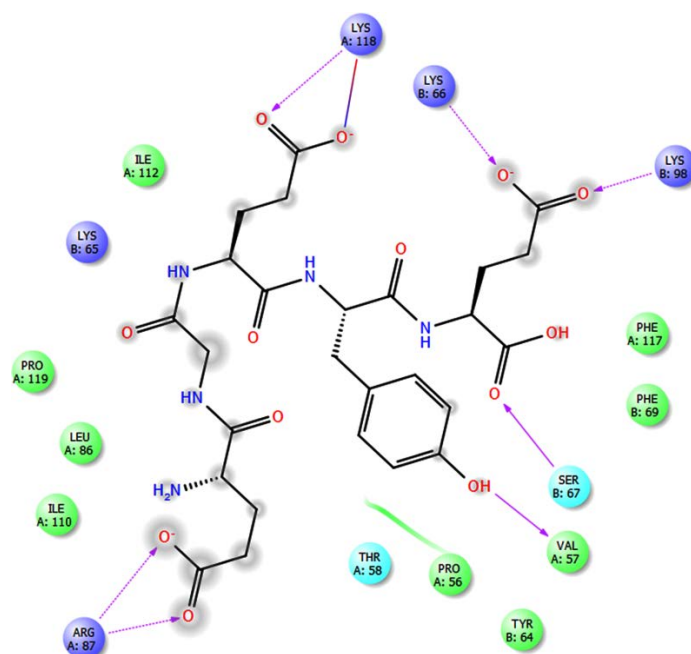


**Figure 45:** Interaction of the designed peptide EGEYE according to *S. aureus* DHNA thioesterase structure. Peptide molecules are shown in stick mode and residues involved in the interaction are shown as balls colored as pink: negatively charged, purple: positively charged, green: hydrophobic, cyan: polar, magenta arrows indicate hydrogen bonds and green arrow indicate  $\pi$ -stacking interactions. The figure was created with Maestro Molecular Modeling Interface Version 10.1.013, Schrödinger, LLC and the PyMOL Molecular Graphics System, Version 1.7.4 Schrödinger, LLC.



Once docking studies identified possible inhibitors, the thioesterase assays, using the same conditions as for the normal thioesterase activity, were carried out to evaluate the inhibition effect. One hundred micromolar of each peptide was used for this test and preliminary results demonstrated that all three peptides possess influence on the thioesterase activity. Non-measurable activity was detected by the DTNB reagent, implying that the DHNA was not able to act in the thioester bond of the substrate and, thus, its activity was inhibited. To avoid false positive results, two more controls were prepared: the first control was performed by leaving out the substrate to detect any non-specific conversion of DTNB by the peptides. The second was to monitor the rate of the uncatalyzed reaction by leaving out the peptides. In addition, to certify that the inhibition activity was due to an inactive enzyme, native DHNA was used as a positive control. As a result, there was no detectable nonspecific conversion of DTNB by the peptides, as well as the uncatalyzed reaction, and the native DHNA activity was as expected, demonstrating thioesterase activity towards the substrate ( $127 \text{ nMol TNB min}^{-1} [\text{mg protein}]^{-1}$ ).

---

## 6. Discussion

### 6.1. Isochorismate synthase (MenF)

Undoubtedly, the expression of recombinant proteins in microbiological systems has changed biochemistry. The ability to express and purify the desired protein has driven the biochemistry field into a new era of biochemical characterization of proteins [262]. The recombinant expression in a large quantity allows to increase the amount of studies of important target proteins for structure-based drug design investigations, including for example isochorismate synthase, demethylmenaquinone methyltransferase and DHNA-CoA thioesterase, enzymes involved in the menaquinone biosynthesis pathway.

Isochorismate synthase (MenF), the first enzyme of the bacteria vitamin K<sub>2</sub> biosynthesis pathway is a chorismate-utilizing enzyme, which catalyzes the irreversible formation of isochorismate originated from the shikimate pathway [263]. Daruwala and coworkers, in 1996, isolated for the first the isochorismate synthase enzyme specifically involved in the menaquinone biosynthesis. However, only in 2007 the 3D information of the *E. coli* MenF structure was published. [264].

In order to obtain 3D structure information to support drug discovery, *SaMenF* was cloned and expressed as a C-terminal Strep-tagged protein. Test expression and purification demonstrated that *SaMenF* was eluted with minor contaminants from the affinity column. The CD spectroscopy showed that the *SaMenF* secondary structure contains 27%  $\alpha$ -helices, 40%  $\beta$ -sheet, 3% turn and 30% random. For the *EcMenF* homologue (PDB 3BZN), similar percentages were found regarding the secondary structure (30%  $\alpha$ -helices, 35%  $\beta$ -sheet, 2% turn and 33% random structures) [219]. High amounts of random structures indicate that *SaMenF* may possess several flexible parts, which can interact with other proteins and can aggregate as well. Parsons and coworkers [219] observed that magnesium, as well as sulfate ions, were found in the active site of the closed conformation of *EcMenF*. This conformation, in contrast to the open conformation, turned out to be more stable due to limitation of the solvent-exposure of the active site. Such ions were also included in buffers during *SaMenF* purification, however, no difference was observed in the protein stability, indicating that the protein may be already unfolded, explaining the high fluorescence observed during the thermos shift assay.

Despite the low homology of the N-terminus, the sequence alignment of *S. aureus* MenF with the *E. coli* MenF homologue revealed that several amino acids of *SaMenF* possesses similar physico-chemical properties, as well as conservative substitutions with *EcMenF*. In addition, the lysine in position 190 is well conserved, indicating that this residue may be crucial for the activity in *S. aureus* as well. Protein sequence similarities may be an indication that *SaMenF* might crystallize in similar conditions, as described before by Parsons and coworkers [219].

In conclusion, further optimizations in protein expression, as well as in protein purification are essential in order to achieve stable amounts of *SaMenF* suitable for protein crystallization. Moreover, codon optimization, co-expression with fusion partners, as well as co-purifications with the substrate chorismic acid are, among others, different strategies to be considered and explored in future.

## 6.2. Demethymenaquinone methyltransferase

Being part of the last step in the menaquinone pathway, demethylmenaquinone methyltransferase (MenH) is essential for producing a functional vitamin K<sub>2</sub> in bacteria. MenH is an *S*-adenosyl methionine (SAM)-dependent methyltransferase (SAM-MTase) which catalyzes the C-methylation step, converting 2-demethylmenaquinone into menaquinone (vitamin K<sub>2</sub>), showing similarities to the CoQ6 biosynthesis pathway [210].

The only homolog found for MenH by all the predicted model programs was the *Saccharomyces cerevisiae* C-methyltransferase CoQ5. CoQ5 is a lipid-soluble ubiquinone, acting as an electron carrier of the respiratory chain in both eukaryotes and prokaryotes [265]. According to Dai *et al.* [217], the *S. cerevisiae* CoQ5, solved to 2.2 Å resolution, exhibits a homodimer oligomerization in solution. The authors observed that *ScCoQ5* residues in the N-terminal segment could not be observed in the electron density maps, demonstrating a high flexibility in this region. A highly flexible N-terminal was also observed for the *SaMenH* protein sequence. Predicted models exhibited that this portion of the protein possesses different secondary structure conformations, showing the disordered nature of the N-terminus. Furthermore, the universal glycine-rich box E/DxGxGxG, present in *ScCoQ5*, was also observed in the MenH protein sequence, with a minor variation of cysteine instead of glycine

---

(DVCCGTG). The glycine-rich box is known to be essential for the ribose binding, present in the *S*-adenosylmethionine substrate [266].

Protein-protein interactions was a major problem faced during the MenH recombinant protein purification. The protein expression in *E. coli* may differ from the original source regarding pH, osmolarity, and folding mechanisms. The exposure of hydrophobic stretches of unfolded proteins, for instance, may induce unspecific protein-protein interactions of the expressed protein and lead to protein aggregation [267]. Good results were observed when CHAPS, a zwitterion non-denaturant detergent was allowed to interact with protein clear lysate during protein purification. Further investigations in different strategies in order to improve protein stability are crucial to obtain protein crystals for *SaMenH* structure analysis.

### 6.3. 4-hydroxybenzoyl CoA Thioesterase (DHNA-CoA thioesterase)

Thioesters play an important role in cellular metabolism. Known to be involved in cell cycling, gene regulation, signal transduction, as well as in energy production, thioesters have different biological forms, such as acylated glutathione, acylated protein cysteine, acyl carrier protein (ACP) and acyl Coenzyme A (CoA) [268].

Leesong and co-workers discovered an unusual  $\alpha/\beta$  fold structure to dehydratase–isomerase from *E. coli* [269]. In their work, the authors describe FabA (PDB entry 1MKA) possessing a central long  $\alpha$ -helix surrounded by a determined number of  $\beta$ -sheets, naming this particular structure a “HotDog fold”, in which the long  $\alpha$ -helix is similar to the “sausage” and the  $\beta$ -strand  $\beta$ -sheet resembles the “bun”.

In general, the central fold topology consists an antiparallel  $\beta$ -sheet cluster ordered 1-3-4-5-2 and the long HotDog helix is positioned in the centre of strands  $\beta_1$  and  $\beta_2$ . Occasionally, some enzymes may also exhibit additional  $\beta$ -strands in their “bun”, as demonstrated for the *SaDHNA* crystal structure. In addition, the minimal functional unit of the HotDog fold is a homodimer, which can be organized into dimers, a dimer of dimers, trimers of dimers as well as in double and triple hotdog folds [270].

The superfamily of  $\alpha/\beta$ -fold hydrolase enzymes, as well as the general HotDog fold, evolved to hydrolyze thioester bonds. Spread in all three kingdoms, the thioesterases comprise the major members of the HotDog fold family. Possessing

---

several functions in cells. Thioesterases also play an important role in the primary and secondary metabolism [271,272].

The HotDog fold comprises six subfamilies well-known by their overall structure [273]. The first and largest subfamily includes the acyl-CoA thioesterases. Representative members of acyl-CoA thioesterases include the human enzymes brown fat adipose tissue thioesterase (BFIT) and cytoplasmic acetyl-CoA hydrolase (CACH) [274,275]. The second subfamily is the YbgC-like. Crystal structures have been solved for the YbgC from *E. coli* (PDB ID: 1S5U), as well as for the YbgC from *Helicobacter pylori* and the YbgC in *Haemophilus influenza* (PDB ID: 2PZH) [276,277]. *EcYbgC*, as well as *HiYbgC*, demonstrated to be more active with short chain substrates. On the other hand, *HpYbgC* was more active for long acyl chains (e.g. palmitoyl- and stearoyl-CoA). In another survey, thioesterases from *Alcaligenes faecalis* [278] and *P. profundum* [251] also share similar results regarding the preference for acyl long chain substrates. The acyl length preferences observed in the thioesterase activity for these organisms might be correlated to the presence of a long tunnel associated with the binding site of the acyl moiety of the substrate. During solvent accessibility analysis, as well as during docking studies of the *SaDHNA* structure, a long tunnel could also be identified. In fact, this long tunnel might explain the reason for *SaDHNA* thioesterase activity towards the long acyl chain of the C<sub>18:0</sub> stearoyl-CoA substrate. Residues identified that surround the tunnel are mainly formed by uncharged amino acids. This may contribute to the hydrophobic nature of the tunnel, assisting the long acyl chain stabilization through hydrophobic non-covalent interactions, such as  $\pi$ -stacking [270]. Despite the hydrophobic nature of the short acyl chain of the C<sub>4:1</sub> crotonyl-CoA, low activity was detected by the DTNB reagent. Analyzing the composition of the amino acid residues near the thioester binding pocket, the hydrophilic environment in this specific region might promote the instability between enzyme-substrate binding and, thus, affect the hydrolysis activity.

From the information acquired through solvent access calculations and thioesterase activity, co-crystallization with the long acyl chain was carried out in order to investigate the binding position of the stearoyl C<sub>18:0</sub> acyl long chain. Co-crystallization was performed for both D16A and E31N mutants, however no complex could be obtained so far. This failure might be attributed to multiple reasons. Firstly, during structure analysis of the D16A mutant, a molecule in the binding site pocket was

detected, probably originating from the affinity chromatography purification or as a metabolism product from the *E. coli* cells. Binding site blockage induced by this alien molecule might hamper the access of the substrate to the binding site pocket and, consequently, make it inaccessible for the stearyl-CoA substrate interaction and binding. Secondly, protein precipitation was observed immediately following the addition of the ligand (about 40%). Protein still present in solution was able to assemble and form protein crystals, however, this always failed to show a protein complex. Production of ligand analogs or short versions of the ligand application, as well as the binding constant knowledge, might help to bypass the precipitation and lead to protein complex crystal formation in future.

Moreover, it is suggested that *SaDHNA* thioesterase might also be active against hydrophilic, as well as aromatic substrates, in particular benzoyl-CoA. In the putative active site analysis of the *SaDHNA* structure, the superposition with the BCA demonstrated that the benzoyl ring hydroxyl group of the substrate might be stabilized due to hydrogen bonds promoted by the benzoyl ring hydroxyl group of Tyr45. Furthermore, the substrate may also be stabilized by a hydrogen bond with residue Glu31 through a water molecule bridge, in a similar process as observed for the *PsHBT*. Such observations prove to be relevant since the main substrate for this enzyme is the 1,4-dihydroxy-2-naphthoyl-CoA, an aromatic compound consisting of a naphthoquinone ring-CoA used during the menaquinone biosynthesis pathway.

The last two HotDog fold thioesterases subfamilies comprise the 4HBT class I (4HBT-I) and the 4HBT class II (4HBT-II). The crystal structure of the 4HBT-II was firstly introduced in a study conducted by Thoden and collaborators [221]. Showing a HotDog fold, the *Arthrobacter* sp. strain SU 4-hydroxybenzoyl-CoA thioesterase has a particular characteristic that differentiates it from other thioesterases: the main  $\alpha$ -HotDog helix ( $\alpha$ -HD) is positioned outwards and the  $\beta$ -sheets inwards, a dimer association known as back-to-back (or sheet-to-sheet). On the other hand, the crystal structure of 4HBT I of the *Pseudomonas* sp. CBS3 4-hydroxybenzoyl-CoA thioesterase, revealed an opposite dimer association, in which  $\beta$ -strands pointing outwards and the main  $\alpha$ -HotDog pointing inwards associate, a dimer association known as face-to-face (or helix-to-helix) [222,273,279,280]. The structure of the *SaDHNA* tetramer revealed a similar oligomerization architecture as observed for 4HBT I from *Pseudomonas*.

According to studies performed with the native *PsHBT* structure, as well as with the *PsHBT* D17N mutant, the residues involved in the thioesterase activity were identified and a catalytic mechanism was proposed [281–283]. The residues responsible for *PsHBT* activity consisted of Tyr24 and Asp17. The Tyr24, positioned in the N-terminus of the main  $\alpha$ -HD helix is responsible for the polarization of the thioester carbonyl group by a hydrogen bond formation from the Tyr24 backbone amide NH. The carbonyl side chain from the closest residue, Asp17, (positioned on the connecting loop  $\beta_1$  and the main  $\alpha$ -HD helix), acts as a nucleophile during the thioester bond cleavage. A mutation of Asp17 halted the hydrolysis of the substrate by *PsHBT*, revealing the importance of this acidic amino acid residue in the thioesterase catalysis. In fact, protein sequence alignment performed between *SaDHNA* and *PsHBT* revealed that this residue is well conserved. Structure superimposition indeed confirmed the position of the aspartic acid. Gathering this information, *SaDHNA* Asp16 might also assume the same function fulfilled by Asp17 in *PsHBT*. Mutagenesis studies performed towards the Asp16 residue in *SaDHNA* thioesterase truthfully altered the catalysis rate, resulting in a decrease in the hydrolysis activity. A similar result was also observed by Zhuang and co-workers [284] for *Bacillus halodurans* C-125 gentisyl-CoA thioesterase, where mutating the residue Asp16, corresponding to Asp17 in *PsHBT* and Asp16 in *SaDHNA*, decreased in approximately 230-fold the catalytic rate. Nonetheless, the D16A mutation in *SaDHNA* thioesterase was not sufficient to entirely halt the thioesterase activity. This controversial result, involving the function of aspartic acid in the catalysis between *PsHBT* and *SaDHNA*, might lead into some possible hypothesis.

Firstly, the lack of the carboxylate side chain of the aspartic acid residue in the active site pocket might allow to bind more water in the active site region and therefore the reaction might occur by a general basis catalysis [285–287]. Secondly, the main catalytic residue might be transferred to a second aspartic acid (Asp31) localized in the main  $\alpha$ -HD helix, on the opposite side of Asp16 within  $\sim 7$  Å of distance. Indeed, the E31N mutation resulted in non-detectable catalytic rates of *SaDHNA*. This result indicates that E31 might be crucial for the catalytic site as well. The turnover of the D32S mutant in *PsHBT* was only 33-fold, in comparison to the wildtype, suggesting that D32 only plays as a supportive role during substrate binding [282]. In the case of the E31N mutant the short side chain of asparagine might influence the protein stability inside the binding site, once this mutant was less stable, in comparison to D16A and

---

native DHNA. These findings might suggest that E31 not only plays a role in supportive substrate binding but is also an essential residue for the protein stability during the thioesterase activity.

Finally, the imidazole ring of the His23 residue might play a role in the catalytic mechanism of *S. aureus* DHNA (Figure 46). The side group of histidine possesses a pKa of approximately 6 to 7, which allows this residue to switch between protonated and unprotonated states under a physiological pH. This particular property enables histidine to participate in general acid-base catalysis, enhancing the nucleophilicity of the hydroxyl and thiol groups [288]. Protonated nitrogen of the imidazole ring can act as a general acid while unprotonated N acts as nucleophile, and consequently, performs as a general base [289]. Basically nitrogen from the imidazole ring of His23 might abstract proton of the nucleophile (a water molecule), and henceforward induce the nucleophilic attack on the carbonyl carbon of the polarized substrate (electrophile). This is a similar reaction described for a general base-catalyzed nucleophile addition to a polarized  $\pi$  bond. In addition, the nitrogen of the imidazole ring might also perform a nucleophilic attack on the polarized carbonyl carbon of the ligand in a general acid catalysis. In conclusion, in order to investigate the implications of His23 on the activity further mutagenesis studies together with substrate analogs co-crystallization are essential to elucidate the mechanisms of action of *Sa*DHNA thioesterase.

One particular characteristic of the members belonging to 4HBT is the absence of a protein sequence consensus, protein length and/or the N or C-termini secondary structure. Members of the HotDog fold possessing a degeneracy in protein sequence share a low sequence identity (10-20%) [290]. This might explain the diversity found in the protein sequence in *S. aureus* DHNA thioesterase, as well as amongst thioesterase homologues, conserving similar quaternary structures, along with the position of the respective active sites at the interface of the two hotdog-fold monomers. In addition, one specific property observed amongst the thioesterases, the largest family within the hotdog-fold protein superfamily, is the well-known substrate promiscuity. A detailed review regarding primary and tertiary structures of thioesterases performed by Cantu and co-workers [291] demonstrates that the HotDog fold thioesterases have an incredible variety of substrate preferences, from short-to-long acyl-CoA (C<sub>4</sub>-C<sub>18</sub>), palmitoyl-CoA, choloyl-CoA, 3,5-tetradecadienoyl-CoA, 4-hydroxybenzoyl-CoA, several hydroxyphenylacetyl-CoA to short-long chain acyl-ACP. Studies with the *E.*



*coli* Hotdog-fold thioesterase paralogs YdiI and YdbB demonstrated that both proteins showed a high promiscuity level regarding the substrate specificity. This situation might be explained in consequence of the huge request for thioester hydrolysis in the cell. In eukaryote cells, for example, thioesterases are present in the cytosol, the endoplasmic reticulum, the mitochondria, as well as in the peroxisomes. This demand might stimulate an upgrade upon HotDog fold functions within cells, suggesting that the substrate promiscuity is a key factor for the rapid gain of novel biological functions during species evolution [292].

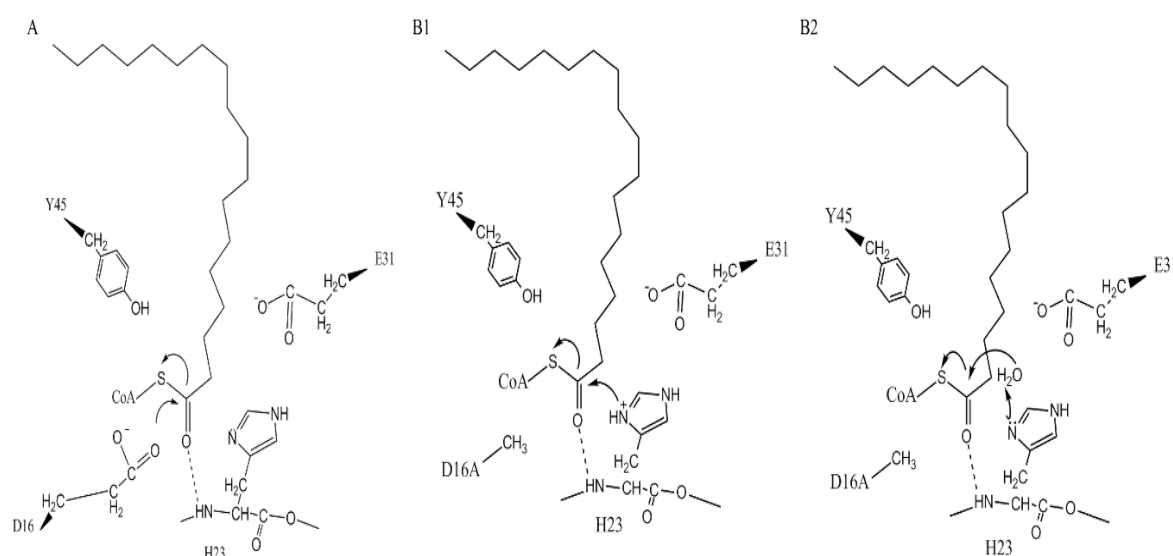


**Figure 46:** *Staphylococcus aureus* DHNA mechanism of action proposed by A: Native *S. aureus* DHNA thioesterase. B1: D16A DHNA mutation, with His23 residue acting as a general acid catalysis and B2: D16A DHNA mutation, with His23 acting as a general base catalysis. The figure was created using the ChemDraw program (PerkinElmer Inc.).

Putative inhibitors were successfully screened and docked to the active site of *Sa*DHNA. The *in vitro* inhibition activity tests performed with the designed peptides might be considered useful for further enzymatic studies of this enzyme. In addition, the predicted interaction might provide some evidence of the mechanism about inhibition.

During the docking studies the peptide YGSDGR, as well as the peptide WRSMGR, were predicted to bind inside the active site, producing a stable interaction via hydrogen bonds. In addition, noncovalent interactions via aromatic stacking ( $\pi$  stacking) between the aromatic ring of tyrosine and tryptophan may also contribute to the peptide stability inside the binding pocket. This stable interaction between the peptide-*Sa*DHNA might block the active site entrance for other substrates, preventing

---

the substrate binding and, thus, cleavage by the enzyme. Furthermore, both peptides possess a remarkable similarity to the benzoyl-CoA substrate, as well as to the natural substrate 1,4-dihydroxy-2-naphthoyl-CoA, confirming the possibility of a stable complex formation in the active site.

Moreover, although the peptide EGEYE was not predicted to bind site in the active site, the surface protein-peptide interaction might also prevent the substrate from binding. Thoden *et al.* [281] observed that the coenzyme A ribose of both 4-hydroxybenzoyl-CoA substrate and the 4-hydroxyphenacyl-CoA inhibitor were positioned in a cleft located on the solvated surface of the dimer. This important observation suggests, that the peptide bond to the *Sa*DHNA protein surface might interfere with the nucleotide moiety binding and reflects the thioesterase activity [293].

Deck and collaborators [294] designed, based on the acyl protein thioesterase I structure, a peptidomimetic with highly selective and inhibitory activity towards the protein palmitoylation. Designed peptidomimetics have shown to be excellent antimicrobial drugs, inhibiting *S. aureus* growth in patients with acute skin infections, as well against MRSA and *S. aureus* biofilms [295,296]. The significant properties of the designed peptidomimetics, combined with base-structure enzymes or proteins, have the potential to be a new generation of antimicrobial agents to overcome bacterial drug resistance. Designed peptides tested in this thesis demonstrated a good inhibition against *Sa*DHNA, indicating that they may have the potential to be new antimicrobial drugs against *S. aureus* infections.

In previous surveys, Kurosu and collaborators [297] showed the importance of MenA (1,4-dihydroxy-2-naphthoate prenyltransferase) within the menaquinone pathway for *Mycobacterium tuberculosis* survival. Based on the *Mt*MenA structure product, the authors developed demethymenaquinone (DMMQ) analogs and evaluated the growth inhibition activity. Several molecules demonstrated strong growth inhibition in concentrations lower than 20  $\mu$ M. In addition, *in vitro* studies showed that the inhibition of this enzyme could not be reversed even when high concentrations of exogenous vitamin K<sub>2</sub> were introduced. Recently, studies from Matarlo and collaborators [223] showed the importance of structural knowledge about the *E. coli* MenE (O-succinylbenzoate-CoA synthetase, OBS-CoA synthetase) active site involved in the menaquinone biosynthesis. Drug design was essential for the synthesis of several secondary amine analogs (OSB-AMS) with high specificity and antimicrobial activity in

---

low concentrations. Furthermore, the effect of these OSB-AMS on the menaquinone levels of *S. aureus* showed a direct interference upon menaquinone biosynthesis. This evidence highlights the significance of the menaquinone biosynthesis in bacterial endurance. An essential enzyme as part of the menaquinone biosynthesis pathway, DHNA-CoA thioesterase of *S. aureus* is a potential target enzyme for intelligent drug design leading to more specific therapeutic drugs, opening an era of novel mechanisms of actions, as well as novel drug discoveries towards MRSA infections.

The structurally and biochemically characterization as well the identification of highly conserved residues, in particular at the active site of a target structure, is extremely important for structure-based drug design. Targeting enzymes in the menaquinone metabolism pathway of *S. aureus*, in order to avoid cross-reaction in the host minimizes drug resistance as well as generates a high specificity of the designed medicaments, however, needs the structural knowledge of the participating enzymes.

In summary, this study presents the structure and biochemical characterization of the HotDog 4-hydroxybenzoyl-CoA thioesterase (DHNA thioesterase) from *S. aureus* involved in the menaquinone biosynthesis pathway. Enzymatic tests and mutagenesis studies demonstrated the preference towards long acyl chain substrates, as well as the importance of the acidic residues Asp16 and Glu31 in the active site and for substrate binding, respectively. Henceforward, a mechanism of action was proposed and shown in Figure 46. Residue D16 might drive the thioesterase activity via nucleophilic attack towards the polarized carbonyl group, whereas Tyr45 and Glu31 might be supportive in substrate binding. In addition, His23 is also proposed to contribute to the thioesterase activity.

Further enzymatic activity towards aromatic substrates, as well as with other polar substrates is essential for characterizing the *Sa*DHNA substrate preferences. Additional mutagenesis investigations together with co-crystallization with substrates and/or analogs are essential for understanding the mechanism of action, as well as the inhibition of the thioesterase activity in *S. aureus*.

Structural information of other enzymes involved in MQ metabolisms, such as MenF and MenH/UbiE in *S. aureus* are still missing. A recombinant expression of these genes in *E. coli* was possible but MenF showed to be unstable, losing the protein stability within 24 hours. Problems regarding protein-protein interactions during

purification did not allow the production of pure samples to perform crystallization screens for MenH. Further optimization in expression duration as well as further purification to remove unspecific interactions is required.

In conclusion, aiming specific targets of the menaquinone metabolism pathway in antibiotic-resistant hospital infections bacteria, such as *S. aureus*, represent an innovative method and might assist the discovery of new antibiotic compounds to treat MRSA.

---

## 7. Summary

Antibiotics, no doubt, are one of the greatest achievements of modern medicine. For many years, antibiotics saved countless lives around the world. However, nowadays, they are in danger of losing effectiveness. Overuse of antibiotics has led to a microbial resistance problem worldwide. Due to selective pressure induced by antimicrobials as well as the remarkable ability of adaptation, the Gram-positive Methicillin-resistant *Staphylococcus aureus* has become the most concerning life-threatening organism in hospital-acquired infections. Only a few therapeutic possibilities are available to treat MRSA infections. To avoid severe side effects promoted by some antibiotics and to help overcome the multidrug resistance issue, targeting metabolic pathways, in particular those absent in humans, such as vitamin K, has become of great interest. Designing medicaments generally requires the structural knowledge of the target (e.g. enzymes or proteins). Structural knowledge of enzymes involved in the metabolic pathway present only in bacteria may contribute to generating highly specific structure-based drug, as well as help to overcome difficulties related to bacterial resistance.

In this work, the structure of DHNA-CoA thioesterase of *S. aureus* was analyzed by X-ray crystallography. The assembly of four identical subunits arranged in dimers form the quaternary structure. Each monomer adopts a HotDog fold comprising a long four-turn  $\alpha$ -helix surrounded by five antiparallel  $\beta$ -sheets and one parallel  $\beta$ -sheet in the order 6-1-3-4-5-2. Mainly a hydrogen bond network formed between each monomer stabilizes the dimer and the dimers are organized in an oligomerization called face-to-face. *Sa*DHNA-CoA thioesterase possesses four putative active sites built into the interface regions between two monomers, with residues Asp16, His23 from one monomer and Glu31, Tyr45 from the other monomer participating in the activity, as well as in substrate binding. In addition, *Sa*DHNA CoA thioesterase is more active against stearyl-CoA, a long chain acyl-CoA substrate, and preliminary tests showed thioesterase inhibition by three designed peptides. Although further studies are necessary regarding the location of the binding site, as well as all of the amino acids involved, the present study provides important information for novel mechanisms of action and novel antibiotic drug development based on structural enzymes, targeting specifically MRSA.

## 8. Zusammenfassung

Antibiotika sind ohne Zweifel eine der größten Errungenschaften der modernen Medizin. Über viele Jahre konnten Antibiotika zahlreiche Menschenleben weltweit retten. Allerdings verlieren diese seit geraumer Zeit ihre Wirkung. Dieses ist darauf zurückzuführen, dass sich durch die Überbenutzung von Antibiotika mikrobielle Resistenzen ausbilden. Der Selektionsdruck, der durch antimikrobielle Substanzen induziert wird, als auch die erstaunliche Anpassungsfähigkeit des grampositivem Methicillin-resistenten *Staphylococcus aureus*, machen diesen Organismus zu einem der lebensbedrohlichsten Auslöser von Krankenhausinfektionen. Die verfügbaren therapeutischen Möglichkeiten zur Behandlung von MRSA Infektionen sind stark begrenzt. Um starken Nebeneffekten vorzubeugen und zur Bekämpfung der weit ausgeprägten Resistenzen werden Stoffwechselwege, insbesondere nicht humane, wie zum Beispiel der Vitamin K Syntheseweg, erforscht. Ein Wissen über der 3D-Struktur des Zielmoleküls ist in der Regel für die Entwicklung eines strukturbasierenden Wirkstoffs erforderlich. Strukturinformationen der Enzyme die an dem Stoffwechsel von Bakterien beteiligt sind können eine Vorlage für hochspezifische strukturbasierte Arzneimittel liefern. Dieses könnte entscheidend für den Kampf gegen Antibiotikaresistenzen sein.

In der vorliegenden Arbeit wurde die Struktur von DHNA-CoA Thioesterase von *S. aureus* mittels Röntgenstrukturanalyse gelöst. Vier identische Untereinheiten, jeweils in Dimeren angeordnet, bilden die Quartärstruktur des Proteins. Jedes Monomer nimmt eine ‚HotDog‘-Faltung an, bestehend aus vier langen, vierfach gewundenen  $\alpha$ -Helices, welche von fünf antiparallelen  $\beta$ -Faltblättern und einem parallelen  $\beta$ -Faltblatt in der Anordnung 6-1-3-4-5-2 umgeben sind. Die Dimere werden hauptsächlich von einem Netzwerk aus Wasserstoffbrücken zwischen den Monomeren stabilisiert und sind in einer ‚face-to-face‘ Oligomerisierung organisiert. *Sa*DHNA-CoA Thioesterase besitzt vier putative aktive Zentren welche sich auf der Grenzfläche zwischen zwei Monomeren befinden, von deren die Aminosäurereste Asp16 und His23 des einen Monomers sowie Glu31 und Tyr45 des anderen zur Aktivität sowie zur Substratbindung beitragen. Des Weiteren weist die *Sa*DHNA CoA Thioesterase eine relative hohe Aktivität gegenüber langkettigen Acyl-CoA, einem Stearoyl-CoA Substrat auf. Die Lösungsmittelzugänglichkeit sowie *Docking* Studien zeigten die Anwesenheit eines länglichen Tunnels, welcher die beiden Untereinheiten verbindet. Drei Peptide wurden

generiert, denen eine Bindung im aktiven Zentrum sowie auf der Proteinoberfläche vorhergesagt wurde. Enzymatische Studien zeigten eine Hemmung der Proteinaktivität für alle untersuchten Peptide. Obwohl zur genauen Lokalisierung der Peptidbindestelle sowie zur Identifizierung aller involvierten Aminosäuren weitere Studien notwendig sind, liefert die vorliegende Arbeit wichtige Informationen bezüglich neuer Wirkmechanismen sowie zur Evaluierung und Entwicklung neuartiger Antibiotika, welche auf strukturellen Daten basieren, zur Behandlung von MRSA.

---

## 9. References

1. Garner JS, Jarvis WR, Emori TG, Horan TC, Hughes JM (1988) CDC definitions for nosocomial infections, 1988. *AJIC Am J Infect Control* 16: 128–140. doi:10.1016/0196-6553(88)90053-3.
2. Horan TC, Emori TG (1997) Definitions of key terms used in the NNIS System. *Am J Infect Control* 25: 112–116. Available: [http://dx.doi.org/10.1016/S0196-6553\(97\)90037-7](http://dx.doi.org/10.1016/S0196-6553(97)90037-7).
3. WHO (2011) World Health Organization: Report on the Burden of Endemic Health Care-Associated Infection Worldwide Clean Care is Safer Care. Geneva, Switzerland.
4. Reed D, Kemmerly SA (2009) Infection control and prevention: a review of hospital-acquired infections and the economic implications. *Ochsner J* 9: 27–31. Available: <http://www.pubmedcentral.nih.gov/articlerender.fcgi?artid=3096239&tool=pmcentrez&rendertype=abstract>.
5. Allegranzi B, Nejad SB, Combescure C, Graafmans W, Attar H, et al. (2011) Burden of endemic health-care-associated infection in developing countries: systematic review and meta-analysis. *Lancet* 377: 228–241. Available: [http://dx.doi.org/10.1016/S0140-6736\(10\)61458-4](http://dx.doi.org/10.1016/S0140-6736(10)61458-4).
6. ECDC (2016) Healthcare-associated infections. Ecdc. Available: [http://ecdc.europa.eu/en/healthtopics/Healthcare-associated\\_infections/pages/index.aspx](http://ecdc.europa.eu/en/healthtopics/Healthcare-associated_infections/pages/index.aspx). Accessed 15 May 2016.
7. ECDC (2008) European Centre for Disease Prevention and Control: Annual Epidemiological Report on Communicable Diseases in Europe 2008. Stockholm.
8. Guggenbichler J, Assadian O, Kramer M (2011) Incidence and clinical implication of nosocomial infections associated with implantable biomaterials – catheters , ventilator-associated pneumonia , urinary tract infections Inzidenz und klinische Folgen implantatassoziiertes nosokomialer. *GMS Krankenhhyg Interdiszip* 6: 1–19. doi:10.3205/dgkh000175.
9. Falci Ercole F, Ernesto Ferreira Starling C, Couto Machado Chianca T, Carneiro M (2007) Applicability of the National Nosocomial Infections Surveillance System Risk Index for the Prediction of Surgical Site Infections: A Review. *BJID Brazilian J Infect Dis* 1111: 134–141. Available: [www.bjid.com.br](http://www.bjid.com.br).
10. Pittet D, Allegranzi B, Storr J, Nejad SB, Dziekan G, et al. (2008) Infection control as a major World Health Organization priority for developing countries. *J Hosp Infect* 6: 285–292.
11. Sydnor ERM, Perl TM (2011) Hospital epidemiology and infection control in acute-care settings. *Clin Microbiol Rev* 24: 141–173. doi:10.1128/CMR.00027-10.
12. Custovic A, Smajlovic J, Hadzic S, Ahmetagic S, Tihic N, et al. (2014) Epidemiological surveillance of bacterial nosocomial infections in the surgical intensive care unit. *Mater Sociomed* 26: 7–11. Available:



- <http://www.pubmedcentral.nih.gov/articlerender.fcgi?artid=3990379&tool=pmcentrez&rendertype=abstract>.
13. Zimlichman E, Henderson D, Tamir O, Franz C, Song P, et al. (2013) Health Care–Associated Infections. *JAMA Intern Med* 173: 2039. Available: <http://archinte.jamanetwork.com/article.aspx?doi=10.1001/jamainternmed.2013.9763>.
  14. ECDC (2015) European Surveillance of Healthcare-Associated Infections in Intensive Care Units.
  15. Nnis (2004) - National Nosocomial Infections Surveillance , Public Health Service, System Report data summary from January 1992 through June 2004, issued October 2004. *Am J Infect Control* 32: 470–485. doi:10.1016/j.ajic.2004.10.001.
  16. Girmenia C, Lo Coco F, Breccia M, Latagliata R, Spadea A, et al. (2003) Infectious complications in patients with acute promyelocytic leukaemia treated with the AIDA regimen. *Leukemia* 17: 925–930. Available: <http://www.ncbi.nlm.nih.gov/pubmed/12750707>.
  17. Lech-Maranda E, Seweryn M, Giebel S, Holowiecki J, Piatkowska-Jakubas B, et al. (2010) Infectious complications in patients with acute myeloid leukemia treated according to the protocol with daunorubicin and cytarabine with or without addition of cladribine. A multicenter study by the Polish Adult Leukemia Group (PALG). *Int J Infect Dis* 14: e132–e140. Available: <http://dx.doi.org/10.1016/j.ijid.2009.02.021>.
  18. Bhatt VR, Viola GM, Ferrajoli A (2011) Invasive fungal infections in acute leukemia. *Ther Adv Hematol* 2: 231–247. doi:10.1177/2040620711410098.
  19. Guinan JL, McGuckin M, Nowell PC (2003) Management of health-care--associated infections in the oncology patient. *Oncol (willist Park)* 17: 415–416.
  20. Thom KA, Kleinberg M, Roghmann M-C (2013) Infection prevention in the cancer center. *Clin Infect Dis* 57: 579–585. Available: [http://umaryland.pure.elsevier.com/en/publications/infection-prevention-in-the-cancer-center\(7bd0739b-1b59-4294-9a16-f24309e7fb85\).html](http://umaryland.pure.elsevier.com/en/publications/infection-prevention-in-the-cancer-center(7bd0739b-1b59-4294-9a16-f24309e7fb85).html).
  21. Xiao J, Gao G, Li Y, Zhang W, Tian Y, et al. (2013) Spectrums of Opportunistic Infections and Malignancies in HIV-Infected Patients in Tertiary Care Hospital, China. *PLoS One* 8. Available: <http://dx.doi.org/10.1371%2Fjournal.pone.0075915>.
  22. Fanosie A, Gelaw B, Tessema B, Tesfay W, Admasu A, et al. (2016) *Mycobacterium tuberculosis* Complex and HIV Co-Infection among Extrapulmonary Tuberculosis Suspected Cases at the University of Gondar Hospital, Northwestern Ethiopia. *PLoS One* 11: 1–15. Available: <http://dx.doi.org/10.1371%2Fjournal.pone.0150646>.
  23. Ercibengoa M, Pérez-Trallero E, Marimón JM (2016) Autochthonous *Nocardia cerradoensis* Infection in Humans, Spain, 2011 and 2014. *Emerg Infect Dis* 22: 109–111. Available: <http://www.ncbi.nlm.nih.gov/pmc/articles/PMC4696691/>.
  24. Wójkowska-Mach J, Merritt TA, Borszewska-Kornacka M, Domańska J, Gulczyńska E, et al. (2016) Device-associated pneumonia of very low birth weight infants in Polish Neonatal Intensive Care Units. *Adv Med Sci* 61: 90–95.

- Available:  
<http://www.sciencedirect.com/science/article/pii/S1896112615000498>.
25. Silwedel C, Vogel U, Claus H, Glaser K, Speer CP, et al. (2016) Outbreak of multidrug-resistant *Escherichia coli* sequence type 131 in a neonatal intensive care unit: efficient active surveillance prevented fatal outcome. *J Hosp Infect*. Available:  
<http://www.sciencedirect.com/science/article/pii/S0195670116001341>.
  26. Ukkonen M, Karlsson S, Laukkarinen J, Rantanen T, Paajanen H (2016) Severe Sepsis in Elderly Patients Undergoing Gastrointestinal Surgery---a Prospective Multicenter Follow-up Study of Finnish Intensive Care Units. *J Gastrointest Surg* 20: 1028–1033. Available: <http://dx.doi.org/10.1007/s11605-016-3076-4>.
  27. Dal-Bó K, Silva RM da, Sakae TM (2012) Infecção hospitalar em uma unidade de terapia intensiva neonatal do Sul do Brasil. *Rev Bras Ter Intensiva* 24: 381–385.
  28. Ribet D, Cossart P (2015) How bacterial pathogens colonize their hosts and invade deeper tissues. *Microbes Infect* 17: 173–183. Available: <http://dx.doi.org/10.1016/j.micinf.2015.01.004>.
  29. Grice EA, Bethesda M, Segre JA (2013) The skin microbiome. *Nat Rev Microbiol* 9: 244–253. doi:10.1038/nrmicro2537.The.
  30. Jung Y, Lee MJ, Sin H-Y, Kim N-H, Hwang J-H, et al. (2012) Differences in characteristics between healthcare-associated and community-acquired infection in community-onset *Klebsiella pneumoniae* bloodstream infection in Korea. *BMC Infect Dis* 12: 1–9. Available: <http://dx.doi.org/10.1186/1471-2334-12-239>.
  31. Mandell LA, Bartlett JG, Dowell SF, File Jr. TM, Musher DM, et al. (2003) Update of practice guidelines for the management of community-acquired pneumonia in immunocompetent adults. *Clin Infect Dis* 37: 1405–1433. Available: <http://www.ncbi.nlm.nih.gov/pubmed/14614663>.
  32. Micek ST, Kollef KE, Reichley RM, Roubinian N, Kollef MH (2007) Health care-associated pneumonia and community-acquired pneumonia: A single-center experience. *Antimicrob Agents Chemother* 51: 3568–3573. doi:10.1128/AAC.00851-07.
  33. Friedman ND, Kaye KS, Stout JE, McGarry S a, Trivette SL, et al. (2002) Health Care - Associated Bloodstream Infections in Adults: A Reason To Change the Accepted Definition of Community - Acquired Infections. *Ann Fam Med*: 791–798. Available: <http://dx.doi.org/10.1097/00019048-200206000-00016>.
  34. Siegman-Igra Y, Fourer B, Orni-Wasserlauf R, Golan Y, Noy A, et al. (2002) Reappraisal of community-acquired bacteremia: a proposal of a new classification for the spectrum of acquisition of bacteremia. *Clin Infect Dis* 34: 1431–1439. doi:10.1086/339809.
  35. Horan TC, Andrus M, Dudeck MA (2008) CDC/NHSN surveillance definition of health care-associated infection and criteria for specific types of infections in the acute care setting. *Am J Infect Control* 36: 309–332. Available: <http://dx.doi.org/10.1016/j.ajic.2008.03.002>.
  36. Nicolle LE (2013) Antimicrobial resistance in community-acquired *Escherichia coli* isolated from urinary infection : Good news or bad ? 24: 123–124.

37. Cimolai N (2006) Community-acquired MRSA infection: An emerging trend. *B C Med J* 48: 116–120.
38. David MZ, Daum RS (2010) Community-associated methicillin-resistant *Staphylococcus aureus*: Epidemiology and clinical consequences of an emerging epidemic. *Clin Microbiol Rev* 23: 616–687. doi:10.1128/CMR.00081-09.
39. Cardoso T, Almeida M, Friedman ND, Aragão I, Costa-Pereira A, et al. (2014) Classification of healthcare-associated infection: a systematic review 10 years after the first proposal. *BMC Med* 12: 40. Available: <http://www.pubmedcentral.nih.gov/articlerender.fcgi?artid=4016612&tool=pmcentrez&rendertype=abstract>.
40. Newsom SWB (2008) Ogston's coccus. *J Hosp Infect* 70: 369–372. Available: <http://dx.doi.org/10.1016/j.jhin.2008.10.001>.
41. Gildeen D (2013) Neuroinfections (What Do I Do Now?). BOOKS Press 19: 30333.
42. Lowy FD (1998) *Staphylococcus aureus* infections. *N Engl J Med* 339: 520–532.
43. Tong SYC, Davis JS, Eichenberger E, Holland TL, Vance G, Fowler J (2015) *Staphylococcus aureus* Infections: Epidemiology, Pathophysiology, Clinical Manifestations, and Management. *Clin Microbiol Rev* 28: 603–661. doi:10.1128/CMR.4.1.52.
44. Holden MTG, Feil EJ, Lindsay J a, Peacock SJ, Day NPJ, et al. (2004) Complete genomes of two clinical *Staphylococcus aureus* strains: Evidence for the rapid evolution of virulence and drug resistance. *Proc Natl Acad Sci U S A* 101: 9786–9791. doi:10.1073/pnas.0402521101.
45. Green BN, Johnson CD, Egan JT, Rosenthal M, Griffith E a., et al. (2012) Methicillin-resistant *Staphylococcus aureus*: An overview for manual therapists. *J Chiropr Med* 11: 64–76. Available: <http://dx.doi.org/10.1016/j.jcm.2011.12.001>.
46. Hoff B, Pöggeler S, Kück U (2008) Eighty years after its discovery, Fleming's *Penicillium* strain discloses the secret of its sex. *Eukaryot Cell* 7: 465–470. doi:10.1128/EC.00430-07.
47. Abraham E (1990) Selective reminiscences of beta-lactam antibiotics: early research on penicillin and cephalosporins. *Bioessays* 12: 601–606. doi:10.1002/bies.950121208.
48. Barber M, Rozwadowska-Dowzenko M (1948) Infection by penicillin-resistant staphylococci. *Lancet (London, England)* 2: 641–644.
49. Demerec M (1945) Production of *Staphylococcus* strains resistant to various concentrations of penicillin. *Proc Natl Acad Sci USA* 31: 16–24. doi:10.1073/pnas.31.1.16.
50. Turlej A, Hryniewicz W, Empel J (2011) Staphylococcal Cassette Chromosome mec (SCCmec) classification and typing methods: An overview. *Polish J Microbiol* 60: 95–103.
51. Chambers HF, Deleo FR (2010) Waves of Resistance: *Staphylococcus aureus* in the Antibiotic Era. *Nat Rev Microbiol* 7: 629–641. doi:10.1038/nrmicro2200.Waves.

52. Jevons MP (1961) "Celbenin"- Resistant Staphylococci. *Br Med J* 1: 124–125.
53. Ito T, Hiramatsu K, Oliveira DC, De Lencastre H, Zhang K, et al. (2009) Classification of staphylococcal cassette chromosome mec (SCCmec): Guidelines for reporting novel SCCmec elements. *Antimicrob Agents Chemother* 53: 4961–4967. doi:10.1128/AAC.00579-09.
54. Katayama Y, Ito T, Hiramatsu K (2000) A new class of genetic element, staphylococcus cassette chromosome mec, encodes methicillin resistance in *Staphylococcus aureus*. *Antimicrob Agents Chemother* 44: 1549–1555. doi:10.1128/AAC.44.6.1549-1555.2000.
55. Suzuki E, Hiramatsu K, Yokota T (1992) Survey of methicillin-resistant clinical strains of coagulase-negative Staphylococci for mecA gene distribution. *Antimicrob Agents Chemother* 36: 429–434. doi:10.1128/AAC.36.2.429.
56. Takeuchi F, Takeuchi F, Watanabe S, Watanabe S, Baba T, et al. (2005) Whole-Genome Sequencing of *Staphylococcus haemolyticus* Uncovers the Extreme Plasticity of Its Genome and the Evolution of Human-Colonizing Staphylococcal Species. *Society* 187: 7292–7308. doi:10.1128/JB.187.21.7292.
57. Tsubakishita S, Kuwahara-Arai K, Sasaki T, Hiramatsu K (2010) Origin and molecular evolution of the determinant of methicillin resistance in staphylococci. *Antimicrob Agents Chemother* 54: 4352–4359. doi:10.1128/AAC.00356-10.
58. Vernozy-rozand C, Mazuy C, Lasne Y, Fiedler F, Etienne J (2000) *Staphylococcus fleurettii* sp . nov ., isolated from goat ' s milk cheeses. *Int J Syst Evol Microbiol*: 1521–1527.
59. García-Álvarez L, Holden MTG, Lindsay H, Webb CR, Brown DFJ, et al. (2011) Methicillin-resistant *Staphylococcus aureus* with a novel mecA homologue in human and bovine populations in the UK and Denmark: A descriptive study. *Lancet Infect Dis* 11: 595–603. doi:10.1016/S1473-3099(11)70126-8.
60. Vandendriessche S, Vanderhaeghen W, Soares FV, Hallin M, Catry B, et al. (2013) Prevalence, risk factors and genetic diversity of methicillin-resistant *Staphylococcus aureus* carried by humans and animals across livestock production sectors. *J Antimicrob Chemother* 68: 1510–1516. doi:10.1093/jac/dkt047.
61. Harrison EM, Paterson GK, Holden MTG, Larsen J, Stegger M, et al. (2013) Whole genome sequencing identifies zoonotic transmission of MRSA isolates with the novel mecA homologue mecC. *EMBO Mol Med* 5: 509–515. doi:10.1002/emmm.201202413.
62. Berglund C, Söderquist B (2008) The origin of a methicillin-resistant *Staphylococcus aureus* isolate at a neonatal ward in Sweden - Possible horizontal transfer of a staphylococcal cassette chromosome mec between methicillin-resistant *Staphylococcus haemolyticus* and *Staphylococcus aureus*. *Clin Microbiol Infect* 14: 1048–1056. Available: <http://dx.doi.org/10.1111/j.1469-0691.2008.02090.x>.
63. Udo EE, Pearman JW, Grubb WB (1993) Genetic analysis of community isolates of methicillin-resistant *Staphylococcus aureus* in Western Australia. *J Hosp Infect* 25: 97–108.
64. Herold B, Immergluck L, Maranan M, Lauderdale DS, Gaskin RE, et al. (1998)

- Community-acquired methicillin-resistant staphylococcus aureus in children with no identified predisposing risk. *JAMA* 279: 593–598. Available: +.
65. Filice GA, Nyman JA, Lexau C, Lees CH, Bockstedt LA, et al. (2010) Excess Costs and Utilization Associated with Methicillin Resistance for Patients with *Staphylococcus aureus* Infection. *Infect Control Hosp Epidemiol* 31: 365–373. Available: <http://www.jstor.org/stable/10.1086/651094>.
  66. Sievert DM, Ricks P, Edwards JR, Schneider A, Patel J, et al. (2013) Antimicrobial-Resistant Pathogens Associated with Healthcare-Associated Infections Summary of Data Reported to the National Healthcare Safety Network at the Centers for Disease Control and Prevention, 2009–2010. *Infect Control Hosp Epidemiol* 34: 1–14. Available: <http://dx.doi.org/10.1086/668770>.
  67. Frazee BW, Lynn J, Charlebois ED, Lambert L, Lowery D, et al. (2005) High Prevalence of Methicillin-Resistant *Staphylococcus aureus* in Emergency Department Skin and Soft Tissue Infections. *Ann Emerg Med* 45: 311–320. Available: <http://dx.doi.org/10.1016/j.annemergmed.2004.10.011>.
  68. Gordon RJ, Lowy FD (2008) Pathogenesis of Methicillin-Resistant *Staphylococcus aureus* Infection. *Clin Infect Dis* 1: 350–359. doi:10.1016/j.biotechadv.2011.08.021.Secreted.
  69. Wright BM, Eiland EH (2011) Retrospective Analysis of Clinical and Cost Outcomes Associated with Methicillin-Resistant *Staphylococcus aureus* Complicated Skin and Skin Structure Infections Treated with Daptomycin, Vancomycin, or Linezolid. *J Pathog* 2011: 347969. doi:10.4061/2011/347969.
  70. Busch BA, Ahern MT, Topinka M, Jenkins II JJ, Weiser MA (2010) Eschar with Cellulitis as a Clinical Predictor in Community-Acquired Methicillin-Resistant *Staphylococcus Aureus* (MRSA) Skin Abscess. *J Emerg Med* 38: 563–566. Available: <http://dx.doi.org/10.1016/j.jemermed.2007.11.072>.
  71. Rutar T, Zwick OM, Cockerham KP, Horton JC (2005) Bilateral Blindness From Orbital Cellulitis Caused by Community-Acquired Methicillin-Resistant *Staphylococcus aureus*. *Am J Ophthalmol* 140: 740–742. Available: <http://dx.doi.org/10.1016/j.ajo.2005.03.076>.
  72. Collins M, Tami TA (2003) Methicillin-resistant *Staphylococcus aureus* (MRSA) in the practice of otolaryngology—an emerging community acquired organism? *Curr Opin Otolaryngol Head Neck Surg* 11. Available: [http://journals.lww.com/co-otolaryngology/Fulltext/2003/06000/Methicillin\\_resistant\\_Staphylococcus\\_aureus\\_\\_MRSA\\_.9.aspx](http://journals.lww.com/co-otolaryngology/Fulltext/2003/06000/Methicillin_resistant_Staphylococcus_aureus__MRSA_.9.aspx).
  73. Sachithanandam ST (2014) Case Report Rising Methicillin-Resistant *Staphylococcus aureus* Infections in Ear , Nose , and Throat Diseases. 2014: 10–13.
  74. Alexander N, Kulbersh B, Heath C, Desmond RA, Caron E, et al. (2011) Mrsa and non-mrsa otorrhea in children: A comparative study of clinical course. *Arch Otolaryngol Neck Surg* 137: 1223–1227. Available: <http://dx.doi.org/10.1001/archoto.2011.198>.
  75. Kumar PS, Cunnion KM (2013) Case Report Acute MRSA Sinusitis with Intracranial Extension and Marginal Vancomycin Susceptibility. 2013.

76. Van Hoecke H, Piette A, De Leenheer E, Lagasse N, Struelens M, et al. (2009) Destructive otomastoiditis by MRSA from porcine origin. *Laryngoscope* 119: 137–140. doi:10.1002/lary.20030.
77. Bamberger DM (2007) Bacteremia and endocarditis due to methicillin-resistant *Staphylococcus aureus*: The potential role of daptomycin. *Ther Clin Risk Manag* 3: 675–684.
78. Cosgrove SE, Fowler, Jr. VG (2008) Management of Methicillin -Resistant *Staphylococcus aureus* Bacteremia. *Clin Infect Dis* 46: S386–S393. Available: <http://cid.oxfordjournals.org/lookup/doi/10.1086/533595>.
79. Pastagia M, Kleinman LC, Lacerda EG, Cruz D, Jenkins SG (2012) Predicting Risk for Death. *Emerg Infect Dis* 18: 1072–1080. Available: <http://www.pubmedcentral.nih.gov/articlerender.fcgi?artid=3376787&tool=pmcentrez&rendertype=abstract>.
80. Otto M (2013) Improved understanding of factors driving epidemic waves: 205–217.
81. Pereira PM, Filipe SR, Tomasz A, Pinho MG (2007) Fluorescence ratio imaging microscopy shows decreased access of vancomycin to cell wall synthetic sites in vancomycin-resistant *Staphylococcus aureus*. *Antimicrob Agents Chemother* 51: 3627–3633. doi:10.1128/AAC.00431-07.
82. Shiu J, Wang E, Tejani AM, Wasdell M (2013) Continuous versus intermittent infusions of antibiotics for the treatment of severe acute infections. *Cochrane database Syst Rev*: CD008481. doi:10.1002/14651858.CD008481.pub2.
83. Appelbaum PC (2007) Reduced glycopeptide susceptibility in methicillin-resistant *Staphylococcus aureus* (MRSA). *Int J Antimicrob Agents* 30: 398–408. Available: <http://dx.doi.org/10.1016/j.ijantimicag.2007.07.011>.
84. Santajit S, Indrawattana N (2016) Mechanisms of Antimicrobial Resistance in ESKAPE Pathogens. *Biomed Res Int* 2016: 1–8. Available: <http://www.hindawi.com/journals/bmri/2016/2475067/>.
85. Howden BP, Davies JK, Johnson PDR, Stinear TP, Grayson ML (2010) Reduced vancomycin susceptibility in *Staphylococcus aureus*, including vancomycin-intermediate and heterogeneous vancomycin-intermediate strains: Resistance mechanisms, laboratory detection, and clinical implications. *Clin Microbiol Rev* 23: 99–139. doi:10.1128/CMR.00042-09.
86. Aoki H, Ke L, Poppe SM, Poel TJ, Weaver EA, et al. (2002) Oxazolidinone Antibiotics Target the P Site on *Escherichia coli* Ribosomes Oxazolidinone Antibiotics Target the P Site on *Escherichia coli* Ribosomes †. *Antimicrob Agents Chemother* 46: 1080–1085. doi:10.1128/AAC.46.4.1080.
87. Gould IM, Cauda R, Esposito S, Gudiol F, Mazzei T, et al. (2011) Management of serious methicillin-resistant *Staphylococcus aureus* infections: what are the limits? *Int J Antimicrob Agents* 37: 202–209. Available: <http://dx.doi.org/10.1016/j.ijantimicag.2010.10.030>.
88. Docobo-Pérez F, López-Rojas R, Domínguez-Herrera J, Jiménez-Mejías ME, Pichardo C, et al. (2012) Efficacy of linezolid versus a pharmacodynamically optimized vancomycin therapy in an experimental pneumonia model caused by methicillin-resistant *Staphylococcus aureus*. *J Antimicrob Chemother* 67: 1961–

1967. doi:10.1093/jac/dks142.
89. Martinez-Olondris P, Rigol M, Soy D, Guerrero L, Agusti C, et al. (2012) Efficacy of linezolid compared to vancomycin in an experimental model of pneumonia induced by methicillin-resistant *Staphylococcus aureus* in ventilated pigs. *Crit Care Med* 40: 162–168. doi:10.1097/CCM.0b013e31822d74a2.
  90. Plosker GL, Figgitt DP (2005) Linezolid: a pharmacoeconomic review of its use in serious Gram-positive infections. *Pharmacoeconomics* 23: 945–964.
  91. Gu B, Kelesidis T, Tsiodras S, Hindler J, Humphries RM (2013) The emerging problem of linezolid-resistant *Staphylococcus*. *J Antimicrob Chemother* 68: 4–11. doi:10.1093/jac/dks354.
  92. Tian Y, Li T, Zhu Y, Wang B, Zou X, et al. (2014) Mechanisms of linezolid resistance in staphylococci and enterococci isolated from two teaching hospitals in Shanghai, China. *BMC Microbiol* 14: 292. Available: <http://www.pubmedcentral.nih.gov/articlerender.fcgi?artid=4245736&tool=pmcentrez&rendertype=abstract> \n<http://www.biomedcentral.com/1471-2180/14/292> \n<http://www.ncbi.nlm.nih.gov/pubmed/25420718> \n<http://www.pubmedcentral.nih.gov/articlerender.fcgi?artid=PMC>.
  93. Locke JB, Hilgers M, Shaw KJ (2009) Novel ribosomal mutations in *Staphylococcus aureus* strains identified through selection with the oxazolidinones linezolid and torezolid (TR-700). *Antimicrob Agents Chemother* 53: 5265–5274. doi:10.1128/AAC.00871-09.
  94. Locke JB, Hilgers M, Shaw KJ (2009) Mutations in ribosomal protein L3 are associated with oxazolidinone resistance in staphylococci of clinical origin. *Antimicrob Agents Chemother* 53: 5275–5278. doi:10.1128/AAC.01032-09.
  95. Wong A, Reddy SP, Smyth DS, Agüero-Rosenfeld ME, Sakoulas G, et al. (2010) Polyphyletic emergence of linezolid-resistant staphylococci in the United States. *Antimicrob Agents Chemother* 54: 742–748. doi:10.1128/AAC.00621-09.
  96. Long KS, Vester B (2012) Resistance to linezolid caused by modifications at its binding site on the ribosome. *Antimicrob Agents Chemother* 56: 603–612. doi:10.1128/AAC.05702-11.
  97. Tsiodras S, Gold HS, Sakoulas G, Eliopoulos GM, Wennersten C, et al. (2001) Linezolid resistance in a clinical isolate of *Staphylococcus aureus*. *Lancet* 358: 207–208. Available: [http://dx.doi.org/10.1016/S0140-6736\(01\)05410-1](http://dx.doi.org/10.1016/S0140-6736(01)05410-1).
  98. Prystowsky J, Siddiqui F, Chosay J, Shinabarger DL, Millichap J, et al. (2001) Resistance to linezolid: Characterization of mutations in rRNA and comparison of their occurrences in vancomycin-resistant enterococci. *Antimicrob Agents Chemother* 45: 2154–2156. doi:10.1128/AAC.45.7.2154-2156.2001.
  99. Olsen KM, Rebuck JA, Rupp ME (2001) Arthralgias and myalgias related to quinupristin-dalfopristin administration. *Clin Infect Dis* 32: e83–e86. doi:10.1086/318702.
  100. Kaka AS, Rueda AM, Shelburne SA 3rd, Hulten K, Hamill RJ, et al. (2006) Bactericidal activity of orally available agents against methicillin-resistant *Staphylococcus aureus*. *J Antimicrob Chemother* 58: 680–683. doi:10.1093/jac/dkl283.
  101. Nørskov-Lauritsen N, Marchandin H, Dowzicky MJ (2009) Antimicrobial

- susceptibility of tigecycline and comparators against bacterial isolates collected as part of the TEST study in Europe (2004-2007). *Int J Antimicrob Agents* 34: 121–130. doi:10.1016/j.ijantimicag.2009.02.003.
102. Schrieffer CA, Fernandez C, Rodvold KA, Danziger LH (2005) Daptomycin: a novel cyclic lipopeptide antimicrobial. *Am J Health Syst Pharm* 62: 1145–1158.
  103. Friedman L, Alder JD, Silverman JA (2006) Genetic changes that correlate with reduced susceptibility to daptomycin in *Staphylococcus aureus*. *Antimicrob Agents Chemother* 50: 2137–2145. doi:10.1128/AAC.00039-06.
  104. Yang S, Kreiswirth BN, Sakoulas G, Yeaman MR, Yan Q, et al. (2010) Enhanced expression of *dltABCD* is associated with development of daptomycin nonsusceptibility in a clinical endocarditis isolate of *Staphylococcus aureus*. 200: 1916–1920. doi:10.1086/648473.Enhanced.
  105. Cui L, Isii T, Fukuda M, Ochiai T, Neoh HM, et al. (2010) An RpoB mutation confers dual heteroresistance to daptomycin and vancomycin in *Staphylococcus aureus*. *Antimicrob Agents Chemother* 54: 5222–5233. doi:10.1128/AAC.00437-10.
  106. Zhanel GG, Trapp S, Gin AS, DeCorby M, Lagacé-Wiens PRS, et al. (2008) Dalbavancin and telavancin: novel lipoglycopeptides for the treatment of Gram-positive infections. *Expert Rev Anti Infect Ther* 6: 67–81. Available: <http://dx.doi.org/10.1586/14787210.6.1.67>.
  107. Chen AY, Zervos MJ, Vazquez JA (2007) Dalbavancin: A novel antimicrobial. *Int J Clin Pract* 61: 853–863. doi:10.1111/j.1742-1241.2007.01318.x.
  108. Jauregui LE, Babazadeh S, Seltzer E, Goldberg L, Krievins D, et al. (2005) Randomized, double-blind comparison of once-weekly dalbavancin versus twice-daily linezolid therapy for the treatment of complicated skin and skin structure infections. *Clin Infect Dis* 41: 1407–1415. doi:10.1086/497271.
  109. Stryjewski ME, O’Riordan WD, Lau WK, Pien FD, Dunbar LM, et al. (2005) Telavancin versus standard therapy for treatment of complicated skin and soft-tissue infections due to gram-positive bacteria. *Clin Infect Dis* 40: 1601–1607. doi:10.1086/429914.
  110. Laohavaleeson S, Kuti JL, Nicolau DP (2007) Telavancin: a novel lipoglycopeptide for serious gram-positive infections. *Expert Opin Investig Drugs* 16: 347–357. doi:10.1517/13543784.16.3.347.
  111. Rodvold KA, Mcconeghy KW (2014) Methicillin-resistant staphylococcus aureus therapy: Past, present, and future. *Clin Infect Dis* 58: 20–27. doi:10.1093/cid/cit614.
  112. Buyck JM, Tulkens PM, Van Bambeke F (2015) RX-P873, a novel protein synthesis inhibitor, accumulates in human THP-1 monocytes and is active against intracellular infections by Gram-positive (*Staphylococcus aureus*) and Gram-negative (*Pseudomonas aeruginosa*) bacteria. *Antimicrob Agents Chemother* 59: 4750–4758. Available: <http://www.ncbi.nlm.nih.gov/pubmed/26014952>.
  113. Kumar K, Chopra S (2013) New drugs for methicillin-resistant *Staphylococcus aureus*: An update. *J Antimicrob Chemother* 68: 1465–1470. doi:10.1093/jac/dkt045.
  114. Rubinchik E, Schneider T, Elliott M, Scott WRP, Pan J, et al. (2011) Mechanism



- of action and limited cross-resistance of new lipopeptide MX-2401. *Antimicrob Agents Chemother* 55: 2743–2754. doi:10.1128/AAC.00170-11.
115. Hashizume H, Sawa R, Harada S, Igarashi M, Adachi H, et al. (2011) Tripropeptin C blocks the lipid cycle of cell wall biosynthesis by complex formation with undecaprenyl pyrophosphate. *Antimicrob Agents Chemother* 55: 3821–3828. doi:10.1128/AAC.00443-11.
  116. Vejbaesya S, Luangtrakool P, Luangtrakool K, Vaughn DW, Endy TP, et al. (2010) Oritavancin exhibits dual mode of action to inhibit cell-wall biosynthesis in *Staphylococcus aureus*. *199: 1442–1448*. doi:10.1086/597422.Tumor.
  117. Pallanza R, Berti M, Goldstein BP, Mapelli E, Randisi E, et al. (1983) Teichomycin: in-vitro and in-vivo evaluation in comparison with other antibiotics. *J Antimicrob Chemother* 11 : 419–425. Available: <http://jac.oxfordjournals.org/content/11/5/419.abstract>.
  118. van Hal SJ, Paterson DL (2011) New Gram-positive antibiotics: better than vancomycin? *Curr Opin Infect Dis* 24: 515–520. doi:10.1097/QCO.0b013e32834ab1de.
  119. Somma S, Gastaldo L, Corti A (1984) Teicoplanin, a new antibiotic from *Actinoplanes teichomyceticus* nov. sp. *Antimicrob Agents Chemother* 26: 917–923. doi:10.1128/AAC.26.6.917.
  120. Blais J, Lewis SR, Krause KM, Benton BM (2012) Antistaphylococcal activity of TD-1792, a multivalent glycopeptide- cephalosporin antibiotic. *Antimicrob Agents Chemother* 56: 1584–1587. doi:10.1128/AAC.05532-11.
  121. Leuthner KD, Vidaillac C, Cheung CM, Rybak MJ (2010) In vitro activity of the new multivalent glycopeptide-cephalosporin antibiotic TD-1792 against vancomycin-nonsusceptible *Staphylococcus* isolates. *Antimicrob Agents Chemother* 54: 3799–3803. doi:10.1128/AAC.00452-10.
  122. Stryjewski ME, Potgieter PD, Li YP, Barriere SL, Churukian A, et al. (2012) TD-1792 versus vancomycin for treatment of complicated skin and skin structure infections. *Antimicrob Agents Chemother* 56: 5476–5483. doi:10.1128/AAC.00712-12.
  123. Mensa B, Howell GL, Scott R, DeGrado WF (2014) Comparative mechanistic studies of brilacidin, daptomycin, and the antimicrobial peptide LL16. *Antimicrob Agents Chemother* 58: 5136–5145. doi:10.1128/AAC.02955-14.
  124. PolyMedix. Brilacidin (PMX-30063) (n.d.) Acute Bacterial Skin and Skin Structure Infections (ABSSSI). Available: <http://www.polymedix.com/pipeline/Brilacidin/absssi>. Accessed 1 July 2016.
  125. Ooi N, Miller K, Hobbs J, Rhys-Williams W, Love W, et al. (2009) XF-73, a novel antistaphylococcal membrane-active agent with rapid bactericidal activity. *J Antimicrob Chemother* 64: 735–740. doi:10.1093/jac/dkp299.
  126. Obiang-Obounou BW, Kang O-H, Choi J-G, Keum J-H, Kim S-B, et al. (2011) The mechanism of action of sanguinarine against methicillin-resistant *Staphylococcus aureus*. *J Toxicol Sci* 36: 277–283.
  127. Pandit N, Singla RK, Shrivastava B (2012) Current Updates on Oxazolidinone and Its Significance. *Int J Med Chem* 2012: 1–24. doi:10.1155/2012/159285.

128. Ippolito JA, Kanyo ZF, Wang D, Franceschi FJ, Moore PB, et al. (2008) Crystal structure of the oxazolidinone antibiotic linezolid bound to the 50S ribosomal subunit. *J Med Chem* 51: 3353–3356. doi:10.1021/jm800379d.
129. Shaw KJ, Poppe S, Schaadt R, Brown-Driver V, Finn J, et al. (2008) In vitro activity of TR-700, the antibacterial moiety of the prodrug TR-701, against linezolid-resistant strains. *Antimicrob Agents Chemother* 52: 4442–4447. doi:10.1128/AAC.00859-08.
130. Lepak AJ, Marchillo K, Pichereau S, Craig WA, Andes DR (2012) Comparative pharmacodynamics of the new oxazolidinone tedizolid phosphate and linezolid in a neutropenic murine *Staphylococcus aureus* pneumonia model. *Antimicrob Agents Chemother* 56: 5916–5922. doi:10.1128/AAC.01303-12.
131. Locke JB, Finn J, Hilgers M, Morales G, Rahawi S, et al. (2010) Structure-activity relationships of diverse oxazolidinones for linezolid-resistant *Staphylococcus aureus* strains possessing the *cfr* methyltransferase gene or ribosomal mutations. *Antimicrob Agents Chemother* 54: 5337–5343. doi:10.1128/AAC.00663-10.
132. Noel GJ, Draper MP, Hait H, Tanaka SK, Arbeit RD (2012) A randomized, evaluator-blind, phase 2 study comparing the safety and efficacy of omadacycline to those of linezolid for treatment of complicated skin and skin structure infections. *Antimicrob Agents Chemother* 56: 5650–5654. doi:10.1128/AAC.00948-12.
133. Sutcliffe JA, O'Brien W, Fyfe C, Grossman TH (2013) Antibacterial activity of eravacycline (TP-434), a novel fluorocycline, against hospital and community pathogens. *Antimicrob Agents Chemother* 57: 5548–5558. doi:10.1128/AAC.01288-13.
134. Tenover FC, Tickler I, Armstrong ES, Kubo A, Lopez S, et al. (2011) Activity of ACHN-490 against methicillin-resistant *Staphylococcus aureus* (MRSA) isolates from patients in US hospitals. *Int J Antimicrob Agents* 38: 352–354. doi:10.1016/j.ijantimicag.2011.05.016.
135. Peyrusson F, Butler D, Tulkens PM, Van Bambeke F (2015) Cellular pharmacokinetics and intracellular activity of the novel peptide deformylase inhibitor GSK1322322 against *Staphylococcus aureus* laboratory and clinical strains with various resistance phenotypes: Studies with human THP-1 monocytes and J774 murine. *Antimicrob Agents Chemother* 59: 5747–5760. doi:10.1128/AAC.00827-15.
136. Corey R, Naderer OJ, O'Riordan WD, Dumont E, Jones LS, et al. (2014) Safety, tolerability, and efficacy of GSK1322322 in the treatment of acute bacterial skin and skin structure infections. *Antimicrob Agents Chemother* 58: 6518–6527. doi:10.1128/AAC.03360-14.
137. Lemaire S, Kosowska-Shick K, Appelbaum PC, Glupczynski Y, van Bambeke F, et al. (2011) Activity of moxifloxacin against intracellular community-acquired methicillin-resistant *Staphylococcus aureus*: Comparison with clindamycin, linezolid and co-trimoxazole and attempt at defining an intracellular susceptibility breakpoint. *J Antimicrob Chemother* 66: 596–607. doi:10.1093/jac/dkq478.
138. Remy JM, Tow-Keogh CA, McConnell TS, Dalton JM, Devito JA (2012)

- Activity of delafloxacin against methicillin-resistant *Staphylococcus aureus*: resistance selection and characterization. *J Antimicrob Chemother* 67: 2814–2820. doi:10.1093/jac/dks307.
139. Stubbings W, Leow P, Yong GC, Goh F, Körber-Irrgang B, et al. (2011) In vitro spectrum of activity of finafloxacin, a novel, pH-activated fluoroquinolone, under standard and acidic conditions. *Antimicrob Agents Chemother* 55: 4394–4397. doi:10.1128/AAC.00833-10.
  140. Patel M V., De Souza NJ, Gupte S V., Jafri MA, Bhagwat SS, et al. (2004) Antistaphylococcal activity of WCK 771, a tricyclic fluoroquinolone, in animal infection models. *Antimicrob Agents Chemother* 48: 4754–4761. doi:10.1128/AAC.48.12.4754-4761.2004.
  141. Bhagwat SS, McGhee P, Kosowska-Shick K, Patel M V., Appelbaum PC (2009) In vitro activity of the quinolone WCK 771 against recent U.S. hospital and community-acquired *Staphylococcus aureus* pathogens with various resistance types. *Antimicrob Agents Chemother* 53: 811–813. doi:10.1128/AAC.01150-08.
  142. Farrell DJ, Liverman LC, Biedenbach DJ, Jones RN (2011) JNJ-Q2, a new fluoroquinolone with potent in vitro activity against *Staphylococcus aureus*, including methicillin- and fluoroquinolone-resistant strains. *Antimicrob Agents Chemother* 55: 3631–3634. doi:10.1128/AAC.00162-11.
  143. Farrell DJ, Turner LL, Castanheira M, Jones RN (2012) Activity of JNJ-Q2 against *Staphylococcus aureus* isolated from patients with acute bacterial skin and skin-structure infection obtained during a Phase 2 clinical trial. *Diagn Microbiol Infect Dis* 74: 73–74. doi:10.1016/j.diagmicrobio.2012.05.031.
  144. Podos SD, Thanassi JA, Leggio M, Pucci MJ (2012) Bactericidal activity of ACH-702 against nondividing and biofilm staphylococci. *Antimicrob Agents Chemother* 56: 3812–3818. doi:10.1128/AAC.00092-12.
  145. Pucci MJ, Podos SD, Thanassi JA, Leggio MJ, Bradbury BJ, et al. (2011) In vitro and in vivo profiles of ACH-702, an isothiazoloquinolone, against bacterial pathogens. *Antimicrob Agents Chemother* 55: 2860–2871. doi:10.1128/AAC.01666-10.
  146. Oefner C, Bandera M, Haldimann A, Laue H, Schulz H, et al. (2009) Increased hydrophobic interactions of iclaprim with *Staphylococcus aureus* dihydrofolate reductase are responsible for the increase in affinity and antibacterial activity. *J Antimicrob Chemother* 63: 687–698. doi:10.1093/jac/dkp024.
  147. Schneider P, Hawser S, Islam K (2003) Iclaprim, a novel diaminopyrimidine with potent activity on trimethoprim sensitive and resistant bacteria. *Bioorg Med Chem Lett* 13: 4217–4221.
  148. Balemans W, Lounis N, Gilissen R, Guillemont J, Simmen K, et al. (2010) Essentiality of FASII pathway for *Staphylococcus aureus*. *Nature* 463: E3–E3. Available: <http://dx.doi.org/10.1038/nature08667>.
  149. Heath RJ, Rock CO (2004) Fatty acid biosynthesis as a target for novel antibacterials. *Curr Opin Investig Drugs* 5: 146–153. doi:10.1097/MPG.0b013e3181a15ae8.Screening.
  150. Karlowsky JA, Kaplan N, Hafkin B, Hoban DJ, Zhanel GG (2009) AFN-1252, a FabI inhibitor, demonstrates a staphylococcus-specific spectrum of activity.

- 
- Antimicrob Agents Chemother 53: 3544–3548. doi:10.1128/AAC.00400-09.
151. Payne DJ, Miller WH, Berry V, Burgess WJ, Chen E, et al. (2002) Discovery of a Novel and Potent Class of FabI-Directed Antibacterial Agents. *Society* 46: 3118–3124. doi:10.1128/AAC.46.10.3118.
  152. Escaich S, Prouvensier L, Saccomani M, Durant L, Oxoby M, et al. (2011) The MUT056399 inhibitor of FabI is a new antistaphylococcal compound. *Antimicrob Agents Chemother* 55: 4692–4697. doi:10.1128/AAC.01248-10.
  153. Schiebel J, Chang A, Shah S, Lu Y, Liu L, et al. (2014) Rational design of broad spectrum antibacterial activity based on a clinically relevant enoyl-acyl carrier protein (ACP) reductase inhibitor. *J Biol Chem* 289: 15987–16005. doi:10.1074/jbc.M113.532804.
  154. Park HS, Yoon YM, Jung SJ, Kim CM, Kim JM, et al. (2007) Antistaphylococcal activities of CG400549, a new bacterial enoyl-acyl carrier protein reductase (FabI) inhibitor. *J Antimicrob Chemother* 60: 568–574. doi:10.1093/jac/dkm236.
  155. Ventola CL (2015) The antibiotic resistance crisis: part 1: causes and threats. *P T A peer-reviewed J Formul Manag* 40: 277–283. Available: <http://www.ncbi.nlm.nih.gov/pubmed/25859123>\n<http://www.pubmedcentral.nih.gov/articlerender.fcgi?artid=PMC4378521>\n<http://www.ncbi.nlm.nih.gov/pubmed/25859123>\n<http://www.pubmedcentral.nih.gov/articlerender.fcgi?artid=PMC4378521>.
  156. CDC (2013) Antibiotic resistance threats in the United States, 2013. Current: 114. Available: <http://www.cdc.gov/drugresistance/threat-report-2013/index.html>.
  157. Lushniak BD (2014) Antibiotic resistance: a public health crisis. *Public Health Rep* 129: 314–316. Available: <http://www.pubmedcentral.nih.gov/articlerender.fcgi?artid=4037453&tool=pmcentrez&rendertype=abstract>.
  158. Bartlett JG, Gilbert DN, Spellberg B (2013) Seven ways to preserve the Miracle of antibiotics. *Clin Infect Dis* 56: 1445–1450. doi:10.1093/cid/cit070.
  159. Boucher HW, Talbot GH, Bradley JS, Edwards JE, Gilbert D, et al. (2009) Bad bugs, no drugs: no ESKAPE! An update from the Infectious Diseases Society of America. *Clin Infect Dis* 48: 1–12. Available: <http://www.ncbi.nlm.nih.gov/pubmed/19035777>.
  160. Silver LL (2011) Challenges of Antibacterial Discovery. *Clin Microbiol Rev* 24: 71–109. Available: <http://cmr.asm.org/cgi/doi/10.1128/CMR.00030-10>.
  161. Bush K (2012) Improving known classes of antibiotics: An optimistic approach for the future. *Curr Opin Pharmacol* 12: 527–534. Available: <http://dx.doi.org/10.1016/j.coph.2012.06.003>.
  162. Power E (2006) Impact of antibiotic restrictions: The pharmaceutical perspective. *Clin Microbiol Infect* 12: 25–34. Available: <http://dx.doi.org/10.1111/j.1469-0691.2006.01528.x>.
  163. Bettiol E, Wetherington JD, Schmitt N, Harbarth S (2015) Challenges and solutions for clinical development of new antibacterial agents: Results of a survey among pharmaceutical industry professionals. *Antimicrob Agents Chemother* 59: 3695–3699. doi:10.1128/AAC.00638-15.

164. Gröber U, Reichrath J, Holick MF, Kisters K (2014) Vitamin K: An old vitamin in a new perspective. *Dermatoendocrinol* 6. doi:10.4161/19381972.2014.968490.
165. McFarlane WD, Graham WR, Richardson F (1931) The Fat Soluble Vitamin Requirements of the Chick. 1. The Vitamin A and D Content of Fish Meal and Fish Meat. *Biochem J* 25: 358.
166. Holst WF, Halbrook ER (1933) A “scurvy-like” disease in chicks. *Science* 77: 354. doi:10.1126/science.77.1997.354.
167. Oldenburg J, Marinova M, Müller-Reible C, Watzka M (2008) The Vitamin K Cycle. *Vitam Horm* 78: 35–62. doi:10.1016/S0083-6729(07)00003-9.
168. Ferland G (2012) The Discovery of Vitamin K and its Clinical Applications. *Ann Nutr Metab* 61: 213–218.
169. Almquist HJ (1936) Purification of the Antihemorrhagic Vitamin by distillation. *J Biol Chem* 241: 589–592.
170. Binkley SB, MacCorquodale DW, Thayer SA, Doisy EA (1939) Isolation of Vitamin K1. *J Biol Chem* 139: 219–234.
171. MacCorquodale DW, Binkley SB, Thayer SA, Doisy EA (1939) ON THE CONSTITUTION OF VITAMIN K1. *J Am Chem Soc* 61: 1928–1929.
172. McKee RW, Binkley SB, Thayer SA, MacCorquodale DW, Doisy EA (1939) The Isolation of Vitamin K2. *J Biol Chem* 131: 327–344.
173. Klack K, Carvalho JF de (2006) Vitamina K: metabolismo, fontes e interação com o anticoagulante varfarina. *Rev Bras Reumatol* 46: 398–406. Available: [http://www.scielo.br/scielo.php?script=sci\\_arttext&pid=S0482-50042006000600007&nrm=iso](http://www.scielo.br/scielo.php?script=sci_arttext&pid=S0482-50042006000600007&nrm=iso).
174. Schurgers LJ, Vermeer C (2000) Determination of Phylloquinone and Menaquinones in Food. *Pathophysiol Haemost Thromb* 30: 298–307. Available: <http://www.karger.com/DOI/10.1159/000054147>.
175. Widhalm JR, Ducluzeau AL, Buller NE, Elowsky CG, Olsen LJ, et al. (2012) Phylloquinone (vitamin K1) biosynthesis in plants: Two peroxisomal thioesterases of lactobacillales origin hydrolyze 1,4-dihydroxy-2-naphthoyl-coa. *Plant J* 71: 205–215. doi:10.1111/j.1365-313X.2012.04972.x.
176. Liibben M (1995) Cytochromes of archaeal electron transfer chains. *Structure* 1229: 1–22.
177. Schoepp-Cothenet B, Lieutaud C, Baymann F, Verméglio A, Friedrich T, et al. (2009) Menaquinone as pool quinone in a purple bacterium. *Proc Natl Acad Sci U S A* 106: 8549–8554. doi:10.1073/pnas.0813173106.
178. Nowicka B, Kruk J (2010) Occurrence, biosynthesis and function of isoprenoid quinones. *Biochim Biophys Acta - Bioenerg* 1797: 1587–1605. Available: <http://dx.doi.org/10.1016/j.bbabi.2010.06.007>.
179. Collins MD, Jones D (1981) Distribution of isoprenoid quinone structural types in bacteria and their taxonomic implication. *Microbiol Rev* 45: 316–354.
180. Kurosu M, Begari E (2010) Vitamin K2 in Electron Transport System: Are Enzymes Involved in Vitamin K2 Biosynthesis Promising Drug Targets? *Molecules* 15: 1531–1553. Available: <http://www.mdpi.com/1420->

- 3049/15/3/1531/.
181. Walther B, Karl JP, Booth SL, Boyaval P (2013) Menaquinones, bacteria, and the food supply: the relevance of dairy and fermented food products to vitamin K requirements. *Adv Nutr* 4: 463–473. Available: <http://www.pubmedcentral.nih.gov/articlerender.fcgi?artid=3941825&tool=pmcentrez&rendertype=abstract>.
  182. Simon J, van Spanning RJM, Richardson DJ (2008) The organisation of proton motive and non-proton motive redox loops in prokaryotic respiratory systems. *Biochim Biophys Acta - Bioenerg* 1777: 1480–1490. Available: <http://dx.doi.org/10.1016/j.bbabi.2008.09.008>.
  183. Soballe B, Poole RK (2008) REVIEW ARTICLE Microbial ubiquinones: multiple roles in respiration, gene regulation and oxidative stress management: 1–14. doi:10.1099/13500872-145-8-1817.
  184. Marcelli SW, Chang H, Chapman T, Chalk PA, Miles RJ, et al. (1996) The respiratory chain of *Helicobacter pylori*: identification of cytochromes and the effects of oxygen on cytochrome and menaquinone levels. *FEMS Microbiol Lett* 138: 59–64. Available: <http://dx.doi.org/10.1111/j.1574-6968.1996.tb08135.x>.
  185. Bayer AS, McNamara P, Yeaman MR, Lucindo N, Jones T, et al. (2006) Transposon disruption of the complex I NADH oxidoreductase Gene (snoD) in *Staphylococcus aureus* is associated with reduced susceptibility to the microbicidal activity of thrombin-induced platelet microbicidal protein 1. *J Bacteriol* 188: 211–222. doi:10.1128/JB.188.1.211-222.2006.
  186. Somerville GA, Proctor RA (2009) At the crossroads of bacterial metabolism and virulence factor synthesis in staphylococci. *MicrobiolMolBiolRev* 73: 233–248. Available: C:\KARSTEN\PDFs\Staphylokokken-PDFs\Staph-2009\Somerville - Proctor -At the crossroads of bacterial metabolism and virulence factor synthesis in staphylococci.pdf.
  187. Haddock BA, Jones CW (1977) Bacterial respiration. *Bacteriol Rev* 41: 47. Available: <http://eutils.ncbi.nlm.nih.gov/entrez/eutils/eflink.fcgi?dbfrom=pubmed&id=140652&retmode=ref&cmd=prlinks\npapers3://publication/uuid/1E728532-CE74-4E78-B95D-CB359C136C98>.
  188. Richardson DJ (2000) Bacterial respiration: A flexible process for a changing environment. *Microbiology* 146: 551–571. doi:so.
  189. Kröger A, Geisler V, Lemma E, Theis F, Lenger R (1992) Bacterial fumarate respiration. *Arch Microbiol* 158: 311–314. Available: <http://dx.doi.org/10.1007/BF00245358>.
  190. Farrand SK, Taber HW (1974) Changes in menaquinone concentration during growth and early sporulation in *Bacillus subtilis*. *J Bacteriol* 117: 324–326.
  191. Dunphy PJ, Phillips PG, Brodie AF (1971) Separation and Identification of Menaquinones From Microorganisms. *J Lipid Res* 12: 442 – &. Available: <http://eutils.ncbi.nlm.nih.gov/entrez/eutils/eflink.fcgi?dbfrom=pubmed&id=5005959&retmode=ref&cmd=prlinks\npapers2://publication/uuid/A50BE24E-29D7-400C-8394-A7871E33EFA0>.
  192. Yamada Y, Inouye G, Tahara Y, Kondo K (1976) On the chemical structure of

- menaquinones with the tetrahydrogenated isoprenoid side chain. *Biochim Biophys Acta* 486: 195–203. Available: <http://europepmc.org/abstract/MED/1009133>.
193. Campbell IM, Bentley R (1968) Inhomogeneity of vitamin K<sub>2</sub> in *Mycobacterium phlei*. *Biochemistry* 7: 3323–3327.
194. Downey RJ (1964) VITAMIN K-MEDIATED ELECTRON TRANSFER IN *BACILLUS SUBTILIS*. *J Bacteriol* 88: 904–911.
195. Honaker RW, Dhiman RK, Narayanasamy P, Crick DC, Voskuil MI (2010) DosS responds to a reduced electron transport system to induce the mycobacterium tuberculosis DosR regulon. *J Bacteriol* 192: 6447–6455. doi:10.1128/JB.00978-10.
196. Suvarna K, Stevenson D, Meganathan R, Hudspeth MES (1998) Menaquinone (Vitamin K<sub>2</sub>) Biosynthesis: Localization and Characterization of the menA Gene from *Escherichia coli*. *J Bacteriol* 180: 2782–2787.
197. Ehrhardt DW, Atkinson EM, Faull KF, Freedberg DI, Sutherlin DP, et al. (1995) In vitro sulfotransferase activity of NodH, a nodulation protein of *Rhizobium meliloti* required for host-specific nodulation. *J Bacteriol* 177: 6237–6245.
198. Bishop DHL, Pandya KP, King HK (1961) Ubiquinone and Vitamin K<sub>2</sub> in Bacteria. *Biochem J* 78: 35.
199. Campbell IM, Coscia CJ, Kelsey M, Bentley R (1967) Origin of the aromatic nucleus in bacterial menaquinones. *Biochem Biophys Res Commun* 28: 25–29. Available: <http://www.sciencedirect.com/science/article/pii/0006291X67904007>.
200. Bentley R, Meganathan R (1982) Biosynthesis of Vitamin K (Menaquinone) in Bacteria. *Microbiol Rev* 46: 241–280.
201. Meganathan R (2001) Biosynthesis of menaquinone (vitamin K<sub>2</sub>) and ubiquinone (coenzyme Q): A perspective on enzymatic mechanisms. *Cofactor Biosynthesis. Vitamins & Hormones*. Academic Press, Vol. 61. pp. 173–218. Available: <http://www.sciencedirect.com/science/article/pii/S0083672901610069>.
202. Taber HW, Dellers EA, Lombardo LR (1981) Menaquinone biosynthesis in *Bacillus subtilis*: Isolation of men mutants and evidence for clustering of men genes. *J Bacteriol* 145: 321–327.
203. Daruwala R, Kwon O, Meganathan R, Hudspeth ME (1996) A new isochorismate synthase specifically involved in menaquinone (vitamin K<sub>2</sub>) biosynthesis encoded by the menF gene. *FEMS Microbiol Lett* 140: 159–163.
204. Ming Jiang, Yang Cao, Zu-Feng Guo, Minjiao Chen, Xiaolei Chen, et al. (2007) Menaquinone Biosynthesis in *Escherichia coli*: Identification of 2-Succinyl-5-enolpyruvyl-6-hydroxy-3-cyclohexene-1-carboxylate as a Novel Intermediate and Re-Evaluation of MenD Activity. *Biochemistry* 46: 10979–10989. Available: <http://dx.doi.org/10.1021/bi700810x>.
205. Dawson A, Fyfe PK, Gillet F, Hunter WN (2011) Exploiting the high-resolution crystal structure of *Staphylococcus aureus* MenH to gain insight into enzyme activity. *BMC Struct Biol* 11: 19. Available: <http://www.biomedcentral.com/content/pdf/1472-6807-11-19.pdf>.
206. Sharma V, Meganathan R, Hudspeth ME (1993) Menaquinone (vitamin K<sub>2</sub>)

- biosynthesis: cloning, nucleotide sequence, and expression of the menC gene from *Escherichia coli*. *J Bacteriol* 175: 4917–4921. Available: <http://www.pubmedcentral.nih.gov/articlerender.fcgi?artid=204947&tool=pmcentrez&rendertype=abstract>.
207. Sharma V, Hudspeth ME, Meganathan R (1996) Menaquinone (vitamin K<sub>2</sub>) biosynthesis: localization and characterization of the menE gene from *Escherichia coli*. *Gene* 168: 43–48.
208. Truglio JJ, Theis K, Feng Y, Gajda R, Machutta C, et al. (2003) Crystal Structure of *Mycobacterium tuberculosis* MenB, a Key Enzyme in Vitamin K<sub>2</sub> Biosynthesis. *J Biol Chem* 278: 42352–42360. doi:10.1074/jbc.M307399200.
209. Chen M, Ma X, Chen X, Jiang M, Song H, et al. (2013) Identification of a hotdog fold thioesterase involved in the biosynthesis of menaquinone in *Escherichia coli*. *J Bacteriol* 195: 2768–2775. doi:10.1128/JB.00141-13.
210. Lee PT, Hsu AY, Ha HT, Clarke CF (1997) A C-methyltransferase involved in both ubiquinone and menaquinone biosynthesis: Isolation and identification of the *Escherichia coli* ubiE gene. *J Bacteriol* 179: 1748–1754.
211. Hiratsuka T, Furihata K, Ishikawa J, Yamashita H, Itoh N, et al. (2008) An alternative menaquinone biosynthetic pathway operating in microorganisms. *Science* 321: 1670–1673. doi:10.1126/science.1160446.
212. Hiratsuka T, Itoh N, Seto H, Dairi T (2009) Enzymatic properties of futasoline hydrolase, an enzyme essential to a newly identified menaquinone biosynthetic pathway. *Biosci Biotechnol Biochem* 73: 1137–1141. Available: <http://joi.jlc.jst.go.jp/JST.JSTAGE/bbb/80906?from=CrossRef&nhttp://www.ncbi.nlm.nih.gov/pubmed/19420717>.
213. Arai R, Murayama K, Uchikubo-Kamo T, Nishimoto M, Toyama M, et al. (2009) Crystal structure of MqnD (TTHA1568), a menaquinone biosynthetic enzyme from *Thermus thermophilus* HB8. *J Struct Biol* 168: 575–581. Available: <http://www.sciencedirect.com/science/article/pii/S1047847709001798>.
214. DiNicolantonio JJ, Bhutani J, O’Keefe JH (2015) The health benefits of vitamin K. *Open Hear* 2: e000300. Available: <http://www.pubmedcentral.nih.gov/articlerender.fcgi?artid=4600246&tool=pmcentrez&rendertype=abstract>.
215. Crick M, Kurosu DC (2009) MenA Is a Promising Drug Target for Developing Novel Lead Molecules to Combat *Mycobacterium tuberculosis*. *Med Chem (Los Angeles)* 5: 197–207. Available: <http://www.eurekaselect.com/node/84064/article>.
216. KEGG (n.d.) Ubiquinone and other terpenoid-quinone biosynthesis. Available: [http://www.genome.jp/kegg-bin/show\\_pathway?org\\_name=map&mapno=00130&mapscale=&show\\_description=hide](http://www.genome.jp/kegg-bin/show_pathway?org_name=map&mapno=00130&mapscale=&show_description=hide). Accessed 9 July 2016.
217. Priyadarshi A, Kim EE, Hwang KY (2009) Structural and functional analysis of Vitamin {K<sub>2</sub>} synthesis protein MenD. *Biochem Biophys Res Commun* 388: 748–751. Available: <http://www.sciencedirect.com/science/article/pii/S0006291X09016714>.
218. Patskovsky Y, Toro R, Dickey M, Sauder J., Chang S, et al. (n.d.) Crystal



- structure of o-succinylbenzoic acid-CoA ligase from *Staphylococcus aureus*. To be Publ. doi:10.2210/PDB3IPL/PDB.
219. Parsons JF, Shi KM, Ladner JE (2008) Structure of isochorismate synthase in complex with magnesium. *Acta Crystallogr Sect D Biol Crystallogr* 64: 607–610. doi:10.1107/S0907444908005477.
  220. Dai Y-N, Zhou K, Cao D-D, Jiang Y-L, Meng F, et al. (2014) Crystal structures and catalytic mechanism of the C-methyltransferase Coq5 provide insights into a key step of the yeast coenzyme Q synthesis pathway. *Acta Crystallogr D Biol Crystallogr* 70: 2085–2092. doi:10.1107/S1399004714011559.
  221. Thoden JB, Zhuang Z, Dunaway-Mariano D, Holden HM (2003) The Structure of 4-Hydroxybenzoyl-CoA Thioesterase from *Arthrobacter* sp. strain SU. *J Biol Chem* 278: 43709–43716. doi:10.1074/jbc.M308198200.
  222. Benning MM, Wesenberg G, Liu R, Taylor KL, Dunaway-Mariano D, et al. (1998) The three-dimensional structure of 4-hydroxybenzoyl-CoA thioesterase from *Pseudomonas* sp. strain CBS-3. *J Biol Chem* 273: 33572–33579. Available: [http://www.ncbi.nlm.nih.gov/entrez/query.fcgi?cmd=Retrieve&db=PubMed&doctype=Citation&list\\_uids=9837940](http://www.ncbi.nlm.nih.gov/entrez/query.fcgi?cmd=Retrieve&db=PubMed&doctype=Citation&list_uids=9837940).
  223. Matarlo JS, Evans CE, Sharma I, Lavaud LJ, Ngo SC, et al. (2015) Mechanism of MenE Inhibition by Acyl-Adenylate Analogues and Discovery of Novel Antibacterial Agents. *Biochemistry* 54: 6514–6524. doi:10.1021/acs.biochem.5b00966.
  224. Lundberg KS, Shoemaker DD, Adams MWW, Short JM, Sorge JA, et al. (1991) High-fidelity amplification using a thermostable DNA polymerase isolated from *Pyrococcus furiosus*. *Gene* 108: 1–6. Available: <http://www.sciencedirect.com/science/article/pii/037811199190480Y>. Accessed 18 February 2016.
  225. Yilmaz M, Ozic C, Gok I (2012) Principles of nucleic acid separation by agarose gel electrophoresis. *Gel Electrophor - Princ Basics*: 34–40. doi:10.5772/2205.
  226. Edelheit O, Hanukoglu A, Hanukoglu I (2009) Simple and efficient site-directed mutagenesis using two single-primer reactions in parallel to generate mutants for protein structure-function studies. *BMC Biotechnol* 9: 61. Available: <http://www.pubmedcentral.nih.gov/articlerender.fcgi?artid=2711942&tool=pmcentrez&rendertype=abstract>.
  227. Mandel M, Higa A (1970) Calcium-dependent bacteriophage DNA infection. *J Mol Biol* 53: 159–162. doi:10.1016/0022-2836(70)90051-3.
  228. Chan W-T, Verma CS, Lane DP, Gan SK-E (2013) A comparison and optimization of methods and factors affecting the transformation of *Escherichia coli*. *Biosci Rep* 33: 931–937. Available: <http://www.bioscirep.org/bsr/033/e086/bsr033e086.htm>.
  229. Duong-Ly KC, Gabelli SB (2014) Chapter Seven - Salting out of Proteins Using Ammonium Sulfate Precipitation. In: *Enzymology JLBT-M in*, editor. *Laboratory Methods in Enzymology: Protein Part C*. Academic Press, Vol. Volume 541. pp. 85–94. Available: <http://www.sciencedirect.com/science/article/pii/B9780124201194000070>.
  230. Laemmli UK (1970): (1970) Cleavage of Structural Proteins during Assembly of

- Head of Bacteriophage T4. *Nature* 227. doi:10.1038/227680a0.
231. Neuhoff V, Arold N, Taube D, Ehrhardt W (1988) Improved staining of proteins in polyacrylamide gels including isoelectric focusing gels with clear background at nanogram sensitivity using Coomassie Brilliant Blue G-250 and R-250. *Electrophoresis* 9: 255–262. Available: [http://www.ncbi.nlm.nih.gov/entrez/query.fcgi?cmd=Retrieve&db=PubMed&dopt=Citation&list\\_uids=2466658](http://www.ncbi.nlm.nih.gov/entrez/query.fcgi?cmd=Retrieve&db=PubMed&dopt=Citation&list_uids=2466658)  
[http://onlinelibrary.wiley.com/store/10.1002/elps.1150090603/asset/1150090603\\_ft.pdf?v=1&t=gxkaflld0&s=4c763c9237e3d064781c937854387e742685fa28](http://onlinelibrary.wiley.com/store/10.1002/elps.1150090603/asset/1150090603_ft.pdf?v=1&t=gxkaflld0&s=4c763c9237e3d064781c937854387e742685fa28).
232. Neuhoff V, Stamm R, Eibl H (1985) Clear background and highly sensitive protein staining with Coomassie Blue dyes in polyacrylamide gels: A systematic analysis. *Electrophoresis* 6: 427–448. Available: <http://dx.doi.org/10.1002/elps.1150060905>.
233. Gasteiger E, Hoogland C, Gattiker A, Duvaud S, Wilkins MR, et al. (2005) Protein Identification and Analysis Tools on the ExPASy Server. Walker JM, editor *The Proteomics Protocols Handbook*, Humana Press. 571-607 p.
234. Yang JT, Wu CS, Martinez HM (1986) Calculation of protein conformation from circular dichroism. *Methods Enzymol* 130: 208–269.
235. Shevchenko A, Wilm M, Vorm O, Mann M (1996) Mass Spectrometric Sequencing of Proteins from Silver-Stained Polyacrylamide Gels. *Anal Chem* 68: 850–858. Available: <http://dx.doi.org/10.1021/ac950914h>.
236. Battye TGG, Kontogiannis L, Johnson O, Powell HR, Leslie AGW (2011) iMOSFLM: A new graphical interface for diffraction-image processing with MOSFLM. *Acta Crystallogr Sect D Biol Crystallogr* 67: 271–281. doi:10.1107/S0907444910048675.
237. Kabsch W (2010) Xds. *Acta Crystallogr Sect D Biol Crystallogr* 66: 125–132. doi:10.1107/S0907444909047337.
238. Evans PR, Murshudov GN (2013) How good are my data and what is the resolution? *Acta Crystallogr Sect D Biol Crystallogr* 69: 1204–1214. doi:10.1107/S0907444913000061.
239. Panjikar S, Parthasarathy V, Lamzin VS, Weiss MS, Tucker PA (2005) *Auto-Rickshaw*: an automated crystal structure determination platform as an efficient tool for the validation of an X-ray diffraction experiment. *Acta Crystallogr Sect D* 61: 449–457. Available: <http://dx.doi.org/10.1107/S0907444905001307>.
240. Panjikar S, Parthasarathy V, Lamzin VS, Weiss MS, Tucker PA (2009) On the combination of molecular replacement and single-wavelength anomalous diffraction phasing for automated structure determination. *Acta Crystallogr Sect D Biol Crystallogr* 65: 1089–1097. doi:10.1107/S0907444909029643.
241. Murshudov GN, Vagin AA, Dodson EJ (1997) Refinement of Macromolecular Structures by the Maximum-Likelihood Method. *Acta Crystallogr Sect D* 53: 240–255. Available: <http://dx.doi.org/10.1107/S0907444996012255>.
242. Emsley P, Cowtan K (2004) “Coot: model-building tools for molecular graphics.” *Acta Crystallogr Sect D* 60: 2126–2132.
243. Murshudov GN, Skubák P, Lebedev AA, Pannu NS, Steiner RA, et al. (2011) REFMAC5 for the refinement of macromolecular crystal structures. *Acta*

- Crystallogr Sect D Biol Crystallogr 67: 355–367. doi:10.1107/S0907444911001314.
244. McWilliam H, Li W, Uludag M, Squizzato S, Park YM, et al. (2013) Analysis Tool Web Services from the EMBL-EBI. *Nucleic Acids Res* 41: 597–600. doi:10.1093/nar/gkt376.
245. Altschul SF, Madden TL, Schäffer AA, Zhang J, Zhang Z, et al. (1997) Gapped BLAST and PSI-BLAST: a new generation of protein database search programs. *Nucleic Acids Res* 25: 3389–3402. Available: <http://www.ncbi.nlm.nih.gov/pmc/articles/PMC146917/>.
246. Kissinel E, Henrick K (2007) Inference of macromolecular assemblies from crystalline state. *J Chem Inf Model* 372: 774–797. doi:10.1017/CBO9781107415324.004.
247. Krissinel E, Henrick K (2004) Secondary-structure matching (SSM), a new tool for fast protein structure alignment in three dimensions. *Acta Crystallogr Sect D Biol Crystallogr* 60: 2256–2268. doi:10.1107/S0907444904026460.
248. Laskowski R a (2001) PDBsum: summaries and analyses of PDB structures. *Nucleic Acids Res* 29: 221–222. doi:10.1093/nar/29.1.221.
249. Laskowski R a. (2009) PDBsum new things. *Nucleic Acids Res* 37: 355–359. doi:10.1093/nar/gkn860.
250. Genheden S, Ryde U (2015) The MM/PBSA and MM/GBSA methods to estimate ligand-binding affinities. *Expert Opin Drug Discov* 10: 449–461. Available: <http://www.pubmedcentral.nih.gov/articlerender.fcgi?artid=4487606&tool=pmcentrez&rendertype=abstract>.
251. Rodríguez-Guilbe M, Oyola-Robles D, Schreiter ER, Baerga-Ortiz A (2013) Structure, Activity, and Substrate Selectivity of the Orf6 Thioesterase from *Photobacterium profundum*. *J Biol Chem* 288: 10841–10848. Available: <http://www.ncbi.nlm.nih.gov/pmc/articles/PMC3624464/>.
252. Reed J, Kinzel V (1984) Near- and far-ultraviolet circular dichroism of the catalytic subunit of adenosine cyclic 5'-monophosphate dependent protein kinase. *Biochemistry* 23: 1357–1362.
253. McGuffin LJ, Atkins JD, Salehe BR, Shuid AN, Roche DB (2015) IntFOLD: an integrated server for modelling protein structures and functions from amino acid sequences. *Nucleic Acids Res* 43: W169–W173. doi:10.1093/nar/gkv236.
254. Kelley LA, Mezulis S, Yates CM, Wass MN, Sternberg MJE (2015) The Phyre2 web portal for protein modeling, prediction and analysis. *Nat Protoc* 10: 845–858. Available: <http://dx.doi.org/10.1038/nprot.2015.053>.
255. Kallberg M, Wang H, Wang S, Peng J, Wang Z, et al. (2012) Template-based protein structure modeling using the RaptorX web server. *Nat Protoc* 7: 1511–1522. doi:10.1038/nprot.2012.085.
256. Soding J, Biegert A, Lupas AN (2005) The HHpred interactive server for protein homology detection and structure prediction. *Nucleic Acids Res* 33: W244–W248. doi:10.1093/nar/gki408.
257. Roy A, Kucukural A, Zhang Y (2010) I-TASSER: a unified platform for

- automated protein structure and function prediction. *Nat Protoc* 5: 725–738. Available: <http://dx.doi.org/10.1038/nprot.2010.5>.
258. Fernandez-Fuentes N, Rai BK, Madrid-Aliste CJ, Fajardo JE, Fiser A (2007) Comparative protein structure modeling by combining multiple templates and optimizing sequence-to-structure alignments. *Bioinformatics* 23: 2558–2565. doi:10.1093/bioinformatics/btm377.
259. Greenfield NJ (2006) Using circular dichroism spectra to estimate protein secondary structure. *Nat Protoc* 1: 2876–2890. Available: <http://www.ncbi.nlm.nih.gov/pmc/articles/PMC2728378/>.
260. Jo S, Vargyas M, Vasko-Szedlar J, Roux B, Im W (2008) PBEQ-Solver for online visualization of electrostatic potential of biomolecules. *Nucleic Acids Res* 36: 270–275. doi:10.1093/nar/gkn314.
261. Robert X, Gouet P (2014) Deciphering key features in protein structures with the new ENDscript server. *Nucleic Acids Res* 42: 320–324. doi:10.1093/nar/gku316.
262. Rosano GL, Ceccarelli EA (2014) Recombinant protein expression in *Escherichia coli*: Advances and challenges. *Front Microbiol* 5: 1–17. doi:10.3389/fmicb.2014.00172.
263. Daruwala R, Bhattacharyya DK, Kwon O, Meganathan R (1997) Menaquinone (vitamin K<sub>2</sub>) biosynthesis: overexpression, purification, and characterization of a new isochorismate synthase from *Escherichia coli*. *J Bacteriol* 179: 3133–3138. Available: <http://www.pubmedcentral.nih.gov/articlerender.fcgi?artid=179089&tool=pmcentrez&rendertype=abstract>.
264. Kolappan S, Zwahlen J, Zhou R, Truglio JJ, Tonge PJ, et al. (2007) Lysine 190 Is the Catalytic Base in MenF, the Menaquinone-Specific Isochorismate Synthase from *Escherichia coli*: Implications for an Enzyme Family. *Biochemistry* 46: 946–953. Available: <http://dx.doi.org/10.1021/bi0608515>.
265. Hsieh EJ, Gin P, Gulmezian M, Tran UC, Saiki R, et al. (2007) *Saccharomyces cerevisiae* Coq9 polypeptide is a subunit of the mitochondrial coenzyme Q biosynthetic complex. *Arch Biochem Biophys* 463: 19–26. doi:10.1016/j.abb.2007.02.016.
266. Rogelj B, Godin K, Shaw C, Ule J (2012) the Functions of Glycine-Rich Regions in Tdp-43, Fus and Related Rna-Binding Proteins. *RNA Bind Proteins* 1: 1–17. Available: [http://www.landesbioscience.com/pdf/03Lorkovic\\_Ule\\_.pdf](http://www.landesbioscience.com/pdf/03Lorkovic_Ule_.pdf).
267. Carrio MM, Villaverde A (2001) Protein aggregation as bacterial inclusion bodies is reversible. *FEBS Lett* 489: 29–33.
268. Hunt MC, Alexson SEH (2002) The role Acyl-CoA thioesterases play in mediating intracellular lipid metabolism. *Prog Lipid Res* 41: 99–130.
269. Leesong M, Henderson BS, Gillig JR, Schwab JM, Smith JL (1996) Structure of a dehydratase-isomerase from the bacterial pathway for biosynthesis of unsaturated fatty acids: two catalytic activities in one active site. *Structure* 4: 253–264. doi:10.1016/S0969-2126(96)00030-5.
270. Pidugu L, Maity K, Ramaswamy K, Surolia N, Suguna K (2009) Analysis of proteins with the “hot dog” fold: Prediction of function and identification of catalytic residues of hypothetical proteins. *BMC Struc Biol* 9: 37. Available:

- <http://www.biomedcentral.com/1472-6807/9/37>.
271. Lamden PR, Guest JR (1976) Mutants of *Escherichia coli* K12 Unable to use Fumarate as an Anaerobic Electron Acceptor. *J Gen Microbiol* 97: 145–160.
  272. Wallace BJ, Young IG (1977) Role of quinones in electron transport to oxygen and nitrate in *Escherichia coli*. Studies with a *ubiA*<sup>-</sup> *menA*<sup>-</sup> double quinone mutant. *Biochim Biophys Acta - Bioenerg* 461: 84–100.
  273. Dillon SC, Bateman A (2004) The Hotdog fold: wrapping up a superfamily of thioesterases and dehydratases. *BMC Bioinformatics* 5: 109. doi:10.1186/1471-2105-5-109.
  274. Adams SH, Chui C, Schilbach SL, Yu XX, Goddard AD, et al. (2001) BFIT, a unique acyl-CoA thioesterase induced in thermogenic brown adipose tissue: cloning, organization of the human gene and assessment of a potential link to obesity. *Biochem J* 360: 135–142.
  275. Suematsu N, Isohashi F (2006) Molecular cloning and functional expression of human cytosolic acetyl-CoA hydrolase. *Acta Biochim Pol* 53: 553–561.
  276. Angelini A, Cendron L, Goncalves S, Zanotti G, Terradot L (2008) Structural and enzymatic characterization of HP0496, a YbgC thioesterase from *Helicobacter pylori*. *Proteins* 72: 1212–1221. Available: <http://www.ncbi.nlm.nih.gov/pubmed/18338382>.
  277. Zhuang Z, Song F, Martin BM, Dunaway-Mariano D (2002) The YbgC protein encoded by the *ybgC* gene of the *tol-pal* gene cluster of *Haemophilus influenzae* catalyzes acyl-coenzyme A thioester hydrolysis. *FEBS Lett* 516: 161–163.
  278. Shahi P, Kumar I, Sharma R, Sanger S, Jolly RS (2006) Characterization of a novel long-chain acyl-CoA thioesterase from *Alcaligenes faecalis*. *FEBS J* 273: 2374–2387. Available: <http://www.ncbi.nlm.nih.gov/pubmed/16704412>.
  279. Cao J, Xu H, Zhao H, Gong W, Dunaway-Mariano D (2009) The mechanisms of human hotdog-fold thioesterase 2 (hTHEM2) substrate recognition and catalysis illuminated by a structure and function based analysis. *Biochemistry* 48: 1293–1304. Available: <http://dx.doi.org/10.1021/bi801879z>.
  280. Gonzalez CF, Tchigvintsev A, Brown G, Flick R, Evdokimova E, et al. (2012) Structure and activity of the *Pseudomonas aeruginosa* hotdog-fold thioesterases PA5202 and PA2801. *Biochem J* 444: 445–455. Available: <http://www.pubmedcentral.nih.gov/articlerender.fcgi?artid=3836677&tool=pmcentrez&rendertype=abstract>.
  281. Thoden JB, Holden HM, Zhuang Z, Dunaway-Mariano D (2002) X-ray crystallographic analyses of inhibitor and substrate complexes of wild-type and mutant 4-hydroxybenzoyl-CoA thioesterase. *J Biol Chem* 277: 27468–27476. Available: <http://www.ncbi.nlm.nih.gov/pubmed/11997398>.
  282. Song F, Zhuang Z, Dunaway-Mariano D (2007) Structure-activity analysis of base and enzyme-catalyzed 4-hydroxybenzoyl coenzyme A hydrolysis. *Bioorg Chem* 35: 1–10.
  283. Strain S, Thioesterase CBS, Site A, Zhuang Z, Song F, et al. (2002) Kinetic , Raman , NMR , and Site-Directed Mutagenesis Studies of the *Pseudomonas*: 11152–11160.

284. Zhuang Z, Song F, Takami H, Dunaway-mariano D (2004) The BH1999 Protein of *Bacillus halodurans* C-125 Is Gentsyl-Coenzyme A Thioesterase. *J Bacteriol* 186: 393–399. doi:10.1128/JB.186.2.393.
285. Kotaka M, Kong R, Qureshi I, Ho QS, Sun H, et al. (2009) Structure and catalytic mechanism of the thioesterase CalE7 in enediyne biosynthesis. *J Biol Chem* 284: 15739–15749. doi:10.1074/jbc.M809669200.
286. Cao J, Xu H, Zhao H, Gong W, Dunaway-mariano D (2009) The Mechanisms of Human Hotdog-fold Thioesterase 2 ( hTHEM2 ) Substrate Recognition and Catalysis Illuminated by a Structure and Function Based Analysis The Mechanisms of Human Hotdog-fold Thioesterase 2 ( hTHEM2 ) Substrate Recognition and Catalysis Illu. *Biochemistry* 48: 1293–1304. doi:10.1021/bi801879z.
287. Kunishima N, Asada Y, Sugahara M, Ishijima J, Nodake Y, et al. (2005) A Novel Induced-fit Reaction Mechanism of Asymmetric Hot Dog Thioesterase PaaI. *J Mol Biol* 352: 212–228. Available: <http://www.sciencedirect.com/science/article/pii/S0022283605007850>.
288. Fersht A (1999) Structure and mechanism in protein science: A guide to enzyme catalysis and protein folding. 54-101 p. Available: <http://www.lavoisier.fr/livre/notice.asp?id=OLRHXLG23XSOGO\npapers://df790107-00bb-4d1a-a7c1-3a1abd474f6d/Paper/p4695>.
289. Ingle RA (2011) Histidine Biosynthesis. *Arab B*: 1–9. doi:10.1199/tab.0141.
290. Zhuang Z, Song F, Zhao H, Li L, Cao J, et al. (2008) Divergence of function in the hot dog fold enzyme superfamily: The bacterial thioesterase YciA. *Biochemistry* 47: 2789–2796. doi:10.1021/bi702334h.
291. Cantu DC, Chen Y, Reilly PJ (2010) Thioesterases: A new perspective based on their primary and tertiary structures. *Protein Sci* 19: 1281–1295. doi:10.1002/pro.417.
292. Latham JA, Chen D, Allen KN, Dunaway-mariano D (2015) Divergence of Substrate Specificity and Function in the *Escherichia coli* Hotdog-fold Thioesterase Paralogs YdiI and YbdB. *Biochemistry* 53: 4775–4787. doi:10.1021/bi500334v.
293. Obarska-Kosinska A, Iacoangeli A, Lepore R, Tramontano A (2016) PepComposer: computational design of peptides binding to a given protein surface. *Nucleic Acids Res*: gkw366. Available: <http://nar.oxfordjournals.org/lookup/doi/10.1093/nar/gkw366>.
294. Deck P, Pendzialek D, Biel M, Wagner M, Popkirova B, et al. (2005) Development and biological evaluation of acyl protein thioesterase 1 (APT1) inhibitors. *Angew Chem Int Ed Engl* 44: 4975–4980. doi:10.1002/anie.200462625.
295. Méndez-Samperio P (2014) Peptidomimetics as a new generation of antimicrobial agents: Current progress. *Infect Drug Resist* 7: 229–237. doi:10.2147/IDR.S49229.
296. Haug BE, Stensen W, Kalaaji M, Rekdal Ø, Svendsen JS (2008) Synthetic Antimicrobial Peptidomimetics with Therapeutic Potential. *J Med Chem* 51: 4306–4314. Available: <http://dx.doi.org/10.1021/jm701600a>.

297. Kurosu M, Narayanasamy P, Biswas K, Dhiman R, Crick DC (2007) Discovery of 1,4-dihydroxy-2-naphthoate prenyltransferase inhibitors: New drug leads for multidrug-resistant gram-positive pathogens. *J Med Chem* 50: 3973–3975. doi:10.1021/jm070638m.

## 10. Appendix

**Table 14:** Ammonium sulfate concentration: percentage saturation at 0 °C. Adapted from Duong-Ly and Gabelli [229].

Initial concentration of ammonium sulfate	20	25	30	35	40	45	50	55	60	65	70	75	80	85	90	95	100
	Solid ammonium sulfate (grams) to be added to 100 mL solution																
0	10.6	13.4	16.4	19.4	22.6	25.8	19.1	32.6	36.1	39.8	43.6	47.66	51.6	55.9	60.3	65.0	69.7
5	7.9	10.8	13.7	16.6	19.7	22.9	26.2	29.6	33.1	36.8	40.5	44.4	48.4	52.6	57.0	61.5	66.2
10	5.3	8.1	10.9	13.9	16.9	20.0	23.3	26.6	30.1	33.7	37.4	41.2	45.2	49.3	53.6	58.1	62.7
15	2.6	5.4	8.2	11.1	14.1	17.2	20.4	23.7	27.1	30.6	34.3	38.1	42.0	46.0	50.3	54.7	59.0
20	0	2.7	5.5	8.3	11.3	14.3	17.5	20.7	24.1	27.6	31.2	34.9	38.7	42.7	46.9	51.2	55.7
25		0	2.7	5.6	8.4	11.5	14.6	17.6	21.1	24.5	28.0	31.7	35.5	39.5	43.6	47.8	52.2
30			0	2.8	5.6	8.6	11.7	14.8	18.1	21.4	24.9	28.5	32.3	36.2	40.2	44.5	48.8
35				0	2.8	5.7	8.7	11.8	15.1	18.4	21.8	25.4	29.1	32.9	36.9	41.0	45.3
40					0	2.9	5.8	8.9	12.0	15.3	18.7	22.2	25.8	29.6	33.5	37.6	41.8
45						0	2.9	5.9	9.0	12.3	15.6	19.0	22.6	26.3	30.2	34.2	38.3
50							0	3.0	6.0	9.2	12.5	15.9	19.4	23.0	26.3	30.8	34.8
55								0	3.0	6.1	9.3	12.7	16.1	19.7	23.5	27.3	31.3
60									0	3.1	6.2	9.5	12.9	16.4	20.1	23.9	27.6
65										0	3.1	6.3	9.7	13.2	16.8	20.5	24.4
70											0	3.2	6.5	9.9	13.4	17.1	20.9
75												0	3.2	6.6	10.1	13.7	17.4
80													0	3.3	6.7	10.3	13.9
85														0	3.4	6.8	10.5
90															0	3.4	7.0
95																0	3.5
100																	0



## 11. Acknowledgments

When I found out I was lying down in a bed between life and death due a serious bacterial infection, I finally have discovered how to help to create a better world. This thesis is the result of ten years of the thirst for knowledge improvement and definitely will have positive consequences for the future of my Country.

First, I would like to express my gratitude to my supervisor Prof. Dr. Dr. Christian Betzel and my Co-supervisor Prof. Dr. Carsten Wrenger for this wonderful opportunity to work in their group with an extremely interesting subject, which is the structural biology study in Hamburg. I also would like to thanks, PD Dr. Markus Perbandt for the constructive discussion about protein modeling and protein co-crystallization. I also would like to thank Prof. Dr R. Bredehorst, Prof. Dr. A. Torda and Dr. T. Hackl. Thanks also to our lab technician Petra Belda.

I would like to thanks, Prof. Dr. Hahn, Prof. Dr. Ignatova and Dr. Riedner and their working group for allowing me to use their equipment.

To all my work colleagues from AG Betzel, in special to my friends Theresa Nuguid, Svetlana Kapis, Sabine Botha, Christina Schmidt, Robin Schubert and Rutinéia Ferraz Jansen for all nice moments of scientific discussion and entertainment. My gratitude also to Dr. Madeleine Künz that, together with Robin Schubert, gave me the loveliest “Welcome to Hamburg!” reception. Thanks also to my good friends Dr. Rana Hussein and Dr. Haifa El Kilani for all nice conversations. I couldn’t forget also to thanks, Dr. Carsten “Brazilian team” Thales Kronenberger and “almost Brazilian” Jasmin Lindner who helped me and guided me during the first steps of my Ph.D., as well as for tips for cloning and docking studies.

Thank you, Pablo Barros, Dr. Renata Voltolini and Dr. Helen Costa for all “Brazilian moments” of fun. Thanks to Maria Kokkinidou, the Nove Hradý girls Julia Ermak, Tatyana Prudnikova and Oksana Degtjarik and all friends I have made during this three years. Thank you all for showing me the meaning of a true friendship and for helping me not to be so homesick. Be sure those nice moments will never be forgotten....ever!

This work would not be accomplished without my family love and support. I am eternally grateful to my mother Maria da Conceição M. C. Murad and to my father Jamil Murad for all the sacrifice they have made in this life so I could be here in this moment. My huge gratitude to my best friend and lovely brother Dr. André Murad who support also was extremely important so I could pursuit this Ph.D.

To all who presence was equal important so this work could be accomplished.

Thank you!

## 12. Risks and safety statements

### Chemicals used (GHS classification)

Compound	CAS-No.	Supplier	GHS hazard	Hazard Statements	Precautionary Statements
Acetic acid	64-19-7	Chem-solute	GHS02 GHS05	H226, H314	P280, P305+351+338, P310
Acrylamide 37%	79-06-1	Carl Roth	GHS06 GHS08	H301, H312, H315, H317, H319, H332, H340, H350, H361f, H372	P201, P280, P301+310, P305+351+338, P308+313
Agarose	9012-36-6	Serva	-	-	-
(NH <sub>4</sub> ) <sub>2</sub> SO <sub>4</sub>	7283-20-2	Carl Roth	-	-	-
NH <sub>4</sub> NO <sub>3</sub>	6484-52-2	Applichem	GHS03	H272	P210
Ampicillin	69-52-3	Carl Roth	GHS08	H334, H317	P280, P261, P302+352, P342+311
APS	7727-54-0	Carl Roth	GHS03 GHS07 GHS08	H272, H302, H315, H317, H319, H334, H335	P280, P305+351+338, P302+352, P304+341, P342+311
Bromphenol blue	115-39-9	Applichem	-	-	-
CaCl <sub>2</sub>	10043-52-4	Merck	GHS07	H319	P305+351+338
Chloramphenicol	56-75-7	Sigma	GHS08	H350	P201-P308 + P313
Coomassie Brilliant Blue R250	6104-59-2	Serva	-	-	-
CHES	9005-64-5	Sigma	-	H319	P305+351+338
Crotonyl-CoA trilithium salt	992-67-6	Sigma	-	-	-
Desthiobiotin	533-48-2	Sigma	-	-	-
DTT	578517	Applichem	GHS07	H302, H315, H319, H335	P302+352, P305+351+338
5,5'- Dithiobis(2- nitrobenzoic acid)	69-78-3	Sigma	GHS07	H315-H319- H335	P280-P304 + P340 + P312- P305 + P351 + P338-P337 + P313

## Risk and safety statements

<b>EDTA</b>	60-00-4	Sigma	GHS07	H319	P305+351+338
<b>Ethanol</b>	64-17-5	Carl Roth	GHS02	H225	P210
<b>Ethidium bromide</b>	1239-45-8	Sigma	GHS06 GHS08	H302, H331, H341	P260, P281, P284, P310
<b>Glycerol</b>	56-81-5	Sigma	-	-	-
<b>Guanidinhydrochlorid</b>	50-01-1	Applichem	GHS07	H302, H315, H319	P305+351+388, P302+352
<b>HABA</b>	1634-82-8	Fluka	GHS07	H315, H319, H335	P261, P305+351+338
<b>Hepes</b>	7365-45-9	Sigma Aldrich	-	-	-
<b>Hydrochloric acid &gt;25 %</b>	7647-01-0	Merck	GHS05 GHS07	H314, H335	P261, P280, P310, P305+351+338
<b>Isopropanol</b>	67-63-0	Carl Roth	GHS02 GHS07	H225, H319, H336.	P210, P233, P305+351+338
<b>KCl</b>	7447-40-7	Carl Roth	-	-	-
<b>Kanamycin</b>	70560-51-9	Sigma	GHS08	H360	P201-P308 + P313
<b>K<sub>2</sub>HPO<sub>4</sub></b>	7758-11-4	Carl Roth	-	-	-
<b>KH<sub>2</sub>PO<sub>4</sub></b>	7778-77-0	Carl Roth	-	-	-
<b>Li<sub>2</sub>SO<sub>4</sub></b>	10102-25-7	Merck	GHS07	H302	-
<b>MgCl<sub>2</sub></b>	7786-30-3	Carl Roth	-	-	-
<b>MgSO<sub>4</sub></b>	7487-88-9	Merck	-	-	-
<b>2-Mercaptoethanol</b>	60-24-2	Fisher Scientific	GHS06 GHS09	H302, H411, H315, H335, H311, H319	P280, P312, P302+350, P261, P273, P301+312, P305+351+338
<b>NaCl</b>	7647-14-5	Carl Roth	-	-	-
<b>NaH<sub>2</sub>PO<sub>4</sub></b>	10049-21-5	VWR	-	-	-
<b>Na<sub>2</sub>HPO<sub>4</sub></b>	7558-79-4	VWR	-	-	-
<b>NaOH</b>	1310-73-2	Merck	GHS05	H314	P280, P310, P305+351+338
<b>Paraffin</b>	8002-74-2	Applichem	-	-	-
<b>PEG 3350</b>	25322-68-3	Sigma	-	-	-
<b>PMSF</b>	329-98-6	Applichem	GHS06 GHS05	H301, H314	P280, P305+351+338, P310
<b>SDS</b>	151-21-3	Sigma	GHS02 GHS06	H228, H302, H311, H315, H319, H335	P210, P261, P280, P312, P305+351+338

<b>Sodium borate</b>	1303-96-4	Sigma	GHS08	H360FD	P201, P308 +313
<b>Stearoyl-CoA lithium salt</b>	193402-48-1	Sigma	-	-	-
<b>TEMED</b>	110-18-9	Merck	GHS02 GHS05 GHS07	H225, H302, H314, H332	P261, P280, P305+351+338
<b>Tetracycline</b>	60-54-8	Sigma	GHS07	H302	P280, P284
<b>Tris</b>	1185-53-1	Fluka	GHS07	H315, H319, H335	P261, P305+351+338
<b>Triptone</b>	91079-40-2	Appliche m	-	-	-
<b>Tween 20</b>	9005-64-5	Carl Roth	-	-	-
<b>Yeast Extract</b>	8013-01-2	Serva	-	-	-

### Commercial Protein Screens and Kits

<b>Name</b>	<b>Supplier</b>	<b>GHS hazard</b>	<b>Hazard Statements</b>	<b>Precaution ary Statements</b>
<b>Morpheus</b>	Molecular Dimensions	GHS02 GHS06 GHS07 GHS08 GHS09	H225, H301, H302, H315, H319, H331, H332, H335, H340, H350, H360Fd, H361d, H373, H411	P101, P201, P270, P273, P280, P305+351+ 338, P309+311, P313
<b>PACT premier</b>	Molecular Dimensions	GHS06	H301, H331, H412	P101, P270, P273, P280, P309+311
<b>Stura FootPrint &amp; MacroSol</b>	Molecular Dimensions	GHS02 GHS06 GHS07 GHS08 GHS09	H225, H301, H302, H315, H319, H332, H335, H340, H350, H360FD, H373, H411	P101, P201, P270, P273, P280, P305+351+ 338, P309+311, P313
<b>Classics Suite</b>	Qiagen	GHS02 GHS06 GHS07 GHS08 GHS09	H225, H301, H302, H315, H319, H331, H332, H335, H340, H350, H360FD, H373, H411	P101, P201, P270, P280, P305+351+ 338, P309+311, P313

## Risk and safety statements

<b>JCSG-plus</b>	Molecular Dimensions	GHS02 GHS05 GHS06 GHS07 GHS08	H225, H301, H312, H315, H318, H331, H335, H350, H411	P101, P201, P270, P280, P305+351+ 338, P309+311, P313
------------------	-------------------------	-------------------------------------	--	--

Name	Supplier	GHS hazard	Hazard Statements	Precautionary Statements
<b>GeneJET Plasmid Miniprep Kit</b>	Thermo Fisher Scientific	GHS05 GHS07	H314	P260, P303+361+ 353, P305+351+ 338, P310, P405, P501
<b>GeneJET Gel Extraction Kit</b>	Thermo Fisher Scientific	GHS07	H302, H412	P264, P270, P273, P301+312, P330, P501

### GHS pictograms



Figure 47: GHS pictograms (source: <https://www.osha.gov/dsg/hazcom/pictograms/index.html>).

### GHS Hazard Statements

<b>H225</b>	Highly flammable liquid and vapor
<b>H226</b>	Flammable liquid and vapor
<b>H228</b>	Flammable solid
<b>H272</b>	May intensify fire; oxidizer
<b>H301</b>	Toxic if swallowed
<b>H302</b>	Harmful if swallowed

---

<b>H311</b>	Toxic in contact with skin
<b>H312</b>	Harmful in contact with skin
<b>H314</b>	Causes severe skin burns and eye damage
<b>H315</b>	Causes skin irritation
<b>H317</b>	May cause an allergic skin reaction
<b>H318</b>	Causes serious eye damage
<b>H319</b>	Causes serious eye irritation
<b>H330</b>	Fatal if inhaled
<b>H331</b>	Toxic if inhaled
<b>H332</b>	Harmful if inhaled
<b>H334</b>	May cause allergy or asthma symptoms or breathing difficulties if inhaled
<b>H335</b>	May cause respiratory irritation
<b>H336</b>	May cause drowsiness or dizziness
<b>H340</b>	May cause genetic defects
<b>H341</b>	Suspected of causing genetic defects
<b>H350</b>	May cause cancer
<b>H350i</b>	May cause cancer by inhalation
<b>H360</b>	May damage fertility or the unborn child
<b>H360D</b>	May damage the unborn child
<b>H360Fd</b>	May damage fertility. Suspected of damaging the unborn child
<b>H360FD</b>	May damage fertility. May damage the unborn child
<b>H361</b>	Suspected of damaging fertility or the unborn child
<b>H361d</b>	Suspected of damaging the unborn child.
<b>H361f</b>	Suspected of damaging fertility
<b>H370</b>	Cause damage to organs
<b>H372</b>	Causes damage to organs through prolonged or repeated exposure
<b>H373</b>	May cause damage to organs through prolonged or repeated exposure.

<b>H410</b>	Very toxic to aquatic life with long lasting effects
<b>H411</b>	Toxic to aquatic life with long lasting effects
<b>H412</b>	Harmful to aquatic life with long lasting effects.



---

**Curriculum Vitae****Aline Melro MURAD**

Born in Brasília, Brazil, on November 1984. Female. Double citizenship Brazilian/Portuguese.

**Bibliographic Citation** MURAD, Aline Melro

**Areas of Expertise** Major Area: Biological Sciences / Area: Biochemistry

**Formal Education / Degree****2013 – 2016**

**PhD. In Structural Biology.** Laboratory for Structural Biology of Infection and Inflammation c/o DESY, Institute for Biochemistry and Molecular Biology, University of Hamburg, Germany. Research Project: Structure-Function-Analysis of DHNA-CoA Thioesterase Involved in Menaquinone (Vitamin K<sub>2</sub>) Biosynthesis Pathway of *Staphylococcus aureus*

*Year of degree:* 2016. Advisor: Dr. Dr. Christian Betzel.

**Grantee of:** Coordenação de Aperfeiçoamento de Pessoal de Nível Superior, **CAPES**, Brazil. Ciência sem Fronteiras Grant: 754513-9

**2008 – 2010**

**Master's in Genomic Science and Biotechnology.** Catholic University of Brasília, UCB/DF, Brazil. Research Project: *Proteomic analysis of Saccharum spp. cultivars with contrasting drought tolerance phenotypes under salt stress conditions*

*Year of degree:* 2010. Advisor:  Betania Ferraz Quirino.

**Grantee of:** Conselho Nacional de Desenvolvimento Científico e Tecnológico, **CNPq**, Brazil

**2003 – 2007**                      **Graduation in Biological Sciences**, Catholic University of Brasília, UCB/DF, Brasil

*Advisor:* Maria Fátima Grossi de Sá /Thales Lima Rocha.  
**Grantee of:** Conselho Nacional de Desenvolvimento Científico e Tecnológico ,**CNPq** ,Brazil

### Complementary Education

**2014 – 2014**                      **Advanced Methods in Macromolecular Crystallization VI**  
 University of South Bohemia, Czech Republic

**2012 – 2012**                      **Basic Training for Biosafety**  
 Catholic University of Brasília, UCB/DF, Brazil

**2009 – 2009**                      **Analysis of Gene Expression in Plants**  
 Federal University of Ceará

**2007 – 2007**                      **Safety Notions in Laboratory**  
 Embrapa Genetic resources and Biotechnology

**2007 – 2007**                      **Good Laboratory Practice**  
 Embrapa Genetic resources and Biotechnology

**2007 – 2007**                      **Update on Nematology**  
 Federal University of Goiás

**2007 – 2007**                      **Strategy of New Drugs Discovery**  
 Brazilian Society of Pharmacognosy

**2005 – 2005**                      **Plant Diversity in Mined Aereas in the Cerrado**  
 Catholic University of Brasília, UCB/DF, Brazil

### Professional Experience

**2013 – 2016**                      **Laboratory for Structural Biology of Infection and Inflammation c/o DESY, Institute for Biochemistry and Molecular Biology, University of Hamburg.**

Research Projects

- *Structure-Function-Analysis of DHNA-CoA Thioesterase Involved in Menaquinone (Vitamin K<sub>2</sub>) Biosynthesis Pathway of Staphylococcus aureus*

<b>2006 – 2010</b>	<p><b>Embrapa Genetic Resources and Biotechnology / Embrapa Agrienergy</b></p> <p>Research <span style="float: right;">Projects</span></p> <p>- <i>Proteomic analysis of Saccharum spp. cultivars with contrasting drought tolerance phenotypes under salt stress conditions.</i></p> <p>- <i>Prospecting of biomolecules to control phytonematodes and phytopathogenic fungi.</i></p>
<b>2003 – 2005</b>	<p><b>Catholic University of Brasília</b></p> <p>Research and development</p>

### **Scientific and Technological Production**

#### **Publication**

- **Murad AM**, Molinari HBC, Magalhães BS, Franco AC, Takahashi FSC, de Oliveira- NG, Franco OL, Quirino, BF (2014) Physiological and Proteomic Analyses of *Saccharum* spp. Grown under Salt Stress. PLoS ONE 9(6): e98463. doi:10.1371/journal.pone.0098463

#### **Summary published in proceedings of conferences**

- **MURAD, Aline Melro**, PERBANDT, M., WRENGER, C., BETZEL, C. 2015, Rovinj, Croatia. Structure-Function-Analysis of proteins involved in the metabolic pathway of vitamin K acting as major pathogenic factors in *Staphylococcus aureus*, 2015. 29<sup>th</sup> European Crystallographic Meeting, p. 40.
- **MURAD, Aline Melro**; MOLINARI, H. B. C.; OLIVEIRA JUNIOR, N. G. ; MAGALHAES, B. S. ; O. L. Franco; QUIRINO, B. F. . , 2010, Foz do Iguaçu. Proteomic analysis of *Saccharum* spp. cultivars with contrasting drought tolerance phenotypes under salt stress conditions, 2010. v. 1. p. 77-77
- **MURAD, Aline Melro** ; MOLINARI, H. B. C. ; TAKAHASHI, F. S. C. ; OLIVEIRA JUNIOR, N. G. ; FRANCO, A. C. ; O. L. Franco; QUIRINO, B. F., 2009, Fortaleza-CE. CBFV XII Congresso Brasileiro de Fisiologia Vegetal, 2009. p. 204-204
- **MURAD, Aline Melro** ; CARNEIRO, R. ; BRILHANTE, O. ; Grossi de Sá, M.F. ; ROCHA, T. L. . , 2007, Goiânia. XVII Congresso Brasileiro de Nematologia, 2007.
- **MURAD, Aline Melro** ; SILVA, M. S. ; ESPINDOLA, L. S. ; PAULA, J. E. ; Grossi de Sá, M.F. ; ROCHA, T. L. . , 2007, Belém. VI Simpósio de Farmacognosia, 2007
- GOMES, K. R. G. ; **MURAD, Aline Melro** ; PAULA, J. E. ; MAGALHAES, A. V. ; ESPINDOLA, L. S., 2007, Belém. VI Simpósio de Farmacognosia, 2007
- **MURAD, Aline Melro** ; Grossi de Sá, M.F. ; ROCHA, T. L. . , 2006, Brasília. XI ENCONTRO DO TALENTO ESTUDANTIL DA EMBRAPA RECURSOS GENÉTICOS E BIOTECNOLOGIA, 2006. v. E-53. p. 122-122.
- **MURAD, Aline Melro** ; Souza, T. M. S. ; Saúde, A. C. M. ; Sousa, A. R. C. ; Noronha, E. F. ; O. L. Franco ; Neto, E. L. . , 2005, Aguas de Lindóia. XXXIV Reunião Anual da Sociedade Brasileira de Bioquímica e Biologia Molecular, 2005. v. E-95. p. 49-49.

- ROCHA, T. L. ; **MURAD, Aline Melro** ; EVARISTO, R. G. S. ; ALMEIDA, W. S. ; MAGALHAES, J. C. C. ; MATTAR, M. C. S. ; Grossi de Sá, M.F. . . 2006.
- Neto, E. L. ; **MURAD, Aline Melro** ; Souza, T. M. S. ; Saúde, A. C. M. ; Sousa, A. R. C. ; O. L. Franco . , 2005, Gramado. 3º CONGRESSO BRASILEIRO DE MELHORAMENTO DE PLANTAS, 2005.
- Souza, T. M. S. ; Saúde, A. C. M. ; P. D. Tagliari ; **MURAD, Aline Melro** ; COSTA, Fabio Teles ; Bloch Jr. C. ; Noronha, E. F. ; O. L. Franco . , 2005, Aguas de Lindóia. XXXIV Reunião Anual da SBBq, 2005. v. E-6.
- Souza, T. M. S. ; GODOI, Andressa V. ; **MURAD, Aline Melro** ; Noronha, E. F. ; O. L. Franco . , 2004, Brasília. Anais do Encontro de Iniciação Científica da UCB/2004, 2004. v. 1. p. 152-152.
- **MURAD, Aline Melro** ; BARROS, D. M. ; P. D. Tagliari ; J. L. Pereira ; Bloch Jr. C. ; O. L. Franco . , 2004, Caxambu - MG. XXIII Reunião Anual da Sociedade Brasileira de Bioquímica e Biologia Molecular., 2004. v. E-63. p. 50-50.

#### Expanded Summary published in proceedings of conferences

- **MURAD, Aline Melro** ; MOLINARI, H. B. C. ; TAKAHASHI, F. S. C. ; OLIVEIRA JUNIOR, N. G. ; MARTINS, M. T. B. ; GOULART, M. O. ; O. L. Franco ; QUIRINO, B. F. . , 2009, Brasília. I Workshop em Ciências Genômicas e Biotecnologia, 2009
- MARTINS, M. T. B. ; SOUZA, A.P. De ; ARENQUE, B ; GOULART, M. O. ; **MURAD, Aline Melro** ; QUIRINO, B. F. ; ANDRADE, A. C. ; BUCKERIDGE, M.S. ; MOLINARI, H. B. C. . , 2009, Brasília. I Workshop em Ciências Genômicas e Biotecnologia, 2009.
- **MURAD, Aline Melro** ; ROCHA, T. L. ; SILVA, M. S. ; LACERDA, A. F. ; ESPINDOLA, L. S. ; SUASSUNA, N. D. ; CHARCHAR, M.J.A. ; ANJOS, J.R.N. ; Grossi de Sá, M.F. . , 2007, Brasília. II Workshop de Interação Molecular Planta Praga, 2007.

#### Presentation of Work

- **MURAD, Aline Melro**, PERBANDT, M., WRENGER, C., BETZEL, C. . . 2015. (Presentation/Conference).
- **MURAD, Aline Melro**; MOLINARI, H. B. C. ; OLIVEIRA JUNIOR, N. G. ; MAGALHAES, B. S. ; O. L. Franco ; QUIRINO, B. F. . . 2010. (Presentation/Congress).
- **MURAD, Aline Melro**; MOLINARI, H. B. C. ; TAKAHASHI, F. S. C. ; OLIVEIRA JUNIOR, N. G. ; FRANCO, A. C. ; O. L. Franco ; QUIRINO, B. F. . . 2009. (Presentation/Congress)
- **MURAD, Aline Melro**; MOLINARI, H. B. C. ; TAKAHASHI, F. S. C. ; OLIVEIRA JUNIOR, N. G. ; MARTINS, M. T. B. ; GOULART, M. O. ; O. L. Franco ; QUIRINO, B. F. . . 2009. (Presentation/Other).
- **MURAD, Aline Melro**. . 2009. (Presentation/Conference or Colloquium).
- **MURAD, Aline Melro** ; MOLINARI, H. B. C. ; TAKAHASHI, F. S. C. ; O. L. Franco ; QUIRINO, B. F. . . 2008. (Presentation/Symposium).

#### Languages

Portuguese: mothertongue

**English: reading: good; writing and conversation: reasonable**

### **Eidesstattliche Erklärung**

Hiermit versichere ich an Eides statt, die vorliegende Dissertation selbst verfasst und keine anderen als die angegebenen Hilfsmittel benutzt zu haben. Ich versichere, dass diese Dissertation nicht in einem früheren Promotionsverfahren eingereicht wurde.

Ferner versichere ich, dass ich noch keine Promotionsversuche an anderen Universitäten unternommen habe.

Hamburg, 15.08.2016

---

Aline Melro Murad

